Faculdade de Engenharia da Universidade do Porto

Study on dynamic behavior on the human ear with the presence of an irregular body

Rodrigo Duzanowski Savaris

Dissertação realizada no âmbito do Mestrado em Mecânica Computacional

Orientador: Prof. Doutor Marco Paulo Lages Parente
07 de Julho de 2018

ABSTRACT

The present work has as objective the study of the mechanical behavior of the human ear. Through the use of a precise human ear model, irregular bodies were placed on the model in order to analyze the variations on the dynamical behavior on different situations.

The project “The visible ear” used a technique called “cryosectioning” to obtain and arrange a set of high quality images from a frozen temporal bone from an 85 year old woman. These images allowed the creation of the computational model used on this work.

Two tridimensional models were developed from that, afterwards. The first one, further entitled the simple model, consisted on the tympanic membrane, ossicles, ligaments and muscles. The second model, further entitled the complete model, introduces air on the external hearing canal and air on the middle ear cavity, while making use of literature values for the properties of the materials.

Then, three different irregular bodies were built to be inserted into the model to simulate the presence of tumors. The first one was applied on the anvil ossicle of the middle ear, the second one was applied on the inside of the stirrup ossicle, and a third, bigger body was inserted on the tympanic membrane.

The three models were used to obtain natural frequencies and displacements on the umbo and on the stirrup for both models, while always comparing the obtained results from the previous literature complete and simple models, and, when possible, to other previous literature which had similar situations.

The models were subjected to a frequency range between 100 Hz and 10 kHz.

The simulations ended up showing that the first two tumor models didn´t have a large impact on the dynamic behavior of the human ear, mostly due to their size, whereas the third tumor model had the largest impact, with significantly higher variations in both natural frequencies and displacement results.

Index

FIGURES INDEX

TABLES INDEX

1 INTRODUCTION

The human ear is an indispensable organ that is responsible for monitoring variations of air pressure, which are related to sound waves propagation, and sending the information towards the brain, where it can be decoded.

There are three main phases when a sound is produced. Prior to the ear´s involvement, an object will create the sound through vibration on matter. Such vibration causes every air particle nearby the vibration to start moving. When those start moving, they force the movement of the ones close to them, creating a cycle that is responsible for the sound wave.

On the first phase of the ear function, the created sound wave reaches the ear and are directed to the external auditive canal, following to the tympanic membrane, making it vibrate. A simple representation of such anatomy can be seen on Figure 1.1 [1].

The second phase consists the sound transmission through three bones that are found within the middle ear, the hammer (Malleus), the anvil (Incus) and stirrup (Stapes), all of which can be seen in Figure 1.1[1], [2]. The stirrup being the smallest bone on the human body. Once all of these are reached, the third phase occurs.

The third phase takes place on the inner ear. The stirrup´s movement creates waves of pressure on the cochlear fluid inside the cochlea. The created waves stimulate the hair cells which transform the pressure variation to electrical impulses, which are sent through the vestibulocochlear nerve to the brain, which is responsible for the decoding of them.

The present work has as objective the study of modifications that can be made present on the transmission of the sound from the outer ear canal up to the stirrup. In order to better study such occasions, it will be made use of the former project “The visible ear”, which had as objective to develop a digital atlas of the temporal bone in high resolution. It could also be used for computational simulations for studies of the inner ear, which are useful for rehearsal and planning of surgeries.

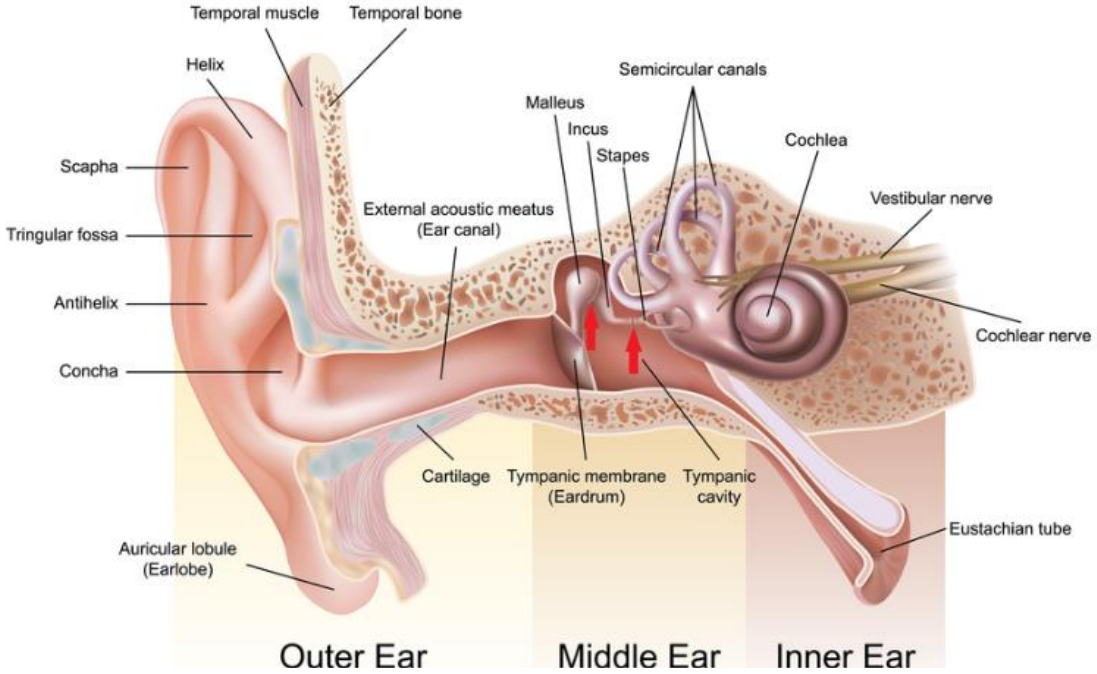

Figure 1.1 - Human ear anatomy [1].

In this work, it will be made use of the Finite Element Method, which is a powerful tool with the capacity to simulate mechanical problems of high complexity, through a geometrical model [3]. The model being used on this work includes tympanic membrane, ossicles, the cochlea, air in the external auditory canal and in the tympanic cavity [4].

The present work will be divided in 7 sections. Introduction, The Human Ear, Acoustics, Dynamics, Finite Element Method, Mechanical Analysis of the Ear, Conclusions and Future Works, References.

In chapter 2, it will be made a basic review of the anatomy of the human auditory system, along it´s main components. It will also be presented the correlations between the auditive sensations and physical characteristics of the sound.

In chapter 3, a brief summary will be presented about the study of acoustics, proceeded with deeper information on it´s aspects.

In chapter 4 the basic concepts of dynamics are explained, along with the composition of a vibratory system.

In chapter 5 the Finite Element Method is thoroughly explained, showing it´s origins and every process involved in using the method for solving a complex calculus problem.

In chapter 6 it is explained about the creation of the model that was the main tool for this work, along with most of the mechanical properties involved, and any changes to which it was subjected to simulate the presence of three different tumors on it are explained. It is also shown the different obtained results for natural frequencies, displacements, and phase angles for several sound pressure levels.

In chapter 7 there is a summary of the complete work, along with conclusions and suggestions for future works.

2 THE HUMAN EAR

2.1 Introduction

Human beings have five fundamental distinct senses, those being sight, touch, smell, taste, and hearing. The one which will be mainly discussed on the present work will be the latter, hearing [5].

The hearing capacity of the human being is rather important for it´s life amongst society. The human organ which is responsible for such sense is the human ear. It is capable of detecting and reading sound waves of frequency between 16 Hz up to 20 kHz [6] and intensities between 0 dB and 130 dB. It is also responsible for our equilibrium. It has the ability to transform wave sounds in electrical signs, and then transmitting such information to the brain.

The human ear is located on the temporal bone, situated on the lateral wall of the skull. The auditive system is divided in two parts, peripheral and central. The peripheral part is composed by the outer ear, middle ear and the inner ear. The central part is composed by the nerves and the cortex. Such anatomy can be seen in Figure 1, shown previously.

The outer ear consists of the auricle, also known as pinna, and the external auditive canal, and ends in the tympanic membrane. The middle ear contains the Eustachian tube and the tympanic box. The inner ear is composed by sensorial organs responsible for both hearing and equilibrium functions, and the inner ear is the only part responsible for the equilibrium [7].

2.2 Outer Ear

The outer ear is the part of the ear that is capable of sound recognition and is responsible to lead it to the inner parts of the ear. It has two major parts, those being the external auditive canal and the auricle (pinna). Figure 2.1 brings a representation. The auricle is disposed on an angle varying from 20° up to 45° from the cranial wall. It has general dimensions varying from 6 to 7 cm in the vertical axes, and 3 to 4 cm on the horizontal axes. Usually speaking, the dimensions achieved by the age of seven can be considered permanent.

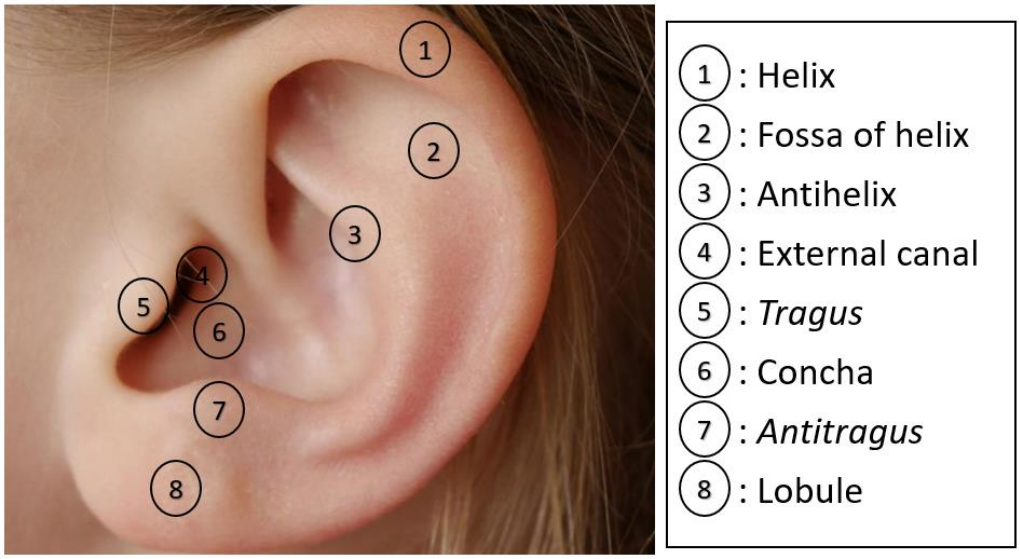

Figure 2.1 - Representation of the outer ear [8].

As can be seen on Figure 2.1, the outstanding margin of the ear is called helix, and the fossa of helix is right under it, being a depression. It is followed by an elevation which is called antihelix, which then branches in two paths. The *tragus* and the *antitragus* are located on the opening of the external auditive canal and right above the lobule, respectively. The lobule is a portion of soft tissue located on the lower parts of the auricle. The concha is located between the antihelix and the *antitragus*.

The external ear canal has the function of transmitting the sounds from the auricle to the tympanic membrane. It also works as resonating chamber and amplifies sounds of certain frequencies [9]. On it´s third external part it is fibrocartilaginous and on it´s remainder it is bony. It is coated with an epidermal cape which is an extension of the skin from the auricle.

In the fibrocartilaginous part the skin is thick, presenting hair and fat. The dermis contains sebaceous glands and the subcutaneous tissue contains ceruminous glands, which are responsible for the production of cerumen, thus avoiding passage of foreign bodies, also protecting the epithelium from maceration, caused by retention of water. It has an approximate size of 25 up to 30 mm from the concha to the tympanic membrane [2]. Figure 2.2 brings a representation.

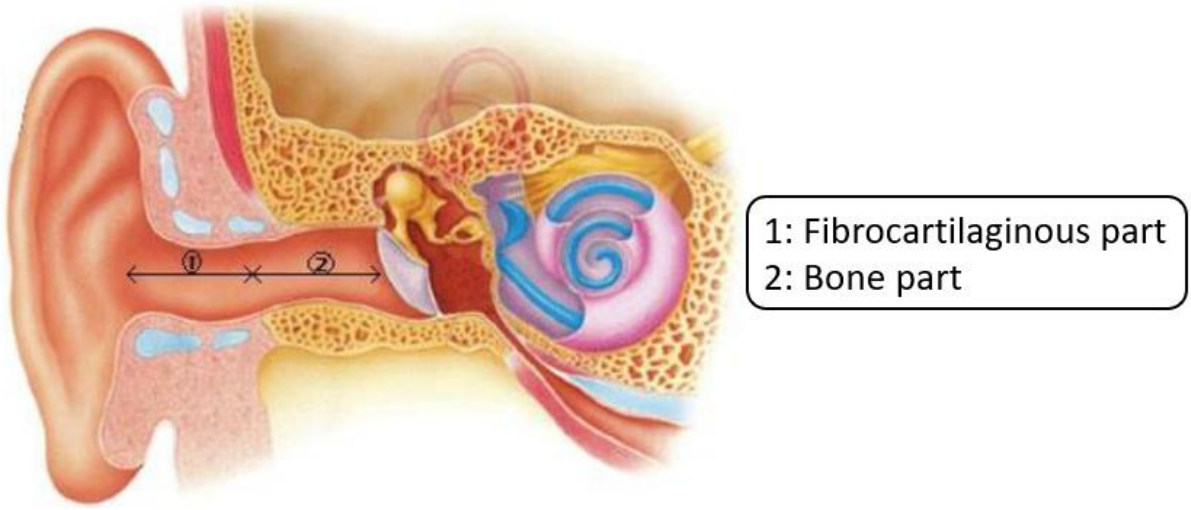

Figure 2.2 - Representation of the outer ear [10].

According to Tröltsch [2], [11] the dimensions, expressed on millimeters, of the four walls of the external ear canal can be seen on Table 2.1.

Table 2.1 - Dimensions for the walls on the external ear canal.

Wall	*Cartilaginous part*	*Bone part*	*Auditive canal*
Inferior	9	18	27
Anterior	10	16	26
Posterior	7	15	22
Superior	7	14	21

2.3 Middle Ear

In the internal part of the outer ear, comes the middle ear. The middle ear is a cavity filled with air, built on an ossicular chain, which is composed of the hammer, the anvil and the stirrup. It has six ligaments, two muscles and a portion of the facial nerve. The external auditive canal conducts sound energy to the tympanic membrane, where it is then transformed into mechanical energy. The dimensions of the tympanic box, for both the anterior-posterior diameters is 15 mm, the transversal diameter has varying dimensions in relation to where it is considered, with it´s lowest part measuring about 4 mm, the middle portion varying 1,5 to 2 mm, and the upper part having between 5 and 6 mm.

On the intern side of the middle ear, two interfaces exist, those being the oval window and the round window, which separate it from the inner ear. One of these opens at the mastoid cells of the mastoid process of the temporal bone. The other, called Eustachian tube, opens into the pharynx and equalizes the pressure between the outside air and the middle ear cavity.

Uneven pressure between the middle ear and the environment is capable of distorting the tympanus, messing with it´s vibrations and therefore making it harder for the hearing process to properly occur. Due to this distortion, when a change of altitudes occurs, it seems like the sounds are stuffy, and a certain amount of pain can be sensed on the tympanum. Such symptoms can be relieved through the opening of Eustachian tube, which then allows the passage of air and even the pressures [4], [9]. This canal also has protection functions of the middle ear, against bacteria and draining of the middle ear, allowing the passage of mucus secreted by the tympanic mucosa. Figure 2.3 brings a representation of the middle ear.

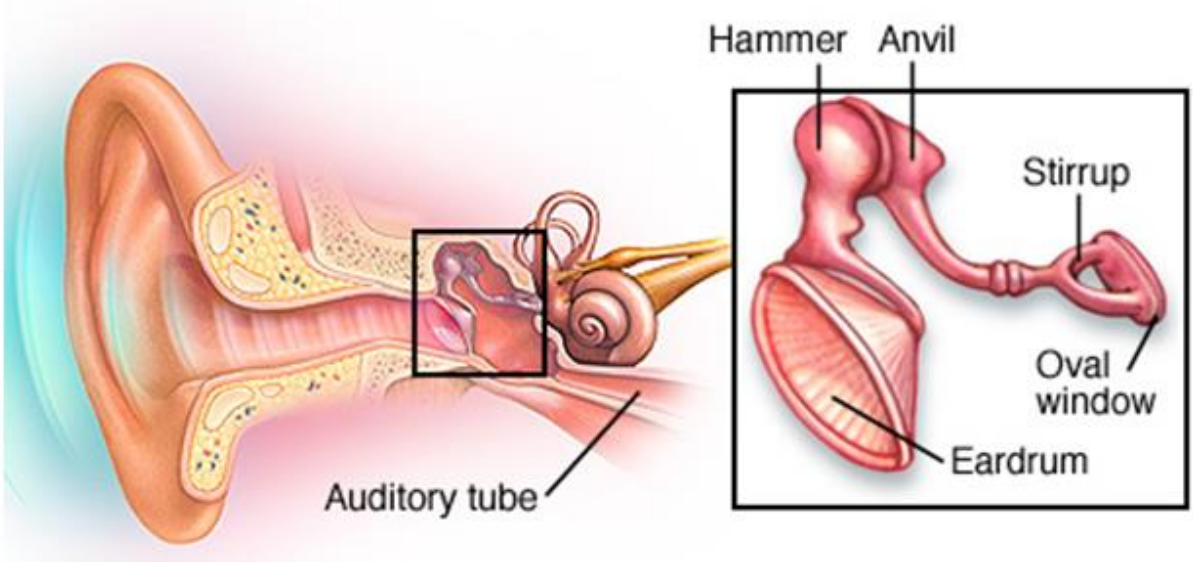

Figure 2.3 - Representation of the middle ear [12].

2.3.1 Tympanic membrane

The tympanic membrane is a thick and semi-transparent membrane which has the function to vibrate when presented with sound stimulation, and then these vibrations proceed to be transmitted to the ossicular chain.

The tympanic membrane has a round shape and has two regions: *pars tensa* and *pars flaccida*

[4]. It has a varying diameter between 9,5 and 10,5 mm, which results in an approximate area of 85 mm^2. Out of that area, a portion of 55 mm^2 is capable of movement, and the rest is rigid. The *pars tensa* has an area of 68,6 mm^2 and the *pars flaccida* has an area of 4,6 mm^2 [13]. Both can be seen on Figure 2.4.

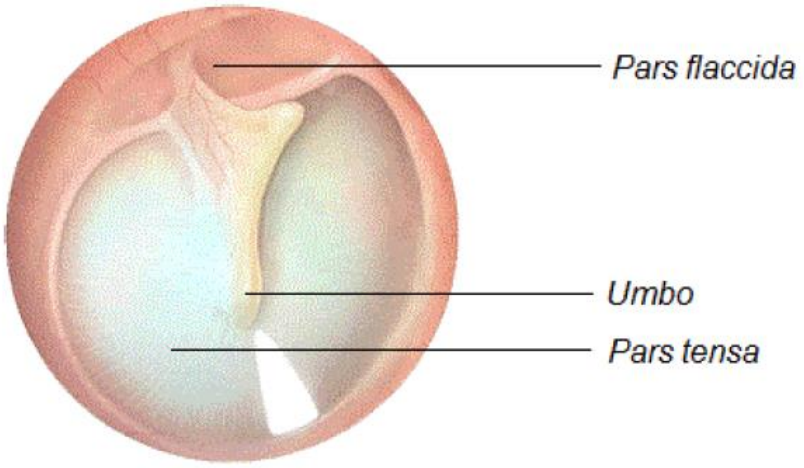

Figure 2.4 - Representation of the tympanic membrane [4], [13].

The tympanic membrane is built upon three layers of tissue, the external, the intermediate and the internal.

The internal layer is composed of epithelial tissue [2], [4]. The intermediate layer is fibrous and is the main responsible part for the vibration response. There are four main types of fiber on it´s composition, those being: Radial fibers, which go from the annular board up to the hammer´s base, thus allowing it´s rotation. Then there are the circular fibers, which form concentric rings on the umbo, and are located inside the hammer´s cable. There are also the parabolic fascicles which go from the short apophysis on the hammer, irradiating from the apophysis to the anterior and posterior part of the membrane, up to the annular ligament. Lastly, there are the semilunar system fibers, which are concave arches and convex arches from the outer membrane up to the umbo.

The external layer is a thin layer and cutaneous which is tethered to the layer that covers the external auditive canal.

The umbo is located on the tympanic membrane, it is the extremity of the hammer´s cable. In the superior part of the tympanic membrane is the *pars flaccida* which has a few fibers, therefore being flaccid. It is composed of a cutaneous layer and a mucous one. On the inferior part of the membrane is the *pars tensa*, composed of three layers. This region has a higher amount of fibers, is elastic, thick, resistant and has low mobility [2], [4].

The membrane can be represented through six different regions, which can be seen on Figure 2.5.

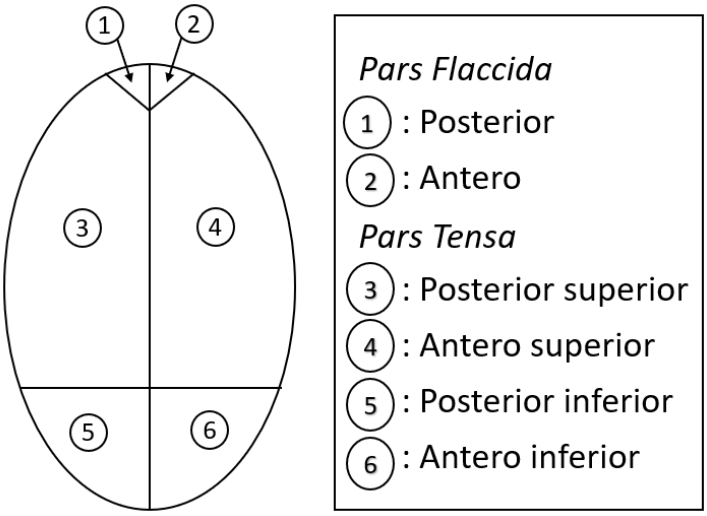

Figure 2.5 - Tympanic membrane regions [2], [4].

2.3.2 Tympanic box

The tympanic box has six main walls: the external, internal, superior, inferior, posterior and anterior. These walls are covered by epithelium and a layer of connective tissue, by the temporal bone. Figure 2.6 brings a representation of the tympanic box.

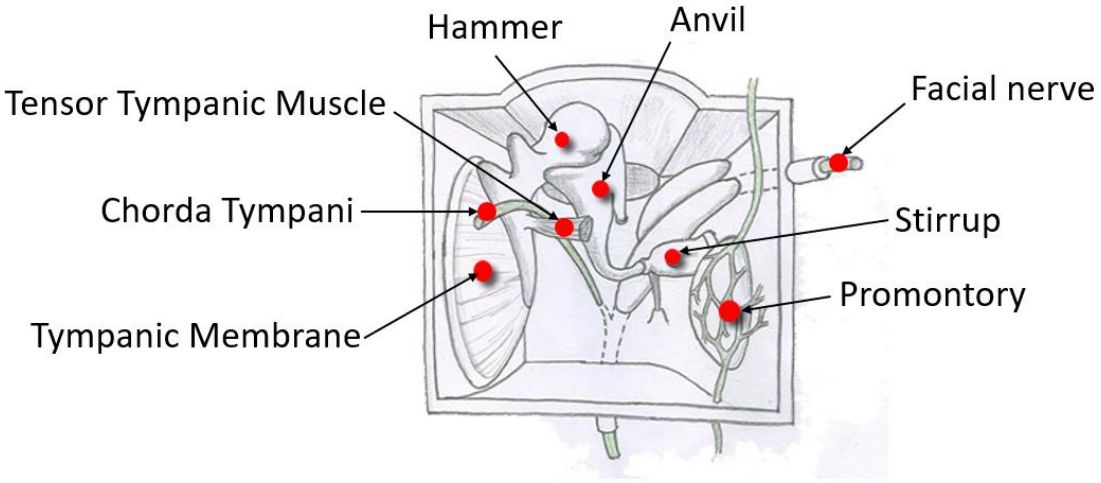

Figure 2.6 - Tympanic box [4].

The external wall, or tympanic, has a bone portion and a membranous portion. The internal wall, or labyrinth, is what separates the inner and the middle ear. It is found the oval window, which is the stirrup´s platinum articulates, the tympanic portion of the canal of the facial nerve, then the round window, the tendon of the tympanic tensor muscle and the promontory, which can be seen on Figure 2.6. The oval window enables communication between the middle ear and the inner ear through the base of the stirrup. The round window is responsible for equalizing

pressure, which allows the incompressible fluid to freely move inside the cochlea. The superior wall is built on a thin bony blade, and separates the middle ear from the cranial cavity. The inferior wall has a petrous tympano structure and forms a sulcus on the anteroposterior direction. It is bounded on the inside by the promontory and on the outside by a bony ridge, where the tympanic membrane is.

The posterior wall possesses an essentially petrous structure, and is the highest of the four walls, with a measurement of approximately 13 mm. The anterior wall has petrous tympano structure and is largely occupied by the Eustachian tube [2], [4].

2.3.3 Ossicles

The middle ear contains three ossicles: the hammer, the anvil and the stirrup, which are responsible for transmitting vibrations from the tympanic membrane to the oval window. Figure 2.7 brings a representation of the hammer.

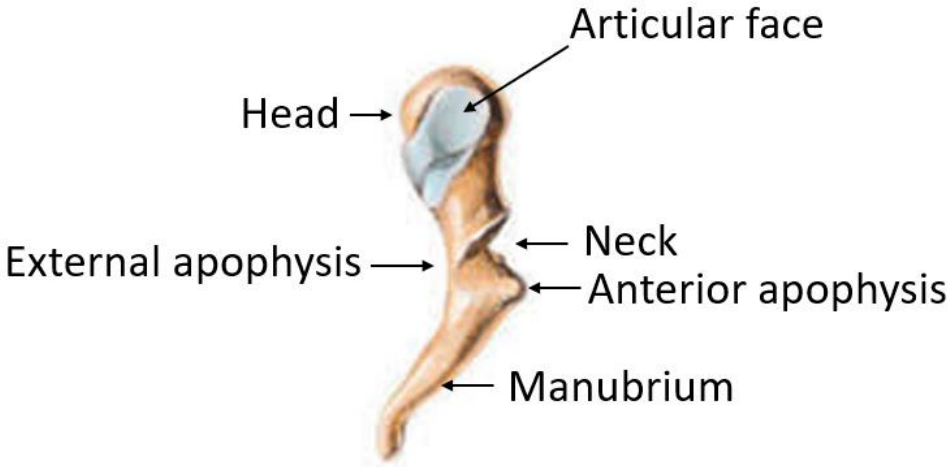

Figure 2.7 - Hammer [2], [14].

The hammer is the most extensive ossicle and is located on the intermediary layer of the tympanic membrane. As can be seen on Figure 2.7, it can be divided into head, neck, manubrium and both apophysis. The head is the superior extremity of the bone, slightly over the tympanic membrane, and is attached to the anvil. The neck is a narrow section which is connected to the *pars flaccida* part of the tympanic membrane. The manubrium is fixated on the superior part of the tympanic membrane, pulling it in. In the neck region is found the tensor tympanic muscle. The external apophysis goes from the neck of the hammer to the superior part of the tympanic membrane, towards the external auditive canal. The anterior apophysis (Raw´s apophysis) also starts on the neck of the hammer, and has a length of approximately 4 to 5 mm [2], [4], [14].

Figure 2.8 brings a representation of the anvil.

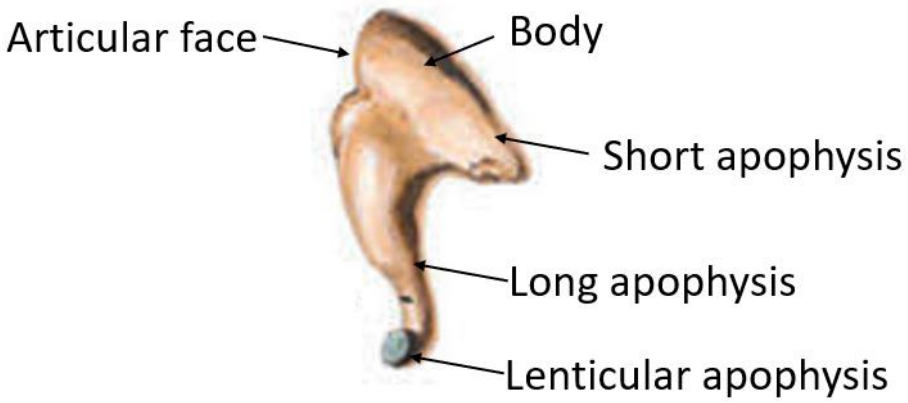

Figure 2.8 - Anvil [2], [14].

As can be observed in Figure 2.8, the anvil is mainly composed of one body and three apophysis. The anvil is the second ossicle, located behind the hammer, and is the heaviest ossicle. The body occupies the upper part of the tympanic box. The short and long apophysis of the anvil separate themselves from the body on it´s inferior part, having a differential angle on the angle between 85° up to 90°. The short apophysis has an approximate length of 5 mm, is directed towards the posterior ligament of the anvil and had a triangular shape. The long apophysis has an approximate length of 7 mm, starts on the body of the anvil and then follows downwards, similarly to the hammer´s manubrium. It ends on the lenticular apophysis, which is then connected to the stirrup´s head [2], [4], [14].

The stirrup is the smallest and last ossicle, with an average weight of 2 mg. Figure 2.9 brings a representation.

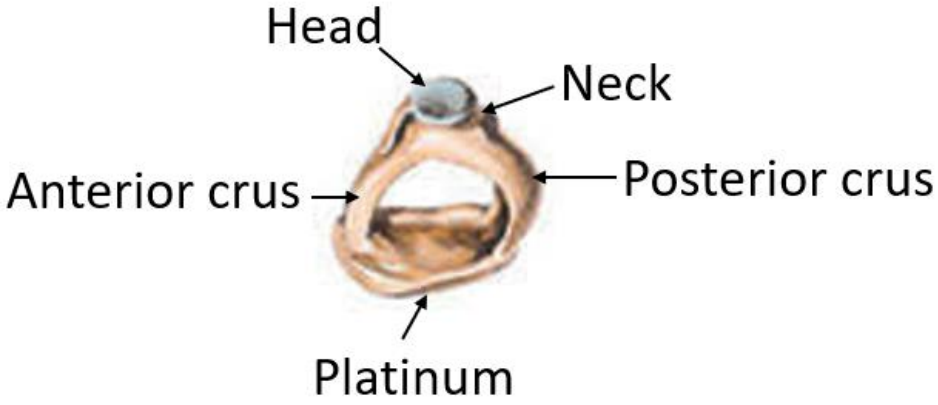

Figure 2.9 - Stirrup [2], [14].

As observed in Figure 2.9, the stirrup can be anatomically split into the head, neck, two crus and the platinum. The head on the extremity of the stirrup has a concave shape, which is connected to the lenticular apophysis of the anvil. The neck connects the head to the posterior and anterior crus, and has a cylindrical shape. The anterior crus and the posterior crus connect the neck to the platinum of the stirrup. The posterior crus is longer and has a wider curve than

the anterior crus. The platinum is a bony irregular plate located on the oval window [2], [4], [6], [14]–[16].

2.3.4 Muscles of the middle ear

There are two muscles connected to the auditive ossicles which have the function of dampening excessively loud noises. Such activity is able to protect the inner ear structures, which are somewhat fragile, from harmful noises. The tympanic tensor muscle is connected to the hammer, and it elongates the tympanic membrane while also causing a rise of pressure on the labyrinthic liquid when there is a presence of strong sounds. The stapedius muscle is connecter to the stirrup and has the function of relaxing the tympanic membrane and lowering the labyrinth pressure. Both muscles are shown in Figure 2.10 [13], [15].

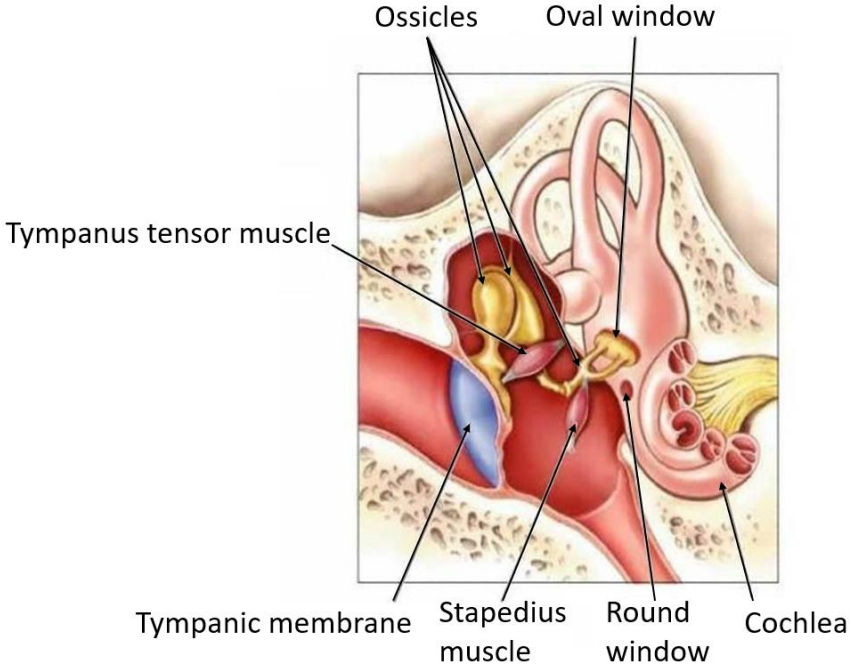

Figure 2.10 - Middle ear muscles [4].

As seen, the anvil is connected to the stirrup. Due to that, every time the tympanic membrane and the hammer´s manubrium move inwards the cochlear liquid is impelled, and when the movement is outward, the liquid is pulled. The articulations are covered by cartilage, which help with possible resonance effects. The ossicles of the middle ear are suspended by ligaments, of which three are connected to the hammer, two on the anvil and one on the stirrup. The stirrup´s platinum and the oval window are covered by cartilage [13], [15].

2.4 Inner Ear

2.4.1 Cochlea

The bone labyrinth is composed of bony canals on the interior of the temporal bone. In the interior of the labyrinth, there is a set of tunnels and chambers with similar shape but smaller,

known as membranous labyrinth, which is filled with a liquid called endolymph, and the space between the membranous and the bone labyrinth is filled by a liquid called perilymph.

The bony labyrinth is divided into three regions: cochlea, vestibule and semicircular canals. The vestibule and the canals are majorly responsible for the equilibrium, while the cochlea is responsible for the hearing. The membranous labyrinth is also divided into three parts, the vestibular scale, the tympanic scale and the cochlear canal [15], [16].

The oval window communicates with the vestibule on the inner ear, which communicates with a cochlear chamber, the vestibular ramp. This ramp goes from the oval window to the helicotrema, which is at the peak of the cochlea. Then there is the tympanic ramp goes from the helicotrema to the round window.

The wall of the membranous labyrinth which is connected to the vestibular ramp is called Reissner´s membrane, and it had the responsibility of separating two chemically distinct fluids. The covering wall of the tympanic ramp is called basilar membrane. The space between the vestibular membrane and the basilar membrane is the cochlear canal and is filled with endolymph. The collagenous fibers of the basilar membrane are oriented through the membrane which resides between the spiral blade and the spiral ligament.

The collagenous fiber´s diameter on the membrane lowers as the basilar membrane enlarges. Therefore, the basilar membrane close to the oval window is shorter and more rigid, having response to high frequency vibrations, while the part closest to the helicotrema is larger and flexible, and has response to lower frequency vibrations. On the cochlear canal is found organ of Corti. This organ contains around 13.000 cells which receive acoustic energy. The structure is resistant, and is capable of blocking sound waves. This structure can be seen on Figure 2.11 [4], [13], [15]–[17].

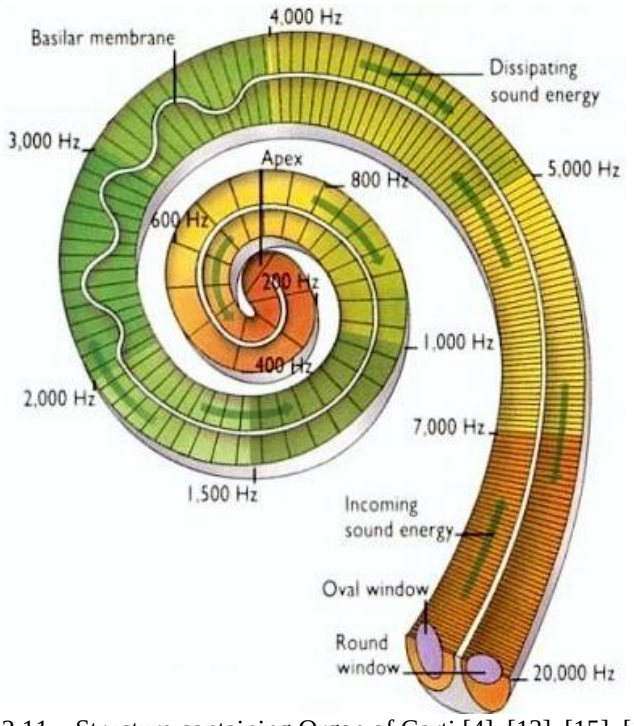

Figure 2.11 – Structure containing Organ of Corti [4], [13], [15]–[17].

2.4.2 Vestibule

The vestibule is a small cavity positioned between the cochlea and the semicircular canals. It is composed of two vesicles, the utricle and the saccule, also known as otolithic organs. The utricle is larger, and is located on the upper part of the vestibule. The saccule is smaller and is located on the lower part. The region in the lining of the utricle and saccule is differentiated into a sensory organ, which is called macula.

The utricle macula stays on the inferior surface of the utricle, and aids on the determination of orientation of the head when the person is standing up. The saccule macula is located on the vertical plane, and aids the equilibrium when the person is laying down. In the saccule exist two small openings, one on the posterior wall, which enables communication with the utricle through the utricle-saccule canal, and another on the inferior part, which communicates the cochlear canal to the Hensen canal.

The utricle walls and the saccule´s are structurally divided into three layers: the external, which is composed of fibrous tissue and contains blood vessels, the intermediary, which is thin and transparent and forms a homogeneous membrane, and the internal, which is composed of epithelial cells. On the utricle´s and saccule´s macula the epithelium is columnar and contains support cells [2], [4], [15], [18].

2.4.3 Semicircular canals

The semicircular canals are three small bony canals which are interconnected, located behind and above the vestibule, starting and finishing on the vestibule. They stand on nearly straight angles from one another, where one of them approaches the transversal plane, the second the frontal plane and the last the sagittal plane. The way they are disposed allows for detection of movement in any direction. The base of the canals expands in ampoule, where can then be found the sensorial organs in the dome. Whenever the head moves on a certain direction, the liquid found on the ampoule, called endolymph, moves at a different speed than the semicircular canals, which causes the dome to move on the opposite direction of the head, therefore producing a relative movement between the dome and the liquid [4], [15].

2.4.4 Sound waves effects on the cochlea

Sound waves originated on the exterior are received through the external ear, proceeded to be amplified by the medium ear and then transformed by the inner ear into nervous impulses which then proceed to the brain. Figure 2.12 brings a representation of the sound waves processes on the cochlea.

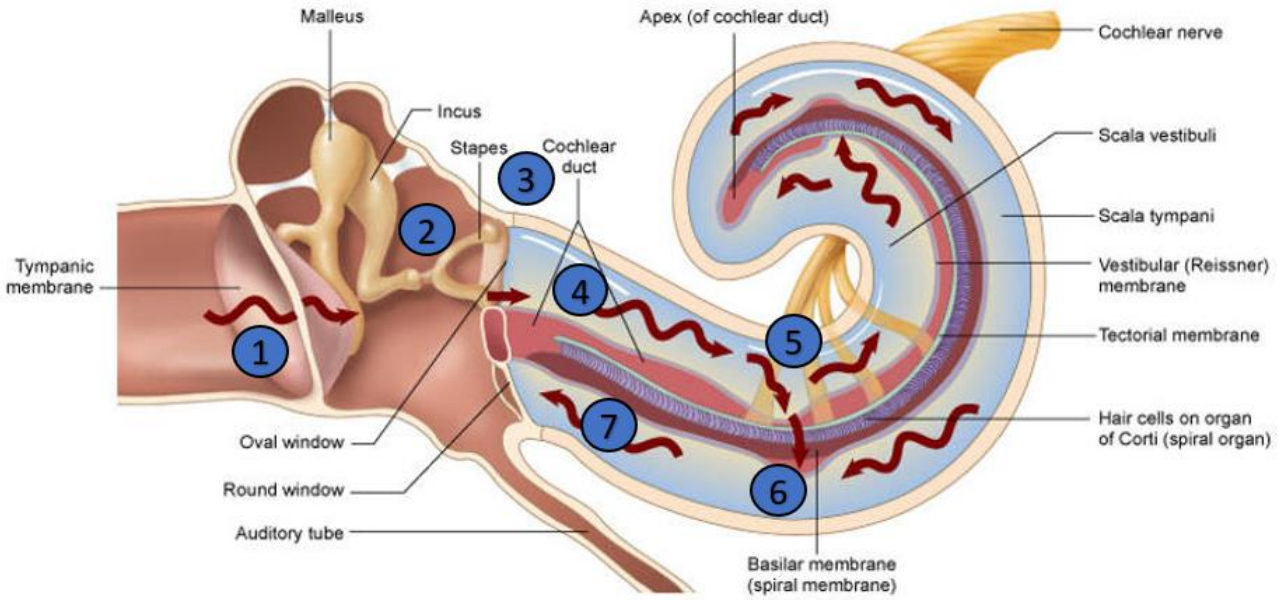

Figure 2.12 - Sound wave effects on the cohclea [2], [4], [15].

The numbered steps observed are:

1- The sound waves hit the tympanic membrane, causing it to vibrate.
2- The vibration of the tympanic membrane also causes the ossicles of the middle ear to vibrate.
3- The base of the stirrup vibrates the oval window.
4- The vibration of the stirrup causes the vibration of the perilymph on the vestibular ramp.
5- The perilymph´s vibration causes displacement of the basilar membrane. The high frequency sound waves excite the basilar membrane closer to the oval window, while the low frequency sound waves make the basilar membrane vibrate farther away from the oval window. The basilar movement is tracked by the cells on the organ of Corti.
6- The vibrations of the perilymph on the vestibule ramp and from the endolymph on the cochlear canal are then transferred to the perilymph on the tympanic ramp
7- The vibrations from the perilymph on the tympanic ramp are then transferred to the round window, there being damped.

3 ACOUSTICS

3.1 Introduction

Acoustic is the field of science responsible for understanding the oscillations and waves on elastic means. It can be defined as the generation, transmission and receival of energy in wave forms on matter. Sound needs a physical, solid, liquid or gas environment in order to properly propagate. When vocal cords vibrate, it creates an oscillation on the air particles that surround us. The impact that is resulted from such oscillation makes is so that it gets propagated through such impact to the nearest air particles, and the cycle keeps repeating itself [19], [20].

There are zones on the air where the pressure is bigger, and there are zones where the pressure is smaller, which is related to the density of particles in such zone. These pressure zones are in constant movement through air and form what is called pressure wave.

The sound has four main attributes: pitch, duration, loudness and timbre.

3.2 Sound structure

3.2.1 Frequency

The core definition of frequency when it comes to the study of sound is that it is a number of cycles in a set time. It is referenced in literature as the letter *f*, and it´s unit is known as Hertz (Hz) which represents cycles per second. Period, on the other hand, is the indication of the amount of time required to fulfill one full cycle. These are related through Equation 3.1 [19], [20].

$$f = \frac{1}{T} \tag{3.1}$$

As can be seen on Equation 3.1, period is simply the inverse of the frequency. Not all frequencies can be rightfully heard by a normal auditory system. The normal frequencies that can be heard with the human system range from 20 Hz up to 20000 Hz. Up to 256 Hz the frequency is considered as low, between that and up to 1000 Hz it is considered medium and anything above that is considered high [2], [4], [19], [20].

In acoustics there is what is called a pure tone. It has a sinusoidal waveform, which consists of a single frequency regardless of other properties, and is the most elemental of all the tones. An equation showing such behavior can be seen on Equation 3.2.

$$x(t) = x_0 * \sin(\omega * \mathrm{t} + \phi) \tag{3.2}$$

In this Equation *x* represents the distance of which the body finds itself from it´s equilibrium position, x_0 is the wave´s amplitude, ω is the angular frequency, *t* is the time in seconds and ϕ is the initial phase angle.

A complex tone is composed of two or more pure tones and is what is more commonly found in nature. Each frequency that constitutes such tone is called a partial frequency. The first partial frequency is what is called the fundamental sound. If a partial´s frequency is a multiple of the fundamental, then it is called harmonic, and if it isn´t, it is called non-harmonic. If the tone is composed only by harmonics, then it is called periodic, and if it has any non-harmonics, it is aperiodic [2], [4].

3.2.2 Pitch

The pitch refers to how the human ear can capitate the fundamental frequency of a sound. A low frequency sound is understood as a low sound, while a high frequency sound is understood as a high sound. The pitch of a sound can be measured, as can be seen in Equation 3.3 [20].

$$m = 1127{,}01048 * log_e(1 + \frac{f}{700}) \tag{3.3}$$

Where *m* represents the pitch. It´s unit is called “mel”. Isolating the frequency on Equation 3.3 it can be read as seen in Equation 3.4.

$$f = 700 * (e^{\frac{m}{1127{,}01048}} - 1) \tag{3.4}$$

Figure 3.1 brings a graphical study of Equation 3.4.

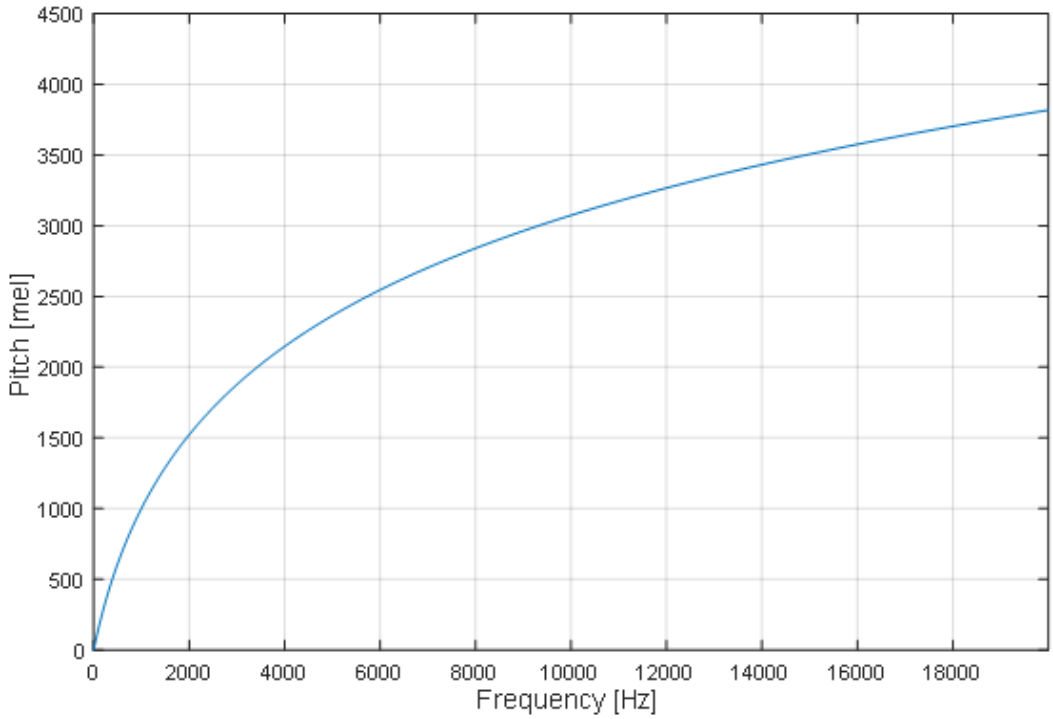

Figure 3.1 - Pitch and frequency relation.

3.2.3 Timbre

Timbre is the responsible property for the determination of the type of sound production, like choir voices, or musical instruments. When two different sounds have the same pitch and loudness, they can be told apart because of the timbre, which dictates where each come from [21].

3.2.4 Sound Wave speed

The speed of sound is affected by what mean it propagates. The physical properties of such mean can have several levels of impact on such speed. The relation between the resulting speed and the properties can be seen on Equation 3.5 [20].

$$v = \sqrt{\frac{k}{\rho}} \tag{3.5}$$

Where k represents a constant that is determined by different materials and concerns it´s elastical properties, and ρ is the density of such material. When it comes to gases and liquids, the k constant is the volumetric module of elasticity, commonly referenced by B (*bulk modulus*). Equation 3.6 brings more information about the modulus.

$$k \dashrightarrow B = -\Delta p * \frac{V}{\Delta V} = -\Delta p * \frac{\rho}{\Delta \rho} \tag{3.6}$$

In Equation 3.6 Δp represents the applied pressure to the gas, V the initial volume and ΔV the variation of the volume brought forth by the pressure. The volumetric module of elasticity is a measure of the elastic properties of the mean. Figure 3.2 brings a graphical representation of the phenomenon [4], [22].

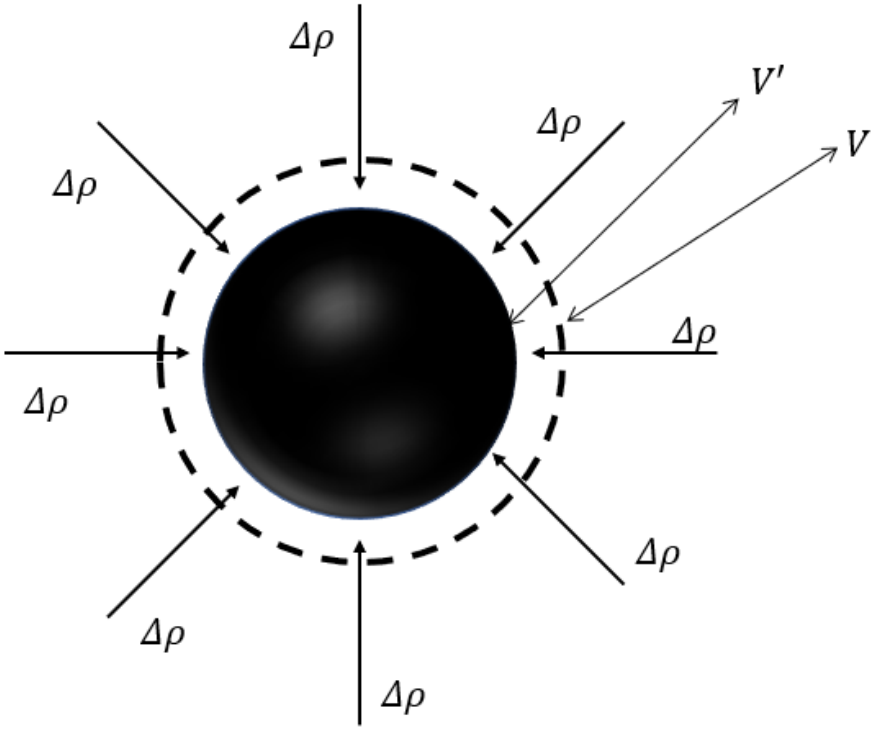

Figure 3.2 - Representation of the volumetric module [4], [22].

3.2.5 Sound power and Sound power level

Sound power is the given name for the amount of energy emitted by a source, in a given set of time. It´s unit of measure is Watts. The sound power level can be calculated through Equation 3.7 [4], [21].

$$L_w = 10 * log\left(\frac{W}{W_0}\right) \tag{3.7}$$

Sound power level is measured in dB, and the term W_0 found in Equation 3.7 is equivalent to $10^{-12}\,W$. Unlike other sound properties, the sound power doesn´t vary depending on the environment or how far the source is found, given it represents the energy emitted by the source. Table 3.1 brings some practical values for this property.

Table 3.1 – Sound power level from several sources.

Source	***Sound Power [W]***	***Sound Power Level [dB]***
Saturn V Rocket	10^8	200
Turbo Jet Plane Engine	10^5	170
Jet Plane Take-off	10^3	160
Turbo Propeller at Take-off	10^2	140
Large Pipe Organ	10	130
Small aircraft Engine	1	120
Chain Saw	10^{-1}	110
Propeller Plane	10^{-2}	100
Lawn Mover	10^{-3}	90
Dishwasher	10^{-4}	80
Vacuum Cleaner	10^{-5}	70
Noisy Home	10^{-6}	60
Average Home	10^{-7}	50
Low Voice	10^{-8}	40
Quiet Conversation	10^{-9}	30
Whisper	10^{-10}	20
Human Breath	10^{-11}	10

3.2.6 Sound Intensity and Sound Intensity Level

Sound intensity is the sound property that measures the power being carried by sound waves in a given area. It is represented as *I* and it´s unit is W/m^2. Same as with the sound power, a sound intensity level can be measured through Equation 3.8 [20].

$$L_I = 10 * log\left(\frac{I}{I_0}\right) \tag{3.8}$$

Where L_I is the intensity level, measured in dB, and the term I_0 is equivalent to $10^{-12}\ W/m^2$.

3.2.7 Sound Pressure and Sound pressure level

When a sound wave propagates itself through a space, such space undergoes a change on its original pressure. The human ear is able to capitate the range between $20\ \mu Pa$ ($0\ dB\ SPL$) up to $20\ Pa$ ($120\ dB\ SPL$) [20], [21].

The sound pressure level is the measurement of the pressure that is applied due to the sound source, on a given space. It´s formulation can be seen on Equation 3.9.

$$L_p = 20 * log\left(\frac{p}{p_0}\right) \tag{3.9}$$

Through experimentation, Fletcher and Munson were able to come up with a correlation between the frequency and the sound pressure level. To do so, they used several people in the age range of eighteen to twenty-five years with normal hearing. The result can be seen on Figure 3.3 [4], [24].

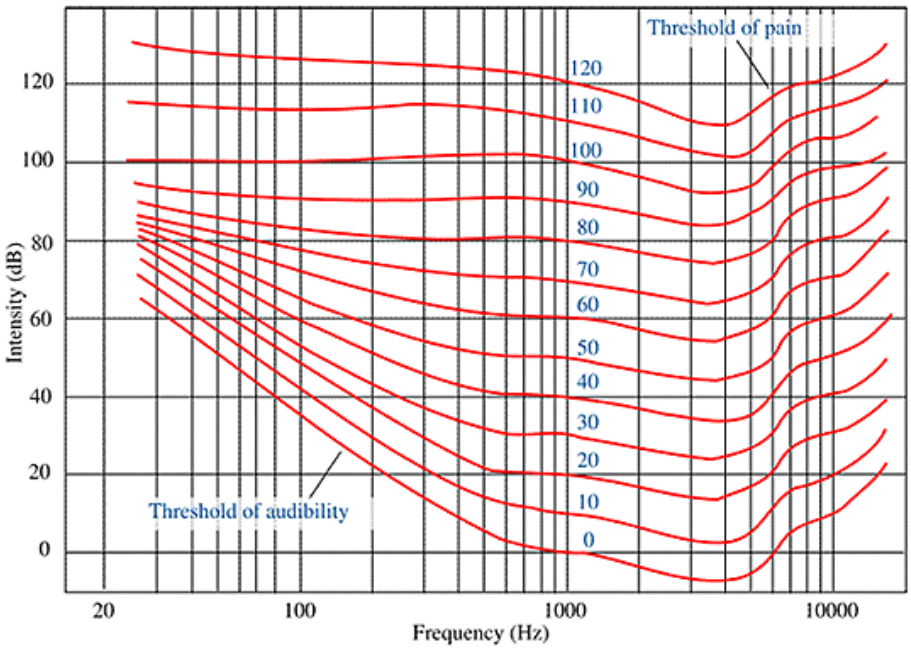

Figure 3.3 - Fletcher diagram [25].

Figure 3.4 brings a graph demonstrating the hearing area for the common human ear and some practical examples that fit in such area.

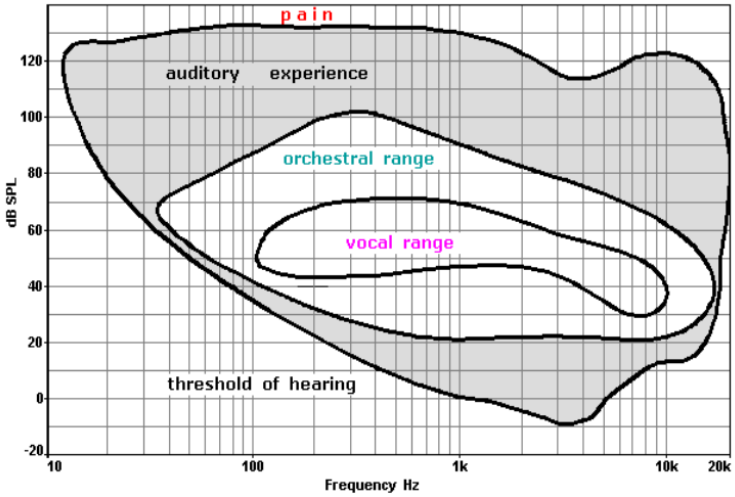

Figure 3.4 - Human hearing boundaries [26].

3.2.8 Acoustic Impedance

Any acoustic system that has the possibility of being converted on analog mechanical systems can be represented as electrical circuits, where the fluid movement is equal to the electrical current and the pressure variation is the equivalent tension in that set part of the circuit. Equation 3.10 brings the acoustic impedance formulation [4], [20], [21].

$$Z = \frac{p}{U} \tag{3.10}$$

Where Z is the acoustic impedance, p is the acoustic pressure on the surface and U is the volumetric velocity on surface. The unit used for the acoustic impedance is $Pa.s/m^3$.

3.2.9 Specific Acoustic Impedance

The specific acoustic impedance is the ratio between acoustic pressure and the particles speed. Equation 3.11 demonstrates such relation, and Equation 3.12 brings the specific acoustic impedance for flat waves.

$$z = \frac{p}{v} \tag{3.11}$$

$$z = \pm \rho c \tag{3.12}$$

The unit of measurement of the acoustic impedance is $Pa.s/m$. Even though the acoustic impedance is a real quantity for progressive flat waves, the same cannot be said for plane or divergent waves. Then, z will usually of complex nature and will be in the form given in Equation 3.13.

$$z = r + jx \tag{3.13}$$

Where r represents the specific acoustic resistance and x represents the specific acoustic resistance of the mean [19], [20].

4 DYNAMICS

4.1 Introduction

There are three main area of study in mechanics: static, cinematic and dynamics.

Static is the field of study which focus the results of the application of forces, along with the boundary conditions for material bodies. It is restricted to cases where such bodies are in equilibrium, therefore have to acceleration.

Cinematic is the area that studies the laws for movement of bodies. By following this area, it is possible to establish for any unique moment the position, speed and acceleration of a body, from a previously appointed referential.

Dynamics is the area that determines the relation between the body movement with the cause for it to happen. The main difference between dynamics and cinematic is the fact that dynamics take inertia into consideration. As result, it is able to predict movement caused by single actions, or determine what action was responsible for a unique movement.

Inside such studies, vibration appears. Vibrating systems are found throughout every day's routine and can have several impacts and results. Using a toothbrush for dental hygiene is achieved through vibrating it. Musical instruments make use of it to produce melodies. It can have unwanted and negative effects such as sound pollution caused by a chainsaw.

It is a key part in most engineering projects. Failing to properly acknowledge it´s effects can lead to a structure entering resonance, which can have fatal effects. Not necessarily so dire, it can also have minor effects, where if not taken into account can undermine a machine´s effectiveness [4], [27], [28].

4.2 Vibrating system

A vibrating system is one that possesses an alternating movement as referenced by a unique position. Generally speaking, it has three main components: an object with the capability to hold potential energy, which is the elastic element. A component that can hold kinetic energy, which is the mass or the inertia of the system. And one object to dissipate the energy, which is the damper. The vibratory movement of a system consists into constantly transforming potential energy into kinetic energy, and vice-versa. If there is a damper, either the system must be fueled somehow to continue it´s movement, or the dissipated energy will occasionally make the system no longer be able to continue to go on [27].

The three components are related to displacement, velocity and acceleration.

4.2.1 Spring element

The spring is related to the displacement. It´s mass is usually disregarded. When a force F_k is applied in an extremity, it must be balanced by another force of same intensity but opposing direction on the other extremity. The application of the force F_k causes a differential displacement on the spring, δ, which is equal to the difference between the extremities' displacements. Equations 4.1,4.2 and 4.3 demonstrate this [28].

$$F_k = k * \delta \tag{4.1}$$

$$\delta = x_2 - x_1 \tag{4.2}$$

$$F_k = k * (x_2 - x_1) \tag{4.3}$$

Where x_1 and x_2 can be better understood through Figure 4.1.

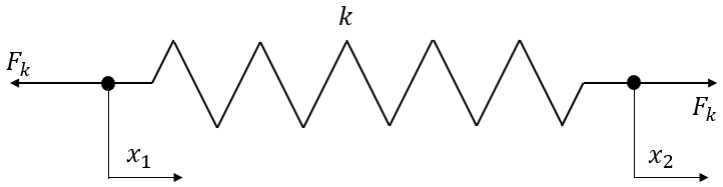

Figure 4.1 - Representation of x_1 and x_2.

And the *k* term represents the spring constant, or stiffness constant. It´s unit of measurement is N/m. The behavior pattern of Equation 4.3 is of linear nature, with *k* determining the slope of the curve. A practical graph of this behavior can be seen on Figure 4.2, where a slope equal to 1 N/m was considered.

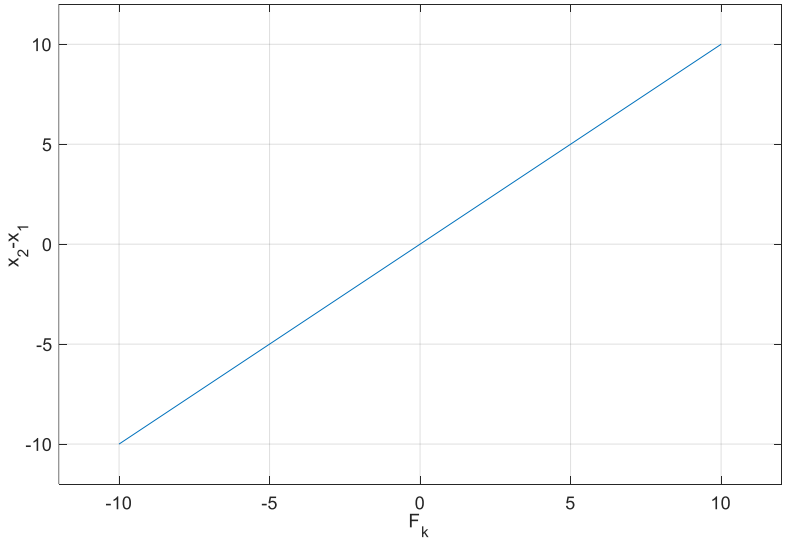

Figure 4.2 – Representation of the linear behavior for Equation 4.3.

4.2.2 Damper

The damper of a system connects the applied forces to the velocity. Like the spring element, it´s mass is generally disregarded, and due to that, the same concept applies that dictates that when a force F_c is applied in one extremity, there will be another force of same intensity but opposing direction in the other extremity. The application of such force creates a difference in velocity. Equations 4.4 demonstrates this.

$$F_c = c * (\dot{x_2} - \dot{x_1}) \tag{4.4}$$

Where $\dot{x_1}$ and $\dot{x_2}$ can be better understood through Figure 4.3.

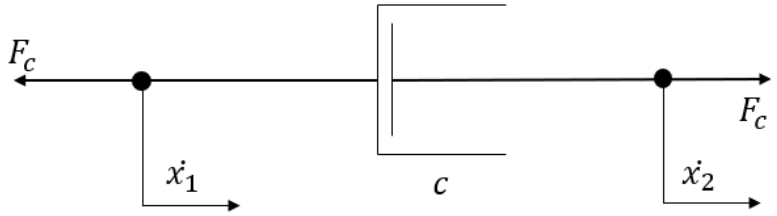

Figure 4.3 - Representation of $\dot{x_1}$ and $\dot{x_2}$.

And the term c represents the damping coefficient. It´s unit of measurement is Ns/m. The behavior pattern of Equation 4.4 is of linear nature, with c determining the slope of the curve [28]. A practical graph of this behavior can be seen on Figure 4.4, where a slope equal to 1 Ns/m was considered.

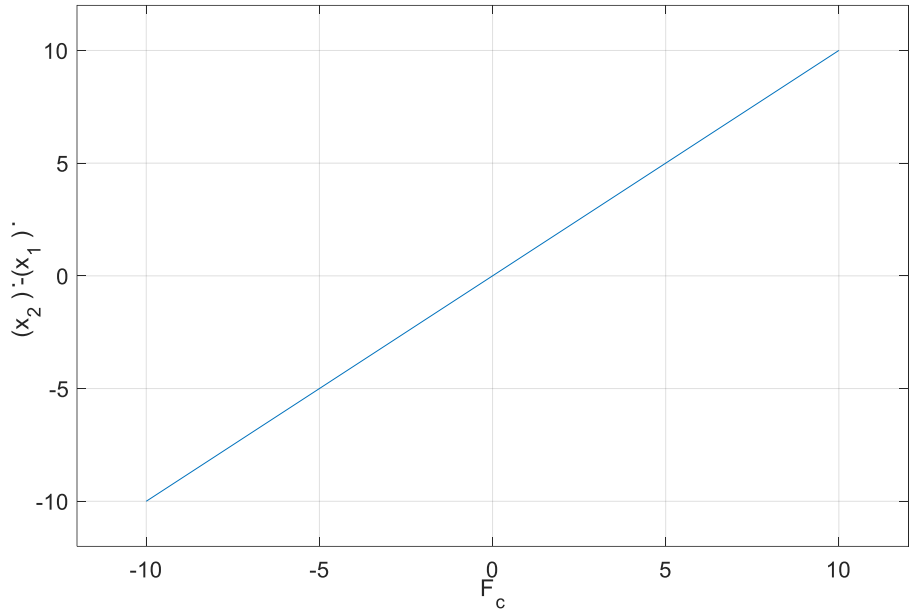

Figure 4.4 – Representation of the linear behavior for Equation 4.4.

4.2.3 Mass Element

The mass element is the one responsible for the relation between the forces and acceleration. Through Newton´s second law, Equation 4.5 is built.

$$F_m = m * \ddot{x} \tag{4.5}$$

Where F_m is the applied force, m is the mass and $\ddot{x}$ the acceleration. The mass m is the constant of proportionality, with it´s unit of measurement being kg [29].

4.3 Degree of freedom

The degree of freedom on a system is defined as the quantity of modes in which the system is able to move. It is equal to the number of displacements. While mechanical problems are usually in two or three dimensions, it is possible for it to have a higher number of degrees of freedom [28], [29].

4.4 Vibration types

Due to the different elements that may be or not on a vibrating system, there are a few possible classifications for it´s vibration. Table 4.1 brings one practical way to do so [29].

Table 4.1 – Possible classifications for a vibration.

Vibration	
Free	Forced
Damped	Undamped
Linear	Non-Linear

4.5 System Excitation

A system can be excited by either an acting force or an imposed displacement. Such excitation can be classified according to it´s variation through time. When it is known at any point in time, such as a sine function, it is named deterministic. When it is of random nature, such as the force from the wind, it´s response can only be predicted through statistical parameters. Figure 4.5 brings a graphical comparison between a deterministic excitation and a random one [29].

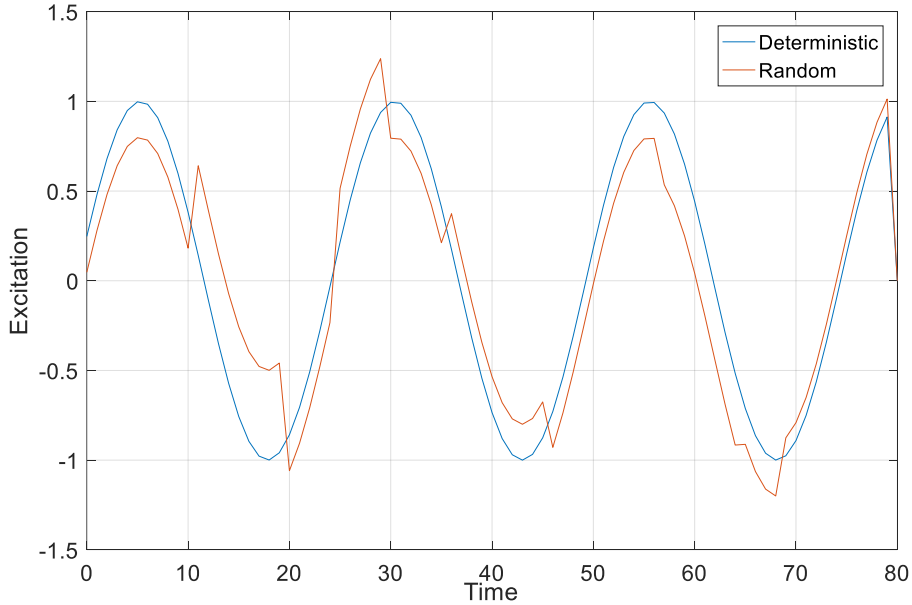

Figure 4.5 – Representation of the difference between deterministic and random excitation.

Figure 4.6 brings a flow chart for a deeper understanding of the formerly explained classifications for vibration types involving the concept of both deterministic and random excitations [29].

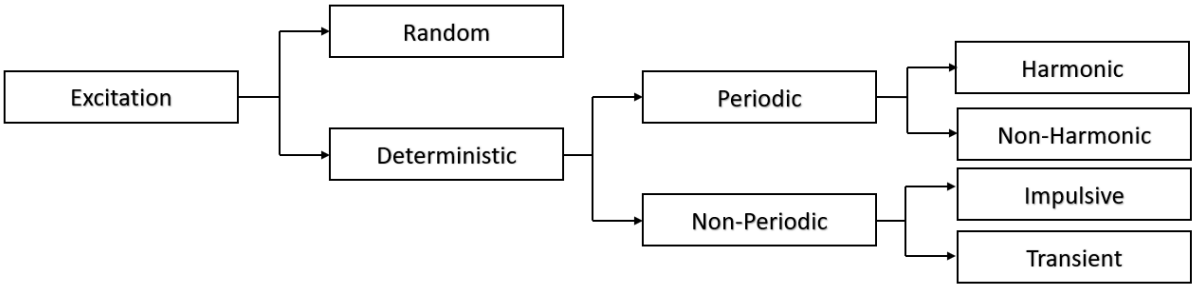

Figure 4.6 - Flow chart for excitation classification.

4.6 Dynamic system with several degrees of freedom

4.6.1 General displacement equations for natural regime

When there is no external excitation on a dynamic system, it is a free system. Such a situation can be formulated through Equation 4.6 [29].

$$[m]\{\ddot{x}(t)\} + [k]\{x(t)\} = \{0\} \tag{4.6}$$

With a free system, the displacement equations are brought in an ordinary homogeneous differential system of equations. In order to solve it, it is necessary to assume that the masses $m_i\ i = 1, \dots, n$ perform a synchronous harmonic motion of frequency ω. With this, it is possible to make the substitution seen on Equation 4.7.

$$\{x(t)\} = \{u\}\cos(\omega t - \phi) \tag{4.7}$$

Where the vector $\{u\}$ brings the values for the movement´s amplitude for $x_i(t)\ i = 1, \dots, n$. Properly inserting Equation 4.7 into Equation 4.6 results in Equation 4.8.

$$\left[-\omega^2[m] + [k]\right]\{u\}\cos(\omega t - \phi) = \{0\} \tag{4.8}$$

The results achieved from Equation 4.8 must satisfy the displacement equations for every time step t where $\cos(\omega t - \phi)$ isn´t equal to zero. With this, the vector $\{u\}$ must satisfy the equation system seen on Equation 4.9. With this, the amplitudes of $\{u\}$ are verified, and Equation 4.6 is verified by $\{u\} = \{0\}$, which confirms static equilibrium for the system and the absence of vibration.

$$\left[[k] - \omega^2[m]\right] = \{0\} \tag{4.9}$$

4.6.2 Characteristic Problem

Equations' 4.9 determinant for the coefficient matrices have to be null, in order to exist non-trivial solutions for vector $\{u\}$. This is demonstrated in Equation 4.10 [29].

$$\Delta(\omega) = |[k] - \omega^2[m]| = \{0\} \tag{4.10}$$

This determinant is the characteristic determinant, and it´s solving leads to a polynomial

equation of n degrees on ω^2, which is then called the characteristic equation. The roots of such equation, $\omega_i^2\ i = 1, \dots, n$, for which the homogeneous system in Equation 4.9 admit non-null solutions for the vector $\{u\}$ are called characteristic values, and are the natural frequencies of the system. The number of the degrees of freedom is equal to the amount of natural frequencies. By introducing in the homogeneous system in Equation 4.9 these roots, it is obtained the amplitude vectors $\{u\}_i\ i = 1, \dots, n$, seen on Equation 4.11.

$$\left[[k] - \omega^2[m]\right]\{u\}_i = \{0\} \quad \text{i} = 1, \dots, \text{n} \tag{4.11}$$

Since a homogeneous system´s solution can be extrapolated through the use of a constant, meaning that if a vector $\{u\}_i\ i = 1, \dots, n$ is a solution, then so is $\alpha\{u\}_i\ i = 1, \dots, n$, given α as a constant.

4.6.3 Displacement Equations for a Forced system

A system with n degrees of freedom will form a equation system with n differential equations of second order. These equations are dependent on one another, which is why they constitute a system of n equations, of which the mass´s movement m_i has influence on the mass´s movement m_j and vice-versa. The complete formulation for this system can be seen on Equation 4.12.

$$[m]\{\ddot{x}(t)\} + [c]\{\dot{x}(t)\} + [k]\{x(t)\} = \{f(t)\} \tag{4.12}$$

Where $[m]$, $[c]$ and $[k]$ are the matrices for mass, damping and stiffness of the system, respectively [4], [28], [29].

4.6.4 Response for a harmonic excitation

For a harmonic excitation with frequency ω, Equations 4.13 brings it´s displacement equations.

$$[m]\{\ddot{x}(t)\} + [c]\{\dot{x}(t)\} + [k]\{x(t)\} = \{F\}e^{j\omega t} \tag{4.13}$$

Admitting a permanent regime, as seen in Equation 4.14, in which generally have a complex vector $\{X(\omega)\}$, and they represent the amplitude and the phase of the movement for each degree of freedom. After proper insertion of Equation 4.14, Equation 4.15 can be achieved.

$$\{x(t)\} = \{X(\omega)\}e^{j\omega t} \tag{4.14}$$

$$\left[-\omega^2[m] + j\omega[c] + [k]\right]\{X(\omega)\} = \{F\} \tag{4.15}$$

The solution for Equation 4.15 is the vector $\{X(\omega)\}$. Substituting the impedance functions $z_{rs}(\omega)\ \ r, s = 1,2, \dots, n$ as seen on Equation 4.16, Equation 4.15 can be rewritten as Equation 4.17.

$$z_{rs}(\omega) = -\omega^2 m_{rs} + \text{j}\omega c_{rs} + k_{rs} \quad r, s = 1,2, \dots, n \tag{4.16}$$

$$[Z(\omega)]\{X(\omega)\} = \{F\} \tag{4.17}$$

Where the matrix $[Z(\omega)]$ is called the impedance matrix. Through matrixial multiplication, $\{X(\omega)\}$ is isolated, as seen on Equations 4.18 and 4.19.

$$[Z(\omega)]^{-1}[Z(\omega)]\{X(\omega)\} = [Z(\omega)]^{-1}\{F\} \tag{4.18}$$

$$\{X(\omega)\} = [Z(\omega)]^{-1}\{F\} \tag{4.19}$$

When the system is undamped, the determinant of the $[Z(\omega)]$ is equal to zero for frequencies equal to the natural frequencies of the system. Through this, when these frequencies are equivalent, the amplitude values for $X_i(\omega) i = 1, \dots, n$ converge to infinite. The regular values for the vector $\{X(\omega)\}$ are generally complex numbers, whose module represents the amplitude and the argument represents the difference between the excitation and the response [4], [28], [29].

4.6.5 Damped Forced regime

4.6.5.1 Normalization of modal vectors

As previously mentioned, modal vectors are defined as less than a constant. It will now be explained the procedure in order to normalize them can transform a modal vector on a unique modal vector without changing it´s natural form. For the normalization of modal vectors for unitary modal masses, it consists on the normalization of the modal vectors so it satisfies the condition expressed on Equation 4.20.

$$\{\phi\}_i^T[m]\{\phi\}_i = 1 \qquad i = 1, \dots, n \tag{4.20}$$

Where $\{\phi\}_i \; i = 1, \dots, n$ are the normalized modal vectors for unitary modal masses. With the normalization, the relation displayed on Equation 4.21 is valid. To obtain the values of $\{\phi\}_i \; i = 1, \dots, n$ it is made use of Equation 4.22, and with that it is possible to construct the modal matrix $[\phi]$ seen on Equation 4.23 [4], [29].

$$\{\phi\}_i^T[k]\{\phi\}_i = \omega_i^2 \qquad i = 1, \dots, n \tag{4.21}$$

$$\{\phi\}_i = \frac{1}{\sqrt{\{u\}_i^T[m]\{u\}_i}}\{u\}_i \tag{4.22}$$

$$[\phi] = [\{\phi\}_1 \quad \{\phi\}_2 \quad \cdots \quad \{\phi\}_n] \tag{4.23}$$

4.6.5.2 Modal coordinates

In order to properly solve a system of differential equations of displacement, it is used a coordinates transformation such as Equation 4.24.

$$\{x(t)\} = [\phi]\{\eta(t)\} \tag{4.24}$$

Since the matrix $[\phi]$ is time dependent, it can be derived twice, achieving the forms seen in

Equation 4.25 and Equation 4.26, and then introducing both in the displacement equation, achieving Equation 4.27.

$$\{\dot{x}(t)\} = [\phi]\{\dot{\eta}(t)\} \tag{4.25}$$

$$\{\ddot{x}(t)\} = [\phi]\{\ddot{\eta}(t)\} \tag{4.26}$$

$$[\phi]^T[m][\phi]\{\ddot{\eta}(t)\} + [\phi]^T[c][\phi]\{\dot{\eta}(t)\} + [\phi]^T[k][\phi]\{\eta(t)\} = [\phi]^T\{f(t)\} \tag{4.27}$$

Considering the properties of orthogonality seen on Equation 4.28 and 4.29, and substituting these on Equation 4.27, it is possible to write Equation 4.30.

$$[\phi]^T[m][\phi] = [I] \tag{4.28}$$

$$[\phi]^T[k][\phi] = [\Omega^2] \tag{4.29}$$

$$[I]\{\ddot{\eta}(t)\} + [\phi]^T[c][\phi]\{\dot{\eta}(t)\} + [\Omega^2]\{\eta(t)\} = \{N(t)\} \tag{4.30}$$

In which $[I]$ and $[\Omega^2]$ represent the identity matrix and a diagonal matrix with terms equal to the square of the natural frequencies, respectively. The differential equation is uncoupled in terms of inertia and stiffness, but it might not be in terms of damping [4], [29].

4.6.5.3 Proportional damping

Taking into consideration a damping matrix $[c]$, achieved from a linear combination of the mass matrix and the stiffness matrix, as seen on Equation 4.31, has a modal base projection seen on Equations 4.32 through 4.35.

$$[c] = \alpha[m] + \beta[k] \tag{4.31}$$

$$[\phi]^T[c][\phi] = \alpha[\phi]^T[m][\phi] + \beta[\phi]^T[k][\phi] \tag{4.32}$$

$$[\phi]^T[c][\phi] = \alpha[I] + \beta[\Omega^2] \tag{4.33}$$

$$[\phi]^T[c][\phi] = [\alpha + \beta\Omega^2] \tag{4.34}$$

$$[\phi]^T[c][\phi] = [2\xi\Omega] \tag{4.35}$$

Which is a diagonal matrix, making it so that the equations of displacement on the modal base are independent equations [4], [29].

4.6.5.4 Modal equations

The modal base equations of displacement for a proportional damping matrix are a set of independent differential equations, with each one of them equivalent to a displacement equation of a system with a single degree of freedom, as seen on Equation 4.36.

$$\ddot{\eta}_i(t) + 2\xi_i\omega_i\dot{\eta}(t) + \omega_i^2\eta(t) = N_i(t) \quad i = 1, \dots, n \tag{4.36}$$

4.6.5.5 Response on modal base

Each equation can be either solved analytically or numerically, according to the system´s excitation. For this, it must be used Duhamel´s integer, seen on Equation 4.37.

$$\ddot{\eta}_i(t) = \frac{1}{\omega_{d_i}} \int_0^t N_i(\tau) e^{-\xi_i \omega_i (t-\tau)} sin\omega_{d_i}(t-\tau) d\tau$$
$$+e^{\xi_i \omega_i t}\left(\frac{\eta_i(0)}{\sqrt{1-\xi^2}}\cos\left(\omega_{d_i} t - \phi_i\right) + \frac{\eta_\iota\ddot{(0)}}{\omega_i} sin\omega_{d_i} t\right) \quad i = 1, \dots, n \tag{4.37}$$

Where the values for ω_{d_i} and ϕ_i can be seen on Equation 4.38 and Equation 4.39 [4], [29].

$$\omega_{d_i} = \omega_i \sqrt{1-\xi_i^2} \tag{4.38}$$

$$\phi_i = tan^{-1} \frac{\xi_i}{\sqrt{1-\xi_i^2}} \tag{4.39}$$

4.6.5.6 Response on modal base

In possession of the response on modal coordinates $\eta_i(t)\ \ i = 1, \dots, n$, it is made needed to calculate the answers on generalized coordinates $x_i(t)$. The change of coordinates is done through Equation 4.40.

$$\{x(t)\} = [\phi]\{\eta(t)\} = \sum_{i=1}^{n} \{\phi_i\}\eta_i(t) \tag{4.40}$$

For a damped system of which the damping matrix is proportional, the displacement can be read as a superposition of the natural forms of vibration from the undamped system multiplied by the damped responses in modal coordinates [4], [29].

4.6.5.7 Vibration classification

There are a few ways to properly classify a vibration. It can be done by it´s displacement, speed, acceleration or with a decibels grade. These classifications can be seen below, where Equation 4.41 brings displacement, Equation 4.42 brings speed and Equation 4.43 brings acceleration.

$$N_{displacement} = 20 * \log\left(\frac{X}{X_{ref}}\right) \qquad X_{ref} = 10^{-12}[m] \tag{4.41}$$

$$N_{speed} = 20 * log\left(\frac{V}{V_{ref}}\right) \qquad V_{ref} = 10^{-9}[m/s] \tag{4.42}$$

$$N_{acceleration} = 20 * log\left(\frac{A}{A_{ref}}\right) \qquad A_{ref} = 10^{-6}[m/s^2] \tag{4.43}$$

The reference values seen can be found in norm to ISO R1683 [4], [29], [30].

5 FINITE ELEMENT METHOD

5.1 Introduction

The first contributions from mathematicians, physicists and engineers towards the Finite Element Method date back to the twenty-century. Ever since, the method has been improved and consolidated as a calculus tool, to project and analyze mechanical structures on continuum mechanics. However, FEM (Finite Element Method) is not limited to this area of application, given that it is capable of producing practical results in the areas of heat transfer, some specific cases for fluid mechanics, diffusion problems, studying electromagnetic potentials, among others [31].

The basic concept behind FEM is the generation of a generic problem of continuum mechanics through the analysis of the discrete parts for which it is then possible to know or obtain a mathematical description of it´s behavior, which has as consequence the possibility of making it so that even the more complex, possibly without a real analytical solution problems can be solved through a structured and sequential resolution originally applied to simpler problems that have analytical solutions.

The structural analysis of the parts is called discretization, where a domain previously considered infinite becomes considered to be finite and, on the possession of a finite number of points (or nodes), it becomes possible to solve an array of problems through simplified formulations and boundary conditions previously established.

One of the first applications of the finite element method was the determination of complex states of tension and deformation on engineering components submitted to several mechanical loads. The method is also necessary for the projecting of a building´s structure, for example.

It is important to note that the finite element method is an approximation method, therefore, should mostly be applied where there is no analytical solution for the problem. When putting it into a practical application, it´s error´s magnitudes should be previously studied and further considered.

For the development of the finite element method, it was necessary to develop technology and the calculus capacity through digital means. Figure 5.1 brings Moore´s Law, showing the evolution of transistors in a computer processor over time.

In current days, several softwares make use of the finite element method, among them: MATLAB, ANSYS and ABAQUS. The latter was the chosen one to properly run the simulations on this work, as will be seen in following sections [33], [34].

Generally speaking, when applying the finite element method, there is a set procedure to be followed. Starting from the general problem, a standard algorithm can be built through the steps seen on the flowchart on Figure 5.2.

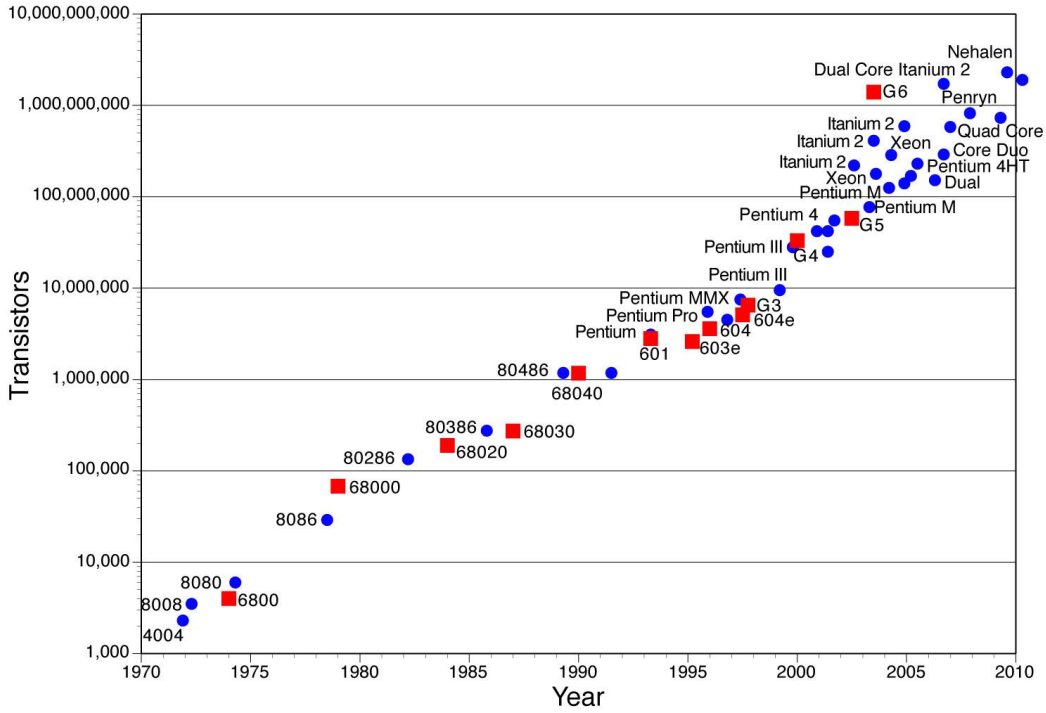

Figure 5.1 - Moore´s Law [32].

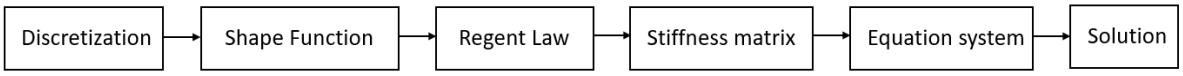

Figure 5.2 – Standard FEM algorithm.

The discretization step refers to the building of the mesh to be used, as well as the choice of which kind of elements will be part of it. The element´s number of dimensions is equal to the mesh´s, meaning that a two-dimensional mesh will have elements like triangles and rectangles, while a three-dimensional mesh will have elements like tetrahedron. The choice of function is done under observation of which function follows the physical behavior of each element.

The regent law can be, for example, Hooke´s Law, which determines the tension-deformation relation. Then, the stiffness matrix is built, better explained in the next sections. With that, the equation system can be arranged, with the boundary conditions properly included.

With that, it becomes possible to solve the system and determine the displacements and deformations.

5.2 Basic concepts

A plain stress can be treated and analyzed through the finite element method through a two-dimensional analysis. This state is characterized by normal stress and shear stress perpendicular to the plane being null. A schematic of the plain stress can be seen on Figure 5.3.

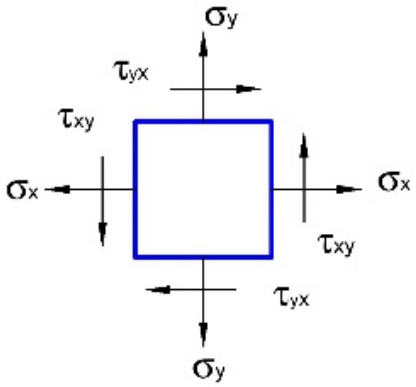

Figure 5.3 - Schematic of the plain stress [35].

With this, considering $\sigma_z = \tau_{xz} = \tau_{yz} = 0$, the tensor for the stresses can be defined as seen on Equation 5.1.

$$\{\sigma\} = \begin{Bmatrix} \sigma_x \\ \sigma_y \\ \tau_{xy} \end{Bmatrix} \tag{5.1}$$

Where σ is the normal stress and τ is the shear stress.

Figure 5.4 brings a representation of the displacements and rotations of the same element under tension state plane. The deformations can be calculated through Equation 5.2 and Equation 5.3.

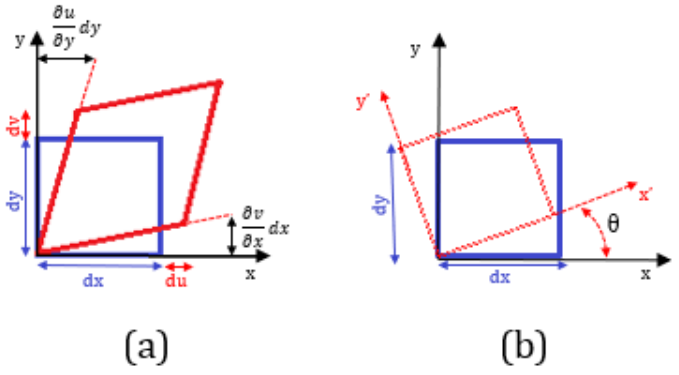

Figure 5.4 – Representation of (a) displacements and (b) rotations on a plain stress.

$$\varepsilon_x = \frac{\partial u}{\partial x} \quad \varepsilon_y = \frac{\partial v}{\partial y} \quad \gamma_{xy} = \frac{\partial u}{\partial y} + \frac{\partial v}{\partial x} \tag{5.2}$$

$$\{\varepsilon\} = \begin{Bmatrix} \varepsilon_x \\ \varepsilon_y \\ \gamma_{xy} \end{Bmatrix} \tag{5.3}$$

Where ε_x and ε_y represent parallel deformations to the xy plane, and γ_{xy} represent the variation of the element´s angle [33].

The relation between the stresses and deformations can be given through Hooke´s law, which can be seen on Equation 5.4.

$$\{\sigma\} = [D]\{\varepsilon\} \tag{5.4}$$

Where [D] represents the constitutive matrix, built solely through material properties, these being the elasticity module and Poisson´s coefficient. The construction of such matrix can be seen on Equation 5.5.

$$[D] = \frac{E}{1-\nu^2}\begin{bmatrix} 1 & \nu & 0 \\ \nu & 1 & 0 \\ 0 & 0 & \dfrac{1-\nu}{2} \end{bmatrix} \tag{5.5}$$

5.3 Discretization, Shape function and Jacobian Matrix

To properly apply the finite element method, the first step is to discretize the problem, which means to divide the problem in a set of finite elements that allow any desired calculation. A representation can be seen on Figure 5.5.

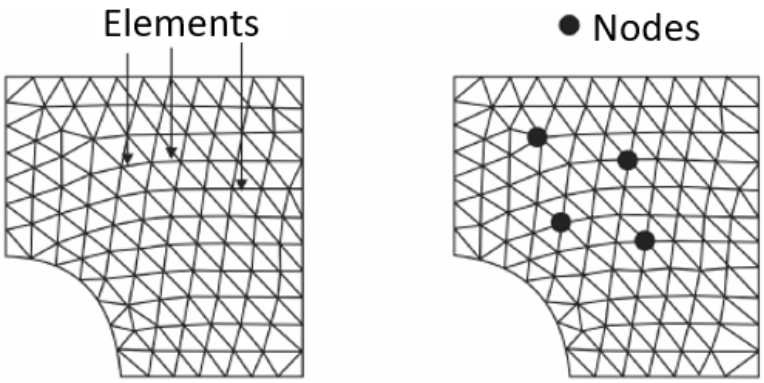

Figure 5.5 – Discretization of a body for finite element analysis [36].

Due to optimizing issues, the most common choice of elements usually resorts to triangles and quadrilateral elements for their natural simplicity. On them, nodes are inserted on the vertices, central points and midpoints on the laterals, according to how much accuracy is needed. The more accurate the result needed, the more nodes should be applied. This choice should not only take accuracy into account, but several other factors should be considered, such as computational power needed to properly calculate every node.

Once these initial choices have been made, the discretization process is done, and the mesh

of the system is created. Then, it is defined a shape function to perform the numerical procedures. For example, it can be used a isoparametric function. Such a function has the ability to perform a change of coordinates, going from global coordinates to local coordinates, simplifying the calculus. Figure 5.6 shows quadrangular elements on local coordinates, and Figure 5.7 shows a mesh on global coordinates and on local coordinates.

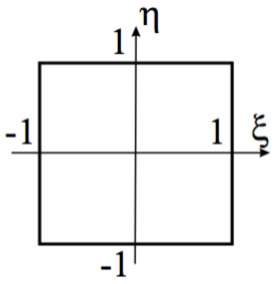

Figure 5.6 – Quadrangular element on local coordinates [37].

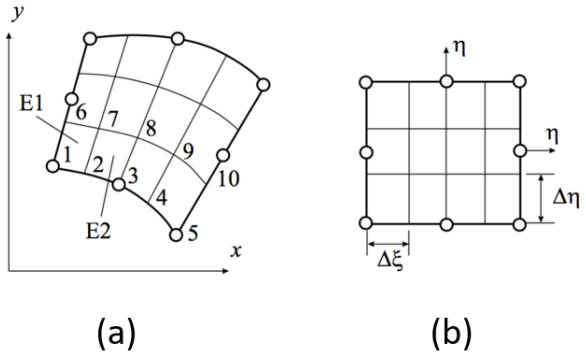

Figure 5.7 – Mesh on (a) global coordinates and (b) local coordinates [37].

With this, on coordinates ξ and η $(-1 \leq \xi, \eta \leq 1)$, the functions are defined, and it becomes possible to achieve Equations 5.6 and 5.7.

$$x = \sum N_i x_i \quad y = \sum N_i y_i \tag{5.6}$$

$$u = \sum N_i u_i \quad v = \sum N_i v_i \tag{5.7}$$

To highlight, N_i are the shape functions of each node, x and y are the points coordinates, x_i and y_i are the nodes coordinates, u and v are the points displacements and u_i and v_i are the nodes displacements. Equations 5.8 through 5.14 are used to achieve the matricidal form.

$$\{x\} = [N]\{x^e\} \tag{5.8}$$

$$\{x\} = \begin{Bmatrix} x \\ y \end{Bmatrix} \tag{5.9}$$

$$\{x^e\} = \begin{Bmatrix} x_1 \\ y_1 \\ x_2 \\ y_2 \\ \vdots \end{Bmatrix} \tag{5.10}$$

$$\{u\} = [N]\{u^e\} \tag{5.11}$$

$$\{u\} = \begin{Bmatrix} u \\ v \end{Bmatrix} \tag{5.12}$$

$$\{u^e\} = \begin{Bmatrix} u_1 \\ v_1 \\ u_2 \\ v_2 \\ \vdots \end{Bmatrix} \tag{5.13}$$

$$[N] = \begin{bmatrix} N_1 & 0 & N_2 & 0 & \cdots \\ 0 & N_1 & 0 & N_2 & \cdots \end{bmatrix} \tag{5.14}$$

In order to properly correlate these shape functions to the displacement´s deformations, it is necessary to use the deformability matrix, which can be obtained from Equations 5.15 through 5.17 [37].

$$\{\varepsilon\} = [B]\{u\} \tag{5.15}$$

$$[B] = [B_1 \quad B_2 \quad \cdots] \tag{5.16}$$

$$[B_i] = \begin{bmatrix} \dfrac{\partial N_i}{\partial x} & 0 \\ 0 & \dfrac{\partial N_i}{\partial y} \\ \dfrac{\partial N_i}{\partial y} & \dfrac{\partial N_i}{\partial x} \end{bmatrix} \tag{5.17}$$

Seeing as the used coordinates are local, it is made use of the Jacobian matrix to perform a change of variables, seen on Equations 5.18 and 5.19.

$$[J] = \begin{bmatrix} \dfrac{\partial N_1}{\partial \xi} & \dfrac{\partial N_2}{\partial \xi} & \cdots & \dfrac{\partial N_i}{\partial \xi} \\ \dfrac{\partial N_1}{\partial \eta} & \dfrac{\partial N_2}{\partial \eta} & \cdots & \dfrac{\partial N_i}{\partial \eta} \end{bmatrix} \begin{bmatrix} x_1 & y_1 \\ x_2 & y_2 \\ \vdots & \vdots \\ x_i & y_i \end{bmatrix} \tag{5.18}$$

$$\begin{bmatrix} \frac{\partial N_i}{\partial x} \\ \frac{\partial N_i}{\partial y} \end{bmatrix} = [J]^{-1} \begin{bmatrix} \frac{\partial N_i}{\partial \xi} \\ \frac{\partial N_i}{\partial \eta} \end{bmatrix} \tag{5.19}$$

With this, the Jacobian determinant can be used to perform the change of variables, seen on Equation 5.20.

$$dxdy = |J| d\xi d\eta \tag{5.20}$$

5.4 Stiffness Matrix, Numerical integration through Gauss Quadrature

The stiffness matrix has as objective to establish a relation between the applied forces on the system with the caused displacements. The matrix, named [K], when multiplied by the displacements, can determine the acting forces.

Given that the finite element method is being studied, an analysis must be made on each element individually, creating a stiffness matrix for each element. These individual matrices can be calculated through Equation 5.21.

$$[K]_e = \int_{\Omega_e} [B]_e^T [D][B]_e \, d\Omega_e \tag{5.21}$$

Where $[B]^T$ is the transposed matrix of deformability, previously seen on Equation 5.16, and [D] is the constitutive matrix, seen on Equation 5.5.

Being able to define the matrix [K], and applying the variable changes originated from the Jacobian matrix, seen on Equation 5.19 and it´s determinant, seen on Equations 5.20, it is possible to perform the calculus for the integral relation, knowing that the utilization of the obtained local coordinates simplifies the calculation.

As example, it is possible to use the Gaussian quadrature as numerical integration technique. Such quadrature makes use of pre-defined points, which´s amount can be determined depending on a number of factors, especially desired accuracy. More points will bring a more accurate results, being theoretically possible to achieve a null error. As a thumb rule, for a choice of quantity of Gaussian points, the polynomial should be of a degree equivalent to $2(n-1)$ where n is the quantity of Gaussian points. Figure 5.8 brings a demonstration of a 3x3 quadrature on an element containing 8 nodes.

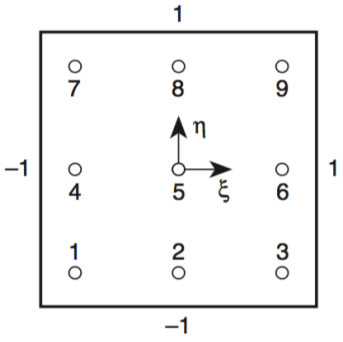

Figure 5.8 – Gaussian points for an 8-node element [38].

The applied integration on this case can be seen on Equation 5.22 [37].

$$I = \int_{-1}^{1}\int_{-1}^{1} f(\xi,\eta)d\xi d\eta = \sum_{i=1}^{n}\sum_{j=1}^{n} f(\xi_i,\eta_j)w_i w_j \tag{5.22}$$

Where f is the function that is wished to be integrated on local coordinates. ξ_i, η_j are coordinates of the Gaussian points and $w_{i,j}$ is the weigth.

Table 5.1 brings some of these values for certain specific quadratures. It is important to note that while Table 5.5 shows only up to a 3x3 quadrature, it is possible to go higher, if required.

Table 5.1 – Gaussian quadratures.

n	ξ_i ou η_j	$w_{i,j}$
1	0	2
2	$\pm\sqrt{\frac{1}{3}}$	1
3	0	$\frac{8}{9}$
	$\pm\sqrt{\frac{3}{5}}$	$\frac{5}{9}$

With this information regarding the points, it is then possible to use Equation 5.23 to determine the stiffness matrix on each element individually.

$$[K]_e = \int_{-1}^{1}\int_{-1}^{1} [B]_e^T [D][B]_e |J| d\xi d\eta = \sum_{i=1}^{n}\sum_{j=1}^{n} [B]_e^T [D][B]_e |J| w_i w_j \tag{5.23}$$

With the individual stiffness matrices properly set up, they can be used to form a global stiffness matrix, which will be used to study phenomenon occurring on the entire body, instead of in small elements. In order to build such global matrix, it is made use of Equation 5.24 [37].

$$[K]_{global} = \sum_{i=1}^{nº\ elem.} [K]_{e,i} \tag{5.24}$$

To properly apply Equation 5.24, some caution is needed. Seeing as each element of the mesh is on different locations, the nodes inside each of them are different from the nodes of the other ones, so their stiffness matrices should be summed accordingly. For example, a imaginary situation where there are only two triangular elements, the first having nodes 1, 2 and 3, and the second having the nodes 2, 3 and 4, there will be two kind of nodes. Those who do not appear on more than one element (1 and 4), and those who appear on more than one element (2 and 3). In this case, on the global stiffness matrix, nodes 1 and 4 will have equal value found in each element, however, elements 2 and 3 will be equivalent to the sum of their respective values on each element.

5.5 Boundary Conditions, Displacement, Deformations, Stresses and Reactions

With the global stiffness matrix properly set, it becomes possible to determine the displacements of which the system is submitted. A manual caution to be taken on this step must be taken, due to the fact that there is no natural way to impose the boundary conditions, so any condition existing on the system must be inserted on this step.

There are two main kinds of boundary conditions: the essential ones, defined by restrictions, which take away the possibility of movement and deformations in set directions, and the natural conditions, which are the acting forces.

To take these conditions into account, it is made use of the “penalty coefficient”. This is a mathematic artifice, in which the values on the global stiffness matrix on the restricted locations are switched for extremely high values, making it so that the displacement on these particular locations is practically zero.

With that, it is now possible to calculate the displacements through Equations 5.25 and 5.26.

$$[K]\{u\} = \{F\} \tag{5.25}$$

$$[K]^{-1}_{global,\alpha}\,\{F\}_{\alpha} = \{u\} \tag{5.26}$$

With the results from Equations 5.26 it can be determined any other information about the system. First, Equation 5.15 is applied to each integration point, and with it´s results, Equation 5.4 can be used to calculate the stresses, for each point individually. And then, to calculate the reaction values, Equation 5.27 can be used.

$$[K]_{global}\{u\} = \{R\} \tag{5.27}$$

On a final note, it is important to note that the stiffness matrix to be used on these last equations is the original stiffness matrix obtained from Equation 5.24, not the one with the modified values of the boundaries [37].

6 MECHANICAL ANALYSIS OF THE HUMAN EAR

6.1 Introduction

This chapter will have as objective the presentation and brief explanation of the predecessor project used for this work, called “The visible ear”, which was conducted in 1995 by Mads Sølvsten Sørensen, MD, *et al.* And formerly continued by students from Aalborg´s University in Denmark [39]. On it, two distinct models were used, the first consisting only on the membrane and the ossicular chain, while the second one was more complete and contained membrane, ossicles, air in the external auditory canal and the tympanic cavity. Once the geometries were properly built and set, it was applied material properties and boundary conditions.

This model was then used to simulate two models: one, which will be entitled the simple model, composed on only the membrane and the ossicles, and the second, entitled the complete model, also included air on the auditory external canal and on the tympanic cavity [4]. Based on this work, the current work takes place, in which in addition to the original model components, irregulars bodies are added to act is if there were tumor body parts. The models with the tumors are simulated on identical situations for the original models, and the results are then compared between them and previous literature.

6.2 Geometric model

The project “The Visible Ear” main goal was to virtually map out the temporal bone, and in the process create a computational simulator to better study the middle ear, which could have benefits in the area of chirurgical procedures. Through the aid of a process called “cryosectioning”, a set of high quality images was taken from the frozen temporal bone of an 85-year-old woman. Figure 6.1 brings an example one of these images [39]. These images would later be used side by side to create the model.

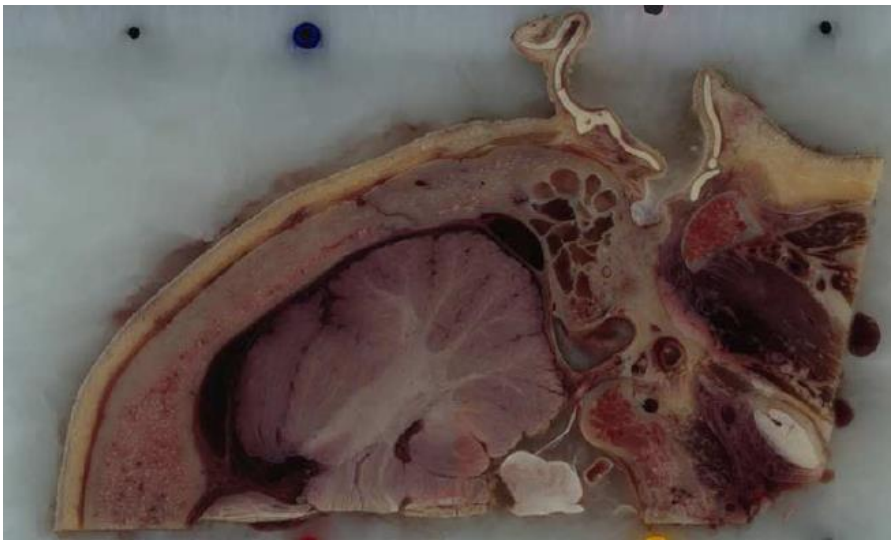

Figure 6.1 – Cross section no. 410 from the Visible Ear Project.

The cut that was made had a width of 25 μm and an image was taken every 50 μm, better described through Figure 6.2, which brings the conversion of these imagens into a volume, and Table 6.1, which brings the dimensions for the slices. In the end, there was a total of 597 images of 24 bits RGB, with a resolution of 50 μm/pixel.

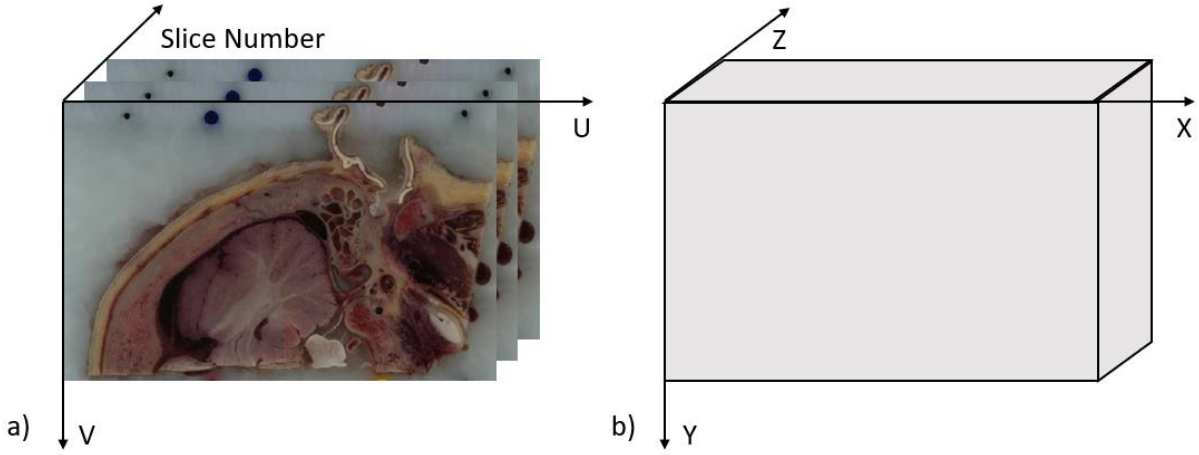

Figure 6.2 – Transition from 2D images to a volume.

Table 6.1 – Dimensions of the slices.

Slices	*X dimension*	*Y dimension*	*Z dimension*
1-70	50	50	100
70-336	50	50	50
336-597	50	50	100

With this, around twenty-six organs were successfully identified in the middle ear, through manual segmentation of each individual image, performed by Mads Sølvsten Sørensen.

Through the results obtained from the images, it was possible to properly build the geometric model for the components of the human ear. In order to actually build the model, it was made use of the software *SolidWorks*, where through detailed analysis a tridimensional solid was formed for each part of the model. As previously said, the project worked with two distinct models, the first one being a simpler model consisting only of membrane, ossicles, cochlea, stapes, tensor of the eardrum and six ligaments, while the second, more complete model, consisted of the entire first model and the addition of a component of air in the external ear canal and in the tympanic cavity, skin, jaw and auricular cartilage. Then, through the software *Abaqus* [40], utilizing the finite element method, the model was discretized and properly assembled [4].

Figure 6.3 brings a discretized view of the tympanic membrane.

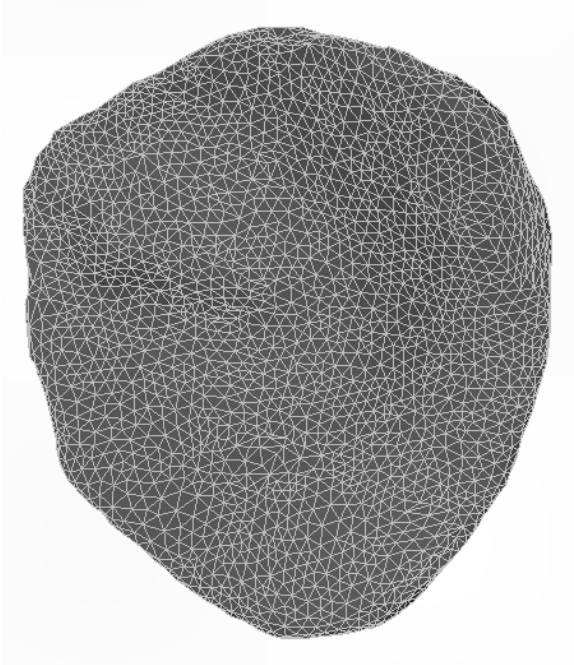

Figure 6.3 - Discretized tympanic membrane.

Table 6.2 brings a comparison of dimensions used on the geometric model to those which could be accessed on previous literature from the work of Wever & Lawrence [41].

Table 6.2 – Comparison of dimensions for the geometric model regarding the tympanic membrane.

Tympanic Membrane	*Parallel distance to the manubrium [mm]*	*Perpendicular distance to the manubrium [mm]*	*Thickness [mm]*
Model	9,45	10,22	0,2 – 0,5
Literature [41]	8,0 - 10,0	7,5 - 9,0	0,1

A quick observation about Table 6.2 is that the Thickness parameter is the parameter that is farthest from the literature range but seeing as the process used for this project is accurate, the dimensions are considered valid. In the model, the tympanic membrane consists of 5455 nodes and 19495 tetrahedral elements or type C3D4. In order to properly simulate the sulcus tympanicus, the elements that connect the membrane to the temporal bone were given a low Young´s module.

The hammer was built with 8111 elements for the head and 3722 elements for the neck, which sums up to 16222 tetrahedral elements of type C3D4. Figure 6.4 brings a view of the hammer on the software.

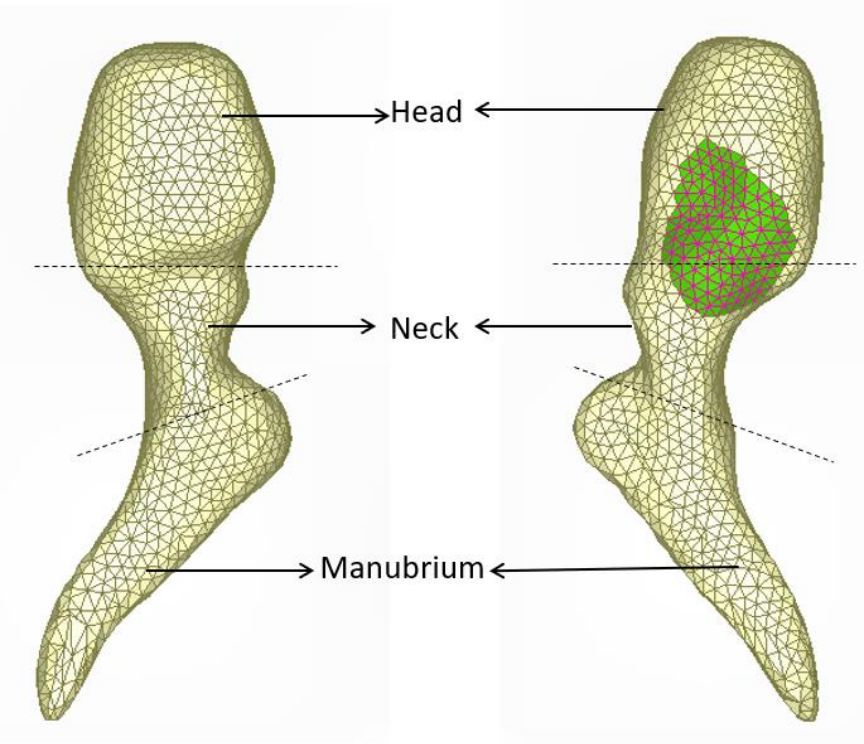

Figure 6.4 - Discretized Hammer and it´s components.

Similar to what was presented for the membrane, Table 6.3 brings a comparison of dimensions used in the model to those present on previous literature of the work from Wever & Lawrence [41].

Table 6.3 – Comparison of dimensions for the geometric model regarding the hammer.

Hammer	*Distance from Manubrium extremity to lateral apophysis [mm]*	*Mass [mg]*	*Total Length[mm]*
Model	4,89	48	8,55
Literature [41]	5,8	23 - 27	7,6 – 9,1

As observed, the mass of the model was higher than the ones found in the literature, which is a consequence from the volume of the manubrium.

The Manubrium was connected to the tympanic membrane through nodes that were adjacent to elements of both parts. The Anvil was built on 18749 tetrahedral elements of type C3D4, containing 3966 nodes. It´s body has 11874 elements. Figure 6.5 brings a view of the anvil.

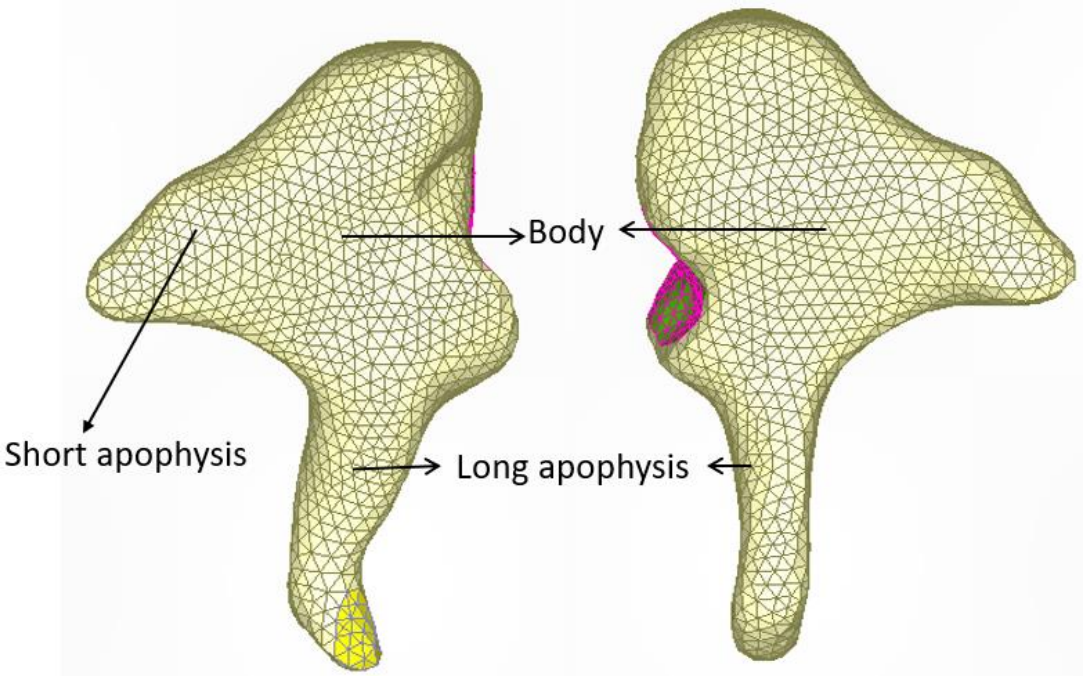

Figure 6.5 - Discretized Anvil and it´s components.

Following the same procedure, Table 6.4 brings a comparison of dimensions used in the model to those present on previous literature of the work from Wever & Lawrence [41].

Table 6.4 – Comparison of dimensions for the geometric model regarding the anvil.

Anvil	*Parallel length to the short apophysis [mm]*	*Parallel length to the long apophysis [mm]*	*Mass [mg]*
Model	4,95	7,26	47,7
Literature [41]	5,0	7,0	25 - 32

The connection between the hammer and the anvil is made up with 988 tetrahedrical elements of type C3D4 consisting on 336 nodes, and it was assumed to have elastic behavior.

The stirrup was built on 17692 elements of type C3D4 consisting on 3995 nodes. Figure 6.6 brings a visualization of it.

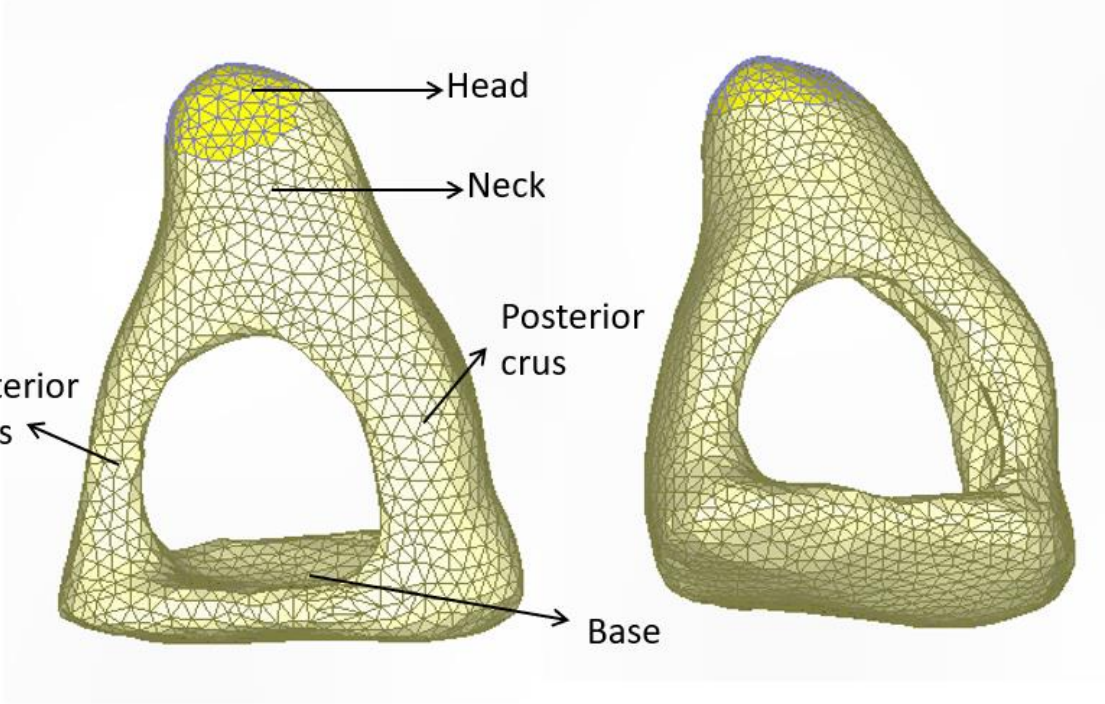

Figure 6.6 - Discretized Stirrup and it´s components.

Once more, Table 6.5 brings a comparison of dimensions from the model and the ones found on the work from Wever & Lawrence [41].

Table 6.5 – Comparison of dimensions for the geometric model regarding the stirrup.

Stirrup	*Height [mm]*	*Base´s length [mm]*	*Base´s width [mm]*	*Mass [mg]*
Model	3,82	3,09	1,92	10,2
Literature [41]	2,5 – 4,0	2,64 – 3,36	0,7 – 1,66	2,05 – 4,35

The connection between the anvil and the stirrup is made up with 1057 tetrahedral elements of type C3D4 consisting on 320 nodes, and it was assumed to have elastic behavior.

The three hammer´s ligaments and the anvil´s two were simulated with beam elements of type T3D2 consisting of two nodes each. For the stapedial muscle and the tympanic tensor muscle, linear elements of type T3D2 were used, consisting on two nodes. Figure 6.7 brings a clearer representation of these ligaments.

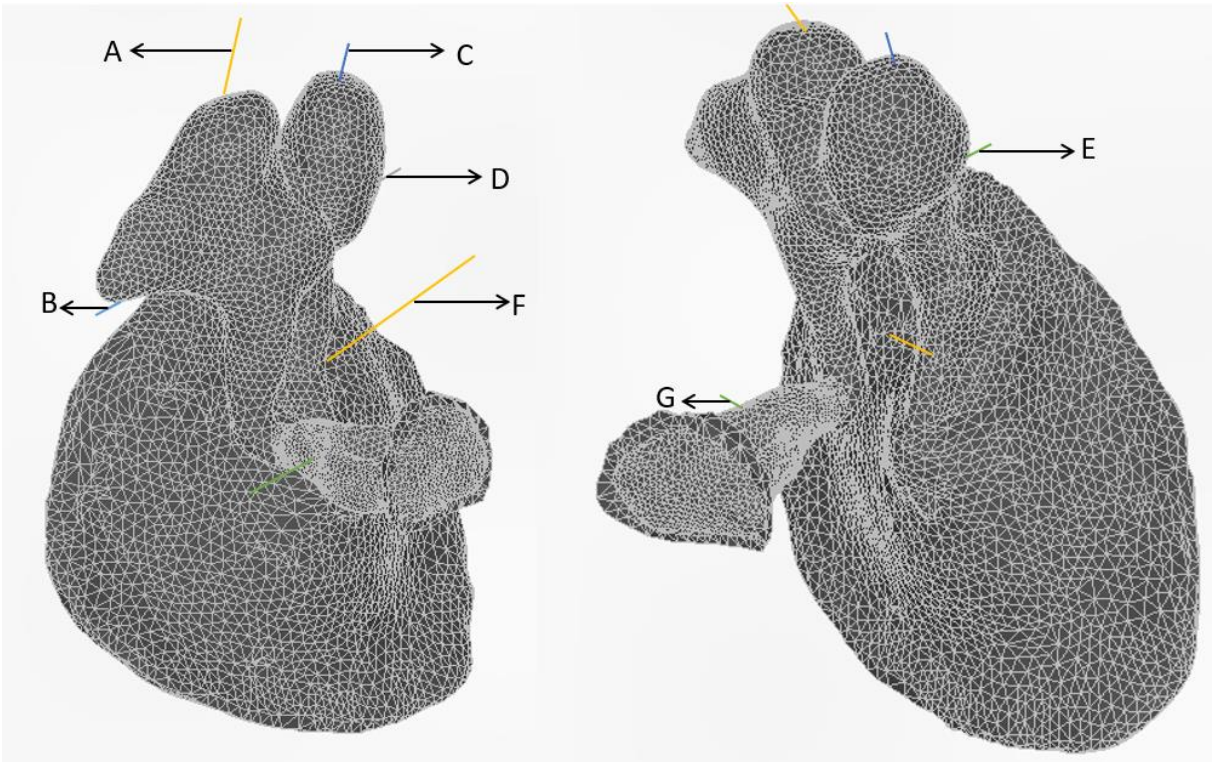

Figure 6.7 - Representation of anvil´s ligaments (A,B), hammer´s ligaments (C,D,E), tympanic tensor muscle (F) and stapedial muscle (G).

The annular ligament was built on 641 elements consisting of 314 nodes, of type C3D4. It connects the stirrup to the bone part of the model, and it can be seen on Figure 6.8.

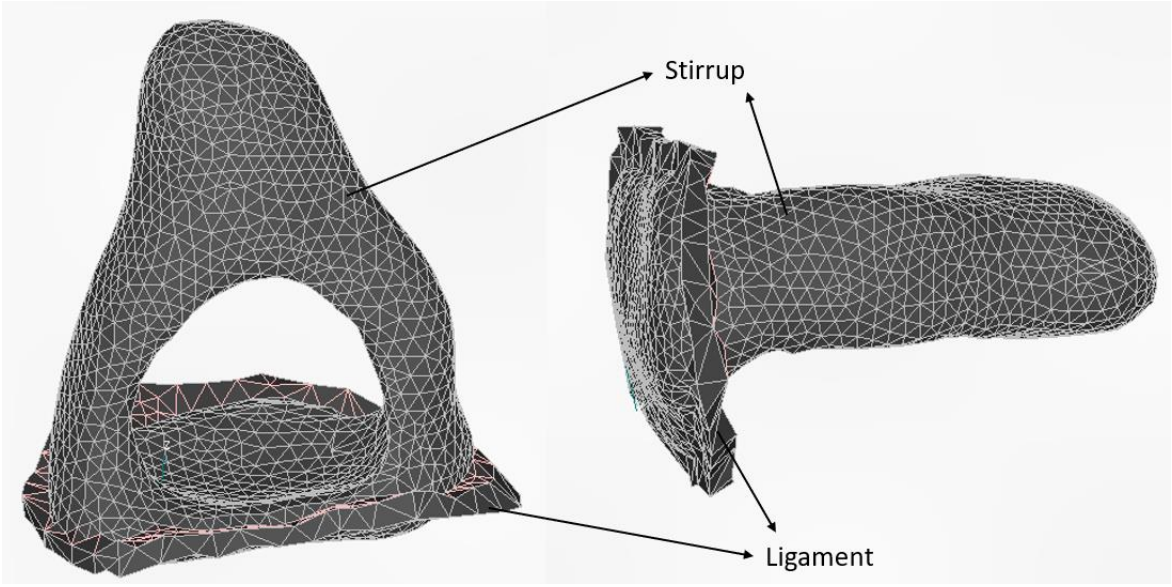

Figure 6.8 – Stirrup´s ligament to the bone.

For the cochlear fluid it were used 41292 acoustic elements of type AC3D4, inside the cochlea, as seen on Figure 6.9.

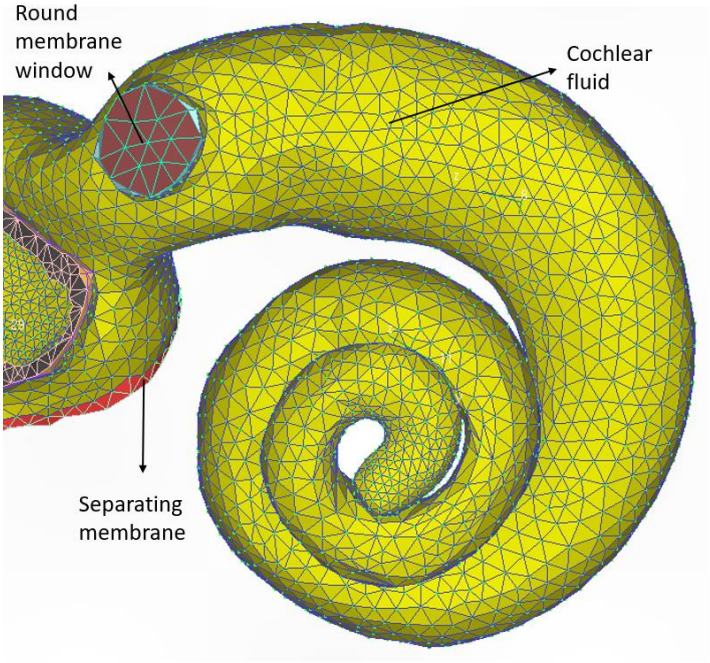

Figure 6.9 – Cochlear fluid.

The bone structure has 4999891 elements consisting of 96273 nodes, of type C3D4. Figure 6.10 brings a representation. Also in the figure, the jaw was built on 32911 C3D4 elements.

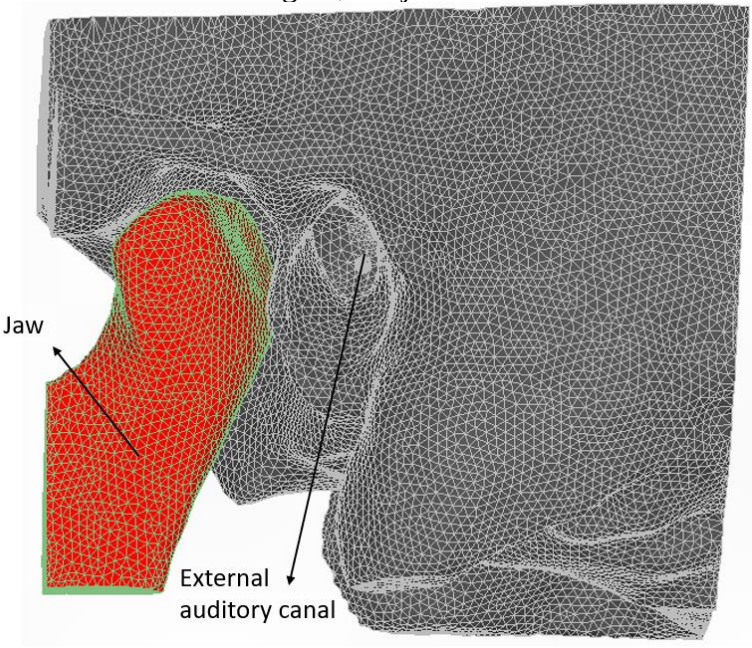

Figure 6.10 – Bone structure.

The skin part was built on 518248 elements of type C3D4, consisting on 107461 nodes. The auricular cartilage has 56310 elements consisting on 15229 nodes, of type C3D4. Both can be seen on Figure 6.11.

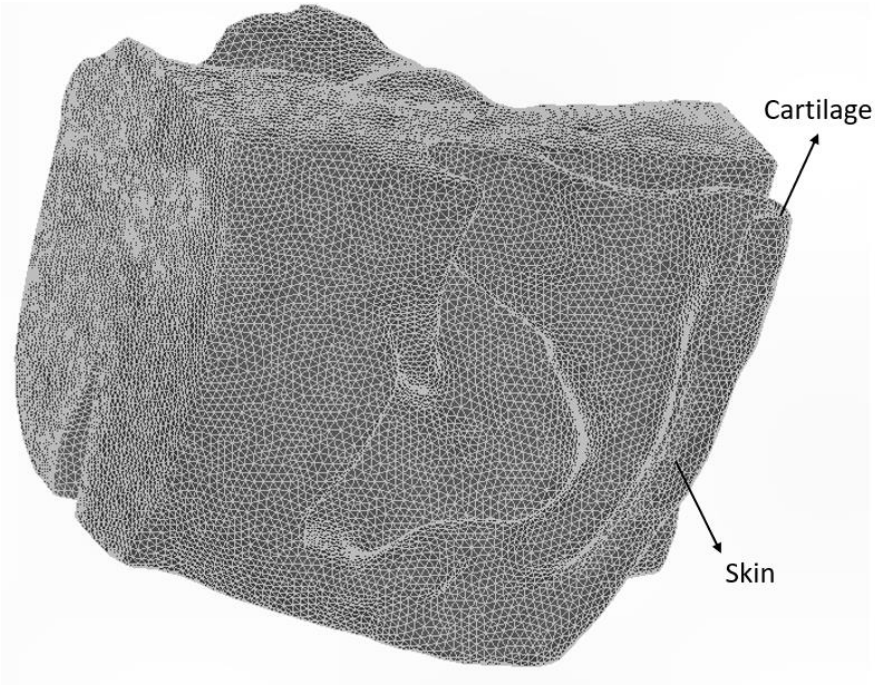

Figure 6.11 – Skin and auricular cartilage.

Figure 6.12 brings a representation of the air in the external auditory canal, which was built on 127875 elements consisting on 25932 nodes and of type AC3D4, and in the tympanic cavity, built on 83230 AC3D4 elements with 17664 nodes.

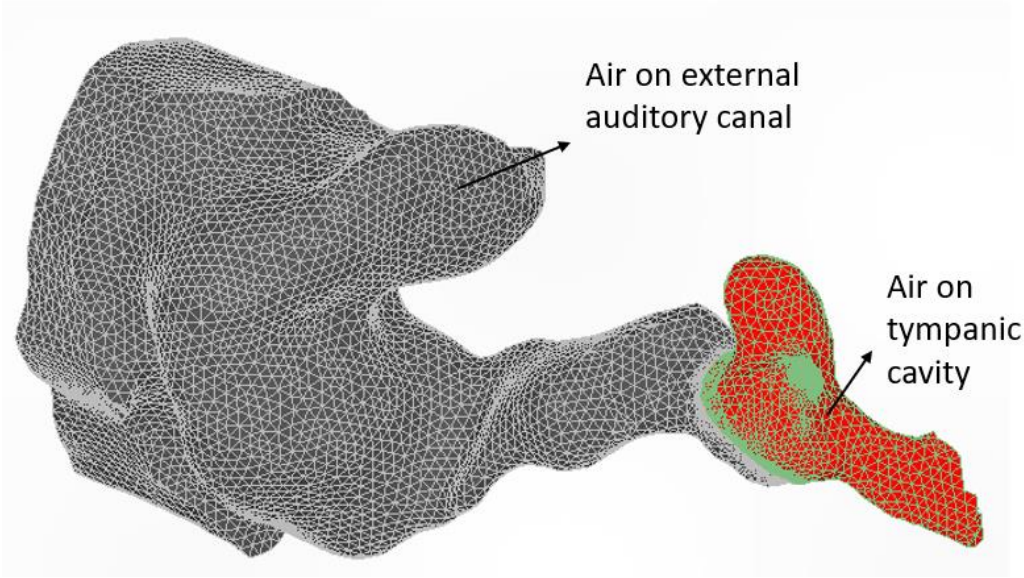

Figure 6.12 – Air on external auditory canal and on the tympanic cavity.

As seen on Table 6.6, the air on the external auditive canal has a volume of 1642,96 mm^3 and the air on the tympanic cavity has 398 mm^3. However, the air in the external auditory canal it were added acoustic elements on the outside of the ear, so it would be included sound reflections due to its anatomic shape, which summed up to a volume of 13650,66 mm^3.

Table 6.6 – Comparison of dimensions for the geometric model regarding air.

Air	*Volume in the external auditive canal [mm^3]*	*Volume in the tympanic cavity [mm^3]*	*Distance from the umbo and the external auditive canal [mm]*
Model	9,45	10,22	0,2 – 0,5
Literature	8,0 - 10,0 [42]	7,5 - 9,0 [43]	0,1 [42]

Figure 6.13 brings the summary of total of elements and nodes for the model.

Elements	
Type	**Quantity**
T3D2	7
AC3D4	252397
C3D4	1186243
Total	1438647

Nodes	
Total	273566

Figure 6.13 – Total count of elements and nodes in the model.

6.3 Model mechanical properties

The materials used on the construction of the model were assumed to have a linear elastic behavior, due to the assumption made that the model would be studied as a linear system. The chosen Poisson´s coefficient was generally 0,3, with the exception of the cartilage, that had a coefficient of 0,4 [44], [45]. A Young´s module of $1{,}41x10^{10}\ Pa$ was used for the ossicles and the articulations present on several components. The tympanic membrane was split on *pars tensa* and *pars flaccida*, with its properties being displayed on Table 6.7, and the membrane´s density set as $1{,}2x10^3\ kg/m^3$.

The ossicles received several values as seen on Table 6.7, along with information for articulations' properties. The damping coefficients for the tympanic membrane, ossicles and articulations were $\alpha = 0s^{-1}$ and $\beta = 0{,}0001s$.

Table 6.7 – Comparison of mechanical properties for the geometric model.

Component	**Value**
Membrane	
Specific mass [kg/m^3]	$1{,}2x10^3$
Pars tensa	
Young´s module [N/m^2]	*Radial:* $3{,}2x10^7$
	Circumferential: $2{,}0x10^7$
Pars flaccida	
Young´s module [N/m^2]	*Radial:* $1{,}0x10^7$
	Circumferential: $1{,}0x10^7$
Hammer	
	Head: $2{,}55x10^3$
Specific mass [kg/m^3]	*Neck:* $4{,}53x10^3$
	Manubrium: $3{,}70x10^3$
Young´s module [N/m^2]	$1{,}41x10^{10}$
Anvil	
	Body: $2{,}36x10^3$
Specific mass [kg/m^3]	*Short apophysis:* $2{,}26x10^3$
	Long apophysis: $5{,}08x10^3$
Young´s module [N/m^2]	$1{,}41x10^{10}$
Stirrup	
Specific mass [kg/m^3]	$3{,}2x10^3$
Young´s module [N/m^2]	$1{,}41x10^{10}$
Incudomaleolar Articulation	
Specific mass [kg/m^3]	$3{,}2x10^3$
Young´s module [N/m^2]	$1{,}41x10^{10}$
Incudoestapedian Articulation	
Specific mass [kg/m^3]	$1{,}2x10^3$
Young´s module [N/m^2]	$6x10^5$
Dampening coefficients for the whole model	
$\alpha = 0s^{-1}$	$\beta = 0{,}0001s$

The assigned section for the ligaments between the hammer and the anvil has an area of $0{,}196\ mm^2$. Once more, an elastic behavior was assumed for these. On the hammer, the superior ligament had a Young´s module equivalent to $4{,}9x10^4\ Pa$, the anterior ligament had it at $2{,}1x10^6\ Pa$ and the lateral ligament had it at $6{,}7x10^4\ Pa$. On the anvil, the section assigned to the superior ligament had $4{,}9x10^4\ Pa$ and the one assigned to the posterior ligament

had $6{,}5x10^5\ Pa$. The stirrup´s ligament´s module was $1x10^4\ Pa$. The tympanic groove was assigned a module of $6{,}0x10^3\ Pa$ and specific mass of 1200 kg/m^3. These informations are more clearly displayed on Table 6.8.

Table 6.8 – Comparison of mechanical properties for the ligaments on the geometric model.

Component and Ligament		**Young´s module [N/m^2]**	**Specific mass [kg/m^3]**
Hammer	Superior	$4{,}9x10^4$	-
	Lateral	$6{,}7x10^4$	-
	Anterior	$2{,}1x10^6$	-
Anvil	Superior	$4{,}9x10^4$	-
	Posterior	$6{,}5x10^5$	-
Stirrup´s annular		$1{,}0x10^4$	-
Tympanic´s annular		$6{,}0x10^3$	1200

The assigned section for the tensor tympanic muscle and the stirrup´s muscle had areas of 5,85 mm^2 and 4,9 mm^2, respectively. These were also assumed to have elastic behavior and had a Young´s module of $2{,}6x10^5\ Pa$ for the tympanic muscle and a module of $5{,}2x10^5\ Pa$ for the stirrup´s [47].

The temporal bone had a Young´s module of $1{,}41x10^{10}\ Pa$ and a specific mass of 2000 kg/m^3, with an assumed isotropic elastic behavior. The jaw was simulated under identical properties. For the skin and the cartilage, a Young´s module of $1{,}67x10^{10}\ Pa$ and one of $2{,}5x10^{10}\ Pa$ were used, respectively, while both received the same specific mass equivalent to 1200 kg/m^3 [44]. All of these components also received dampening coefficients equal to $\alpha = 0s^{-1}$ and $\beta = 0{,}0001s$ [48].

The simulated fluid inside the cochlea was given a volumetric module of $2{,}2x10^9\ Pa$ and a specific mass of 1000 kg/m^3 [49]. The air on the external auditory canal and inside the tympanic cavity were given a volumetric module of $1{,}40x10^5\ Pa$ and a specific mass of 1,164 kg/m^3. Such properties ensured the speed of sound in this mean would be equivalent to $349{,}2\ m/s$ [50].

6.4 Boundary conditions

In the model, the ossicles are connected to the bone part through ligaments and muscles. In the membrane´s outskirts, the tympanic groove connects the membrane to the bone. The annular ligament is responsible for connecting the stirrup to the bone. The temporal bone and the jaw, previously seen on Figure 6.10, were given an encastre boundary. This is represented on Figure 6.14.

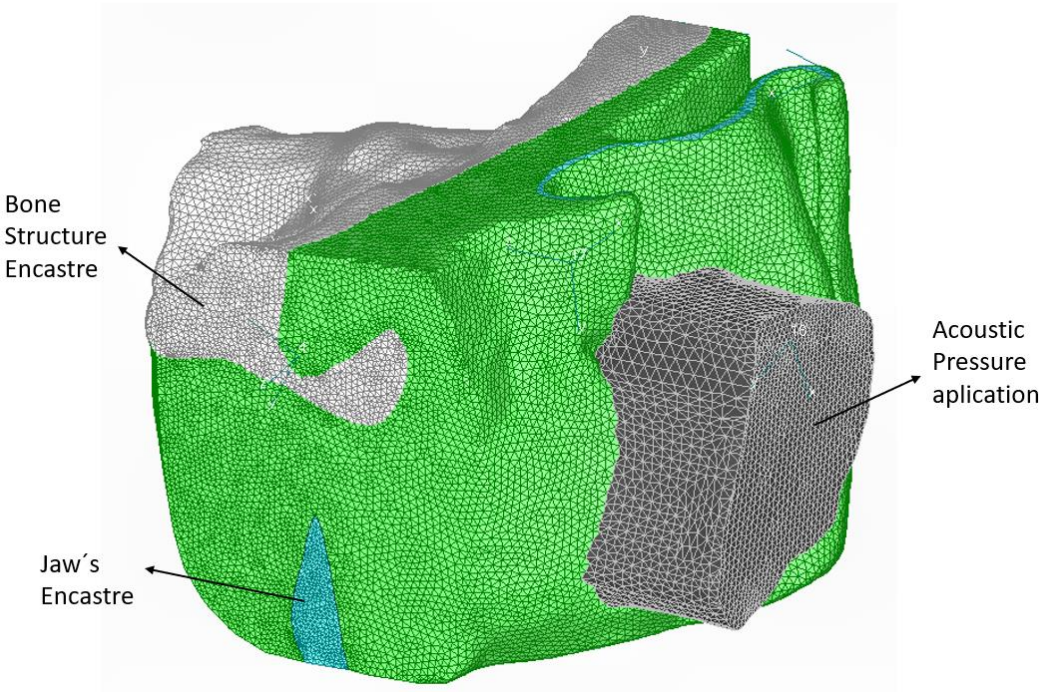

Figure 6.14 – Boundary conditions for the bone structure and the jaw.

In addition to these, acoustic impedance boundaries were also added to simulate the acoustic reflections on the acoustic components. The air on the external auditory canal outside the ear was given an impedance of 406,6 Ns/m^3, and the connection between the air and the bone structure was given an impedance of $6{,}0x10^6$ Ns/m^3 and the connection between the air and the skin was given an impedance of $1{,}99x10^6$ Ns/m^3. The connection between the air and the tympanic membrane was given an impedance of $1{,}99x10^6$ Ns/m^3. This is better displayed on Figures 6.15 through 6.17 [51].

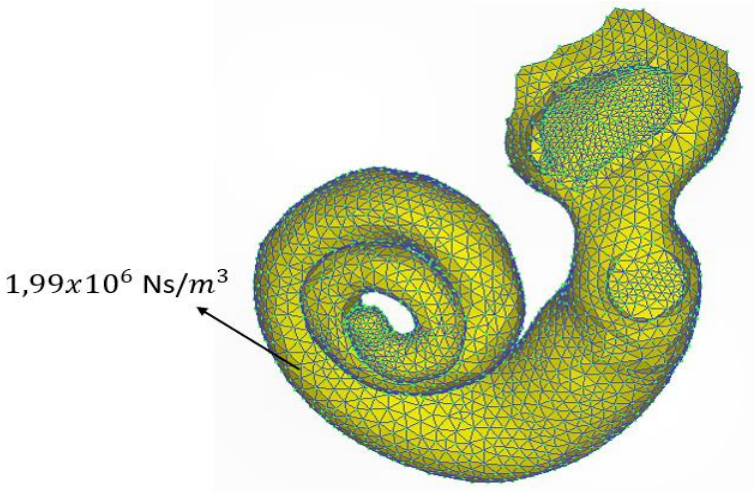

Figure 6.15 – Acoustic impedance.

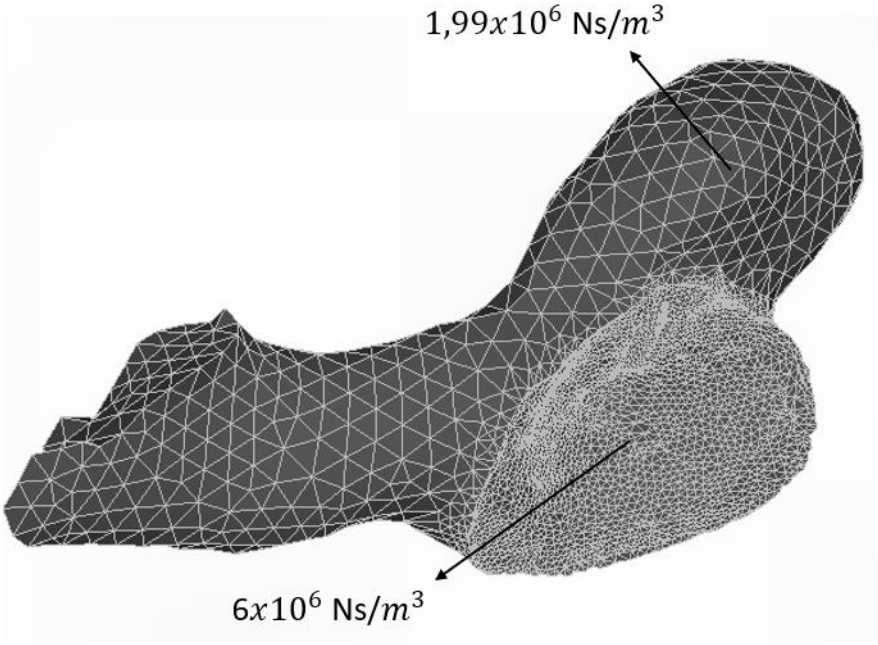

Figure 6.16 – Acoustic impedance.

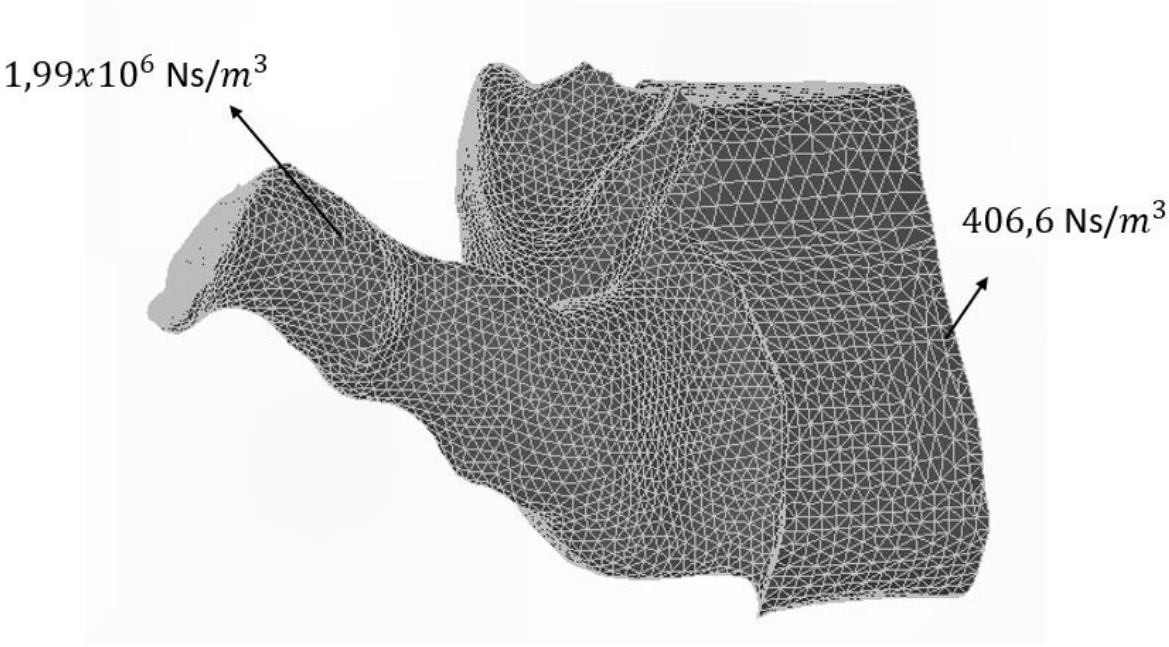

Figure 6.17 – Acoustic impedance.

In order to impose the structural and acoustic interactions on the model, the command TIE, from the software Abaqus, was used.

6.5 Tumors

For the purposes of the present work, three distinct situations were simulated. For the first two models, a small sphere was arbitrarily placed on ossicles of the middle ear, the first on the anvil, the second on the stirrup. Both the spheres were of relatively small size, and received mechanical properties similar to those found on the parts they were attached. The third tumor was based on a real-life condition, and was placed on the tympanic membrane. It received mechanical properties equivalent to blood, since the actual tumor is blood sensitive. The next sections describe each tumor model in detail.

6.5.1 First tumor

The three tumors were built following the same procedure. A regular sphere was placed atop of the place that a tumor was to be simulated, then a surface mesh would be built. After that, any element from such mesh that was in interference with the original elements of the model would be cut out, and a new array of elements connecting the new body to the original would be manually created. With the new body properly connected, a solid mesh was created to fill the surface elements.

Figure 6.18 brings a representation of the first tumor created, and Figure 6.19 shows it properly connected to the anvil ossicle.

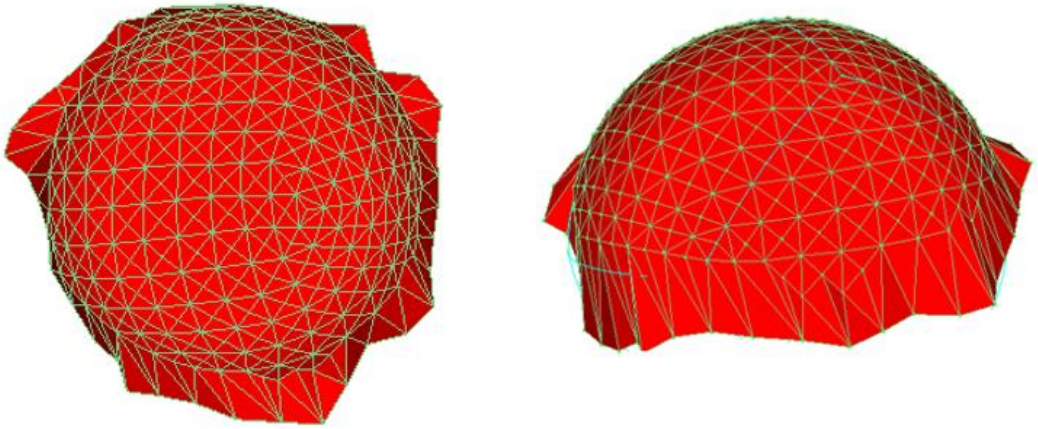

Figure 6.18 – First simulated tumor.

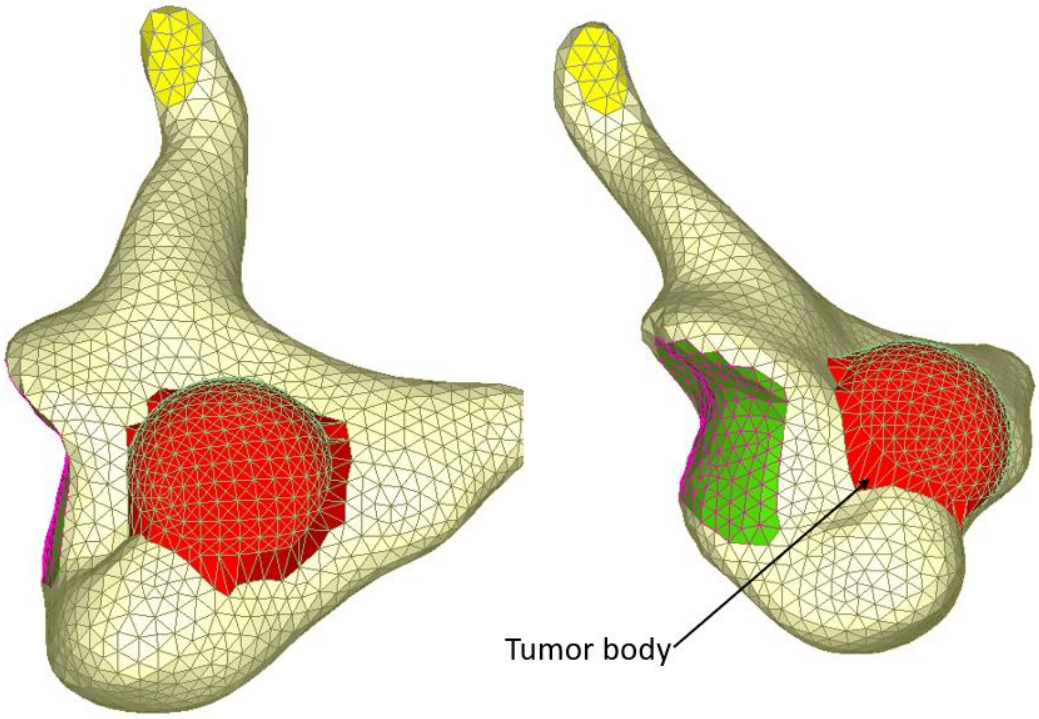

Figure 6.19 – First simulated tumor connected to the anvil ossicle.

Table 6.9 brings information about the quantity of elements and new nodes introduced by the creation of the tumor part of the model.

Table 6.9 – Amount of elements and nodes on the first tumor.

Elements		**Nodes**
Type	Total	Total
C3D4	4912	962

As mentioned, the mechanical properties for the tumor were similar to the ones of the original body. Table 6.10 brings the properties utilized on this case as well as the sphere dimension.

Table 6.10 – Mechanical properties for the first tumor.

Property	*Value*
Density [kg/m^3]	$2{,}36x10^3$
Young´s module [N/m^2]	$1{,}41x10^{10}$
Poisson´s coefficient	0,3
Damping coefficients	$\alpha = 0s^{-1}$ $\beta = 0{,}0001s.$
Sphere radius [mm]	*1*

6.5.2 Second tumor

For the second simulation, it was chosen to simulate a growth simulating a tumor on the inside part of the stirrup. Figure 6.20 brings a representation of the body that was inserted on the stirrup, and Figure 6.21 brings the stirrup with the tumor properly allocated.

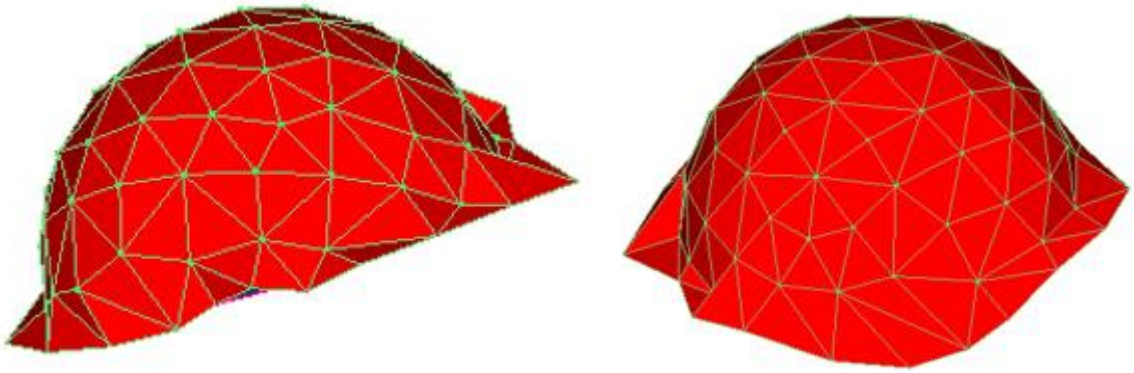

Figure 6.20 – Second simulated tumor.

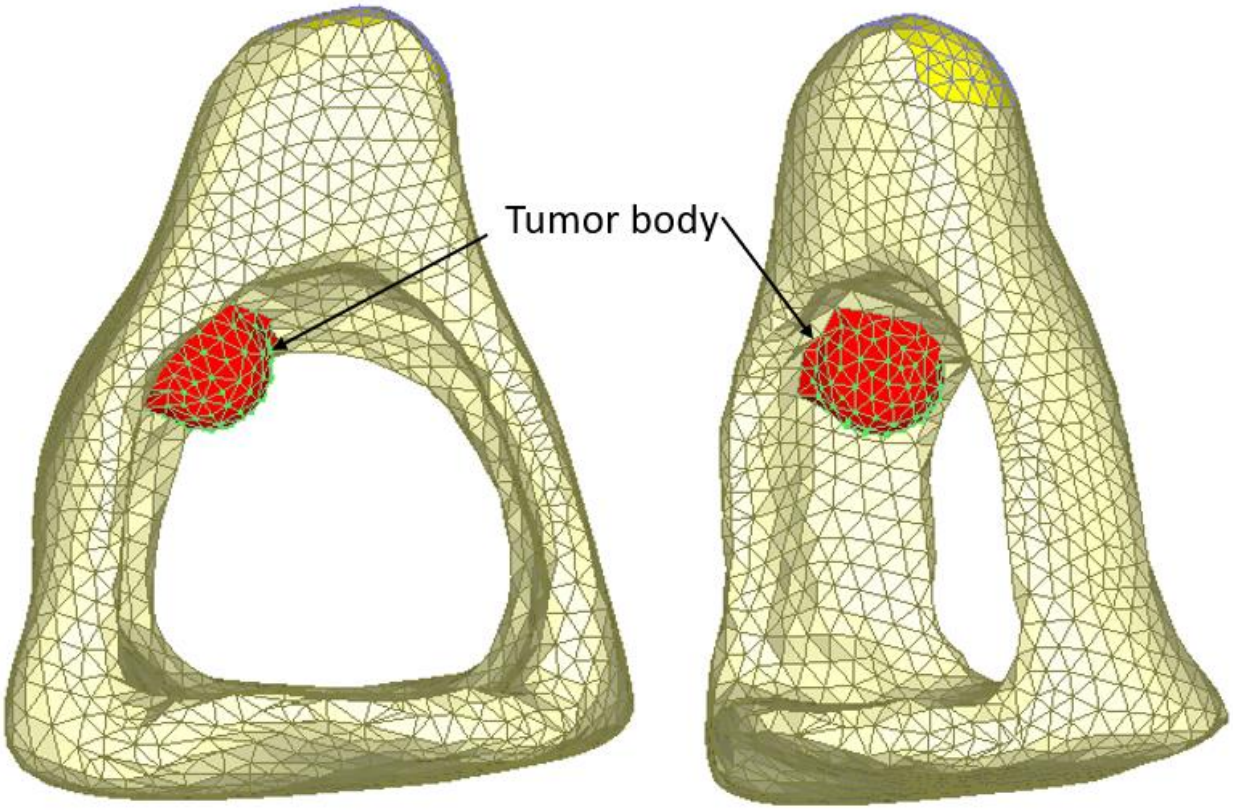

Figure 6.21 – Second simulated tumor connected to the stirrup.

Table 6.11 shows the amount of elements and new nodes introduced to the model through the insertion of the tumor body.

Table 6.11 – Amount of elements and nodes on the second tumor.

Elements		**Nodes**
Type	Total	Total
C3D4	459	88

As previously mentioned, the tumor received similar properties of those present on the body it was attached into, all of which can be seen on Table 6.12, along the dimension for the sphere used to create the tumor.

Table 6.12 – Mechanical properties for the second tumor.

Property	*Value*
Density [kg/m^3]	$3{,}2x10^3$
Young´s module [N/m^2]	$1{,}41x10^{10}$
Poisson´s coefficient	0,3
Damping coefficients	$\alpha = 0s^{-1}$ $\beta = 0{,}0001s.$
Sphere radius [mm]	*0.33*

6.5.3 Third tumor

The tumor built for the third simulation was inspired by Glomus Tumors, the most common benign tumors of the middle ear. Such tumors arise from glomus bodies, which are small regular structures of the middle ear, and have the function of regulating the oxygen pressure through the middle ear and the mastoid [52], [53].

These tumors are blood sensitive, and are mostly built of blood channels flowing through the tumor itself. Figure 6.22 shows and example of the glomus.

Figure 6.22 – Glomus tumor in the middle ear [52].

Following the same procedure as the other tumors, to simulate the tumor body a sphere was incorporated into the model, with the one on this example being the largest of the present work. Figure 6.23 brings a representation of the sphere used for this example.

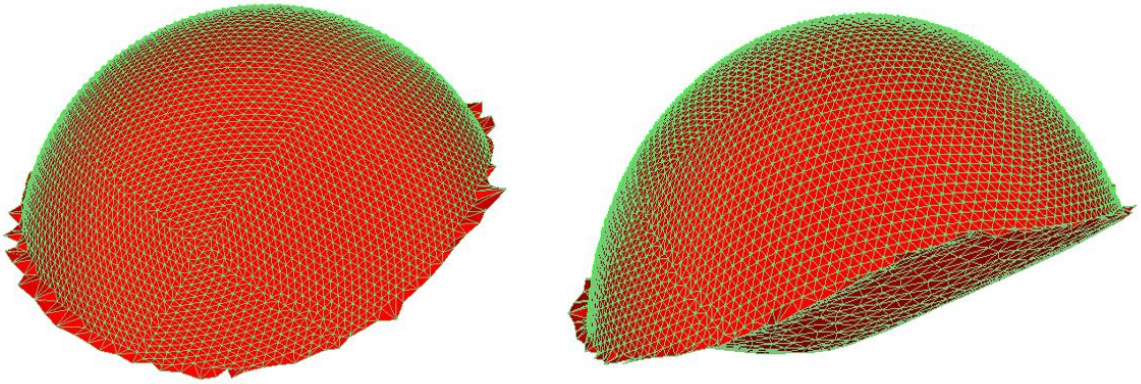

Figure 6.23 – Third simulated tumor.

The tumor body was attached to the membrane to perform the simulation, as can be seen on Figure 6.24.

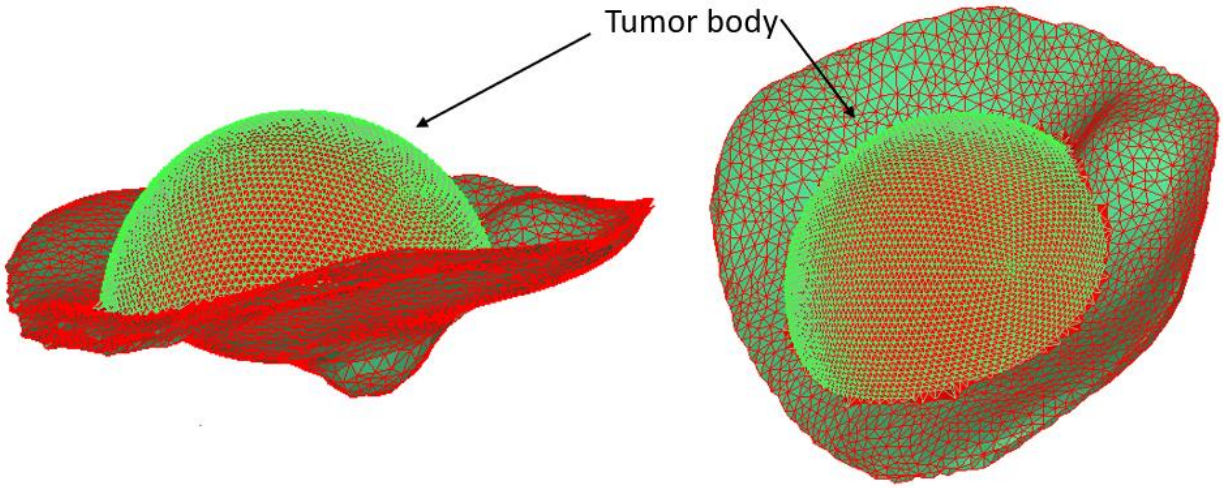

Figure 6.24 – Third simulated tumor connected to the membrane.

Table 6.13 brings information about the quantity of elements and new nodes introduced by the creation of the tumor part of the model.

Table 6.13 – Amount of elements and nodes on the third tumor.

Elements		**Nodes**
Type	Total	Total
C3D4	68846	11720

Since the tumor is built mostly on blood vessels, this tumor received blood mechanical properties. Such properties can be seen on Table 6.14, along with dimensional values for the sphere.

Table 6.14 – Mechanical properties for the third tumor.

Property	*Value*
Density [kg/m^3]	$1{,}06x10^3$ [54]
Young´s module [N/m^2]	$1{,}08x10^7$ [55]
Poisson´s coefficient	0,49 [55]
Damping coefficients	$\alpha = 0s^{-1}$ $\beta = 0{,}0001s.$
Sphere radius [mm]	*4*

6.6 Biomechanical behavior study of the ear

6.6.1 Natural frequencies

The first analysis that the models were subjected had as objective the determination of the forty first natural frequencies of each model, so it could be compared to the values found for the original model and some values found on previous literature for similar situations. Figure 6.25 brings a graph with the comparison of the forty frequencies for the first tumor.

As can be seen on the graph, the values found for the first model are approximate to the ones found on the previous work for the original model. The first natural frequency found on the complete model with the tumor was 214,75 Hz while the first natural frequency found on the original complete model was equal to 212,25 Hz. The tumor´s simple model first natural frequency was 274,58 Hz while the original simple model had a first natural frequency of 272,53 Hz.

Figure 6.26 brings a graphical representation of approximate variations of the values found on the original model to the tumor model, and Table 6.15 brings the average variation value as well as some specific variations.

Table 6.15– Variation statistics for the first tumor regarding natural frequencies.

Complete Model for the First Tumor	
Variation in Natural Frequencies	*Value [%]*
First Natural Frequency	*1,18*
Highest Variation	*5,51*
Average Variation	*2,43*
Membrane and Ossicles Model for the First Tumor	
Variation in Natural Frequencies	*Value [%]*
First Natural Frequency	*0,75*
Highest Variation	*5,13*
Average Variation	*1,12*

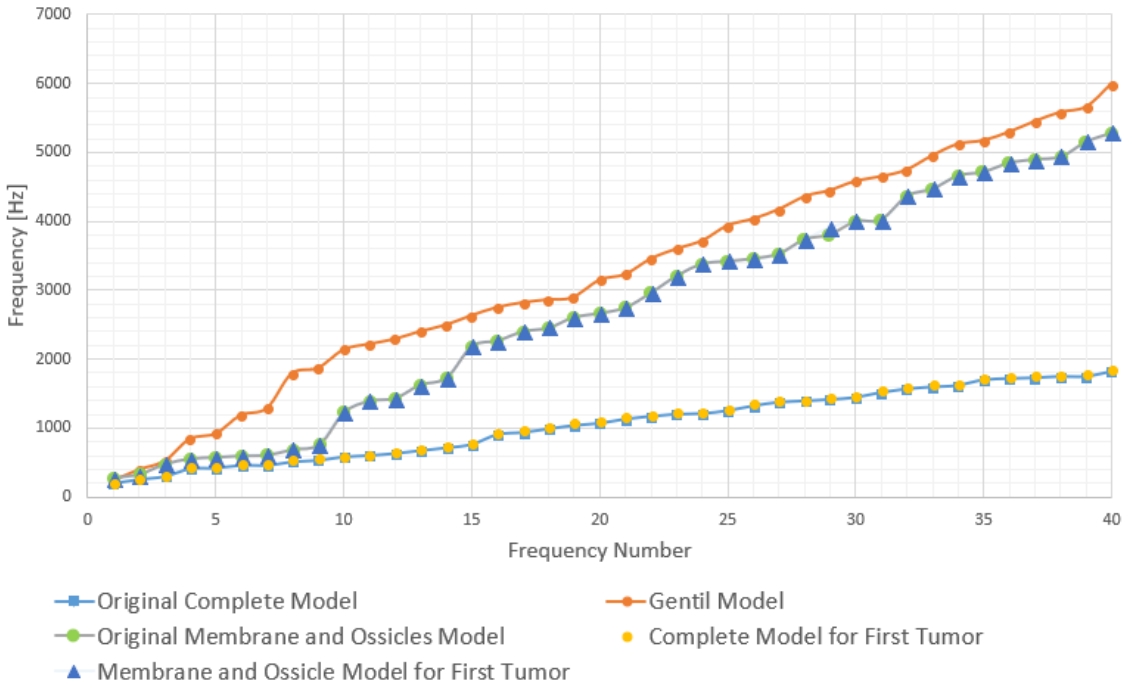

Figure 6.25 – Comparison of first tumor natural frequencies to prior literature [2], [4].

Figure 6.26 – Variations of value between natural frequencies for the original model and the first tumor model [2], [4].

As with the original model, the simple model had the higher natural frequencies in regard to the complete model, with the difference between the two of them becoming larger from the ninth natural frequency.

The highest variation for the complete original model and the tumor complete model was found on the ninth natural frequency with a 5,51% variation of values, where the tumor model had a frequency equal to 567,91 Hz and the original model had 537,96 Hz. The simple original model and the tumor simple model had a peak of variation on the second natural frequency with a variation of 5,13%, of which the tumor model had a frequency of 274,5 Hz and the original model had a frequency of 264,66 Hz.

The tumor model followed a similar behavior in comparison of the original when comparing it to Gentil´s model [2]. The first three natural frequencies had similar values, then from the fourth up to the fourteenth natural frequencies the values had a higher variation in regard to Gentil´s model.

In Figure 6.27 it can be seen the comparison of the natural frequencies for the second tumor, following the same procedure as Figure 6.23 for the first tumor. The first natural frequency found on the second tumor complete model was 212,78 Hz, a similar value to the original complete model which had a first natural frequency of 212,25 Hz. As for the simple models, the second tumor had a first natural frequency equal to 273,2 Hz, also similar to the original model value of 272,53 Hz. The values found for the tumor natural frequencies were always higher than the original model.

Figure 6.28 brings the approximate variations between the second tumor model and the original model, and Table 6.16 presents the average variation of these values along with the highest variation and the first variation.

Table 6.16 – Variation statistics for the second tumor regarding natural frequencies.

Complete Model for the Second Tumor	
Variation in Natural Frequencies	*Value [%]*
First Natural Frequency	*0,25*
Highest Variation	*5,25*
Average Variation	*2,34*
Membrane and Ossicles Model for the Second Tumor	
Variation in Natural Frequencies	*Value [%]*
First Natural Frequency	*0,25*
Highest Variation	*5,19*
Average Variation	*0,54*

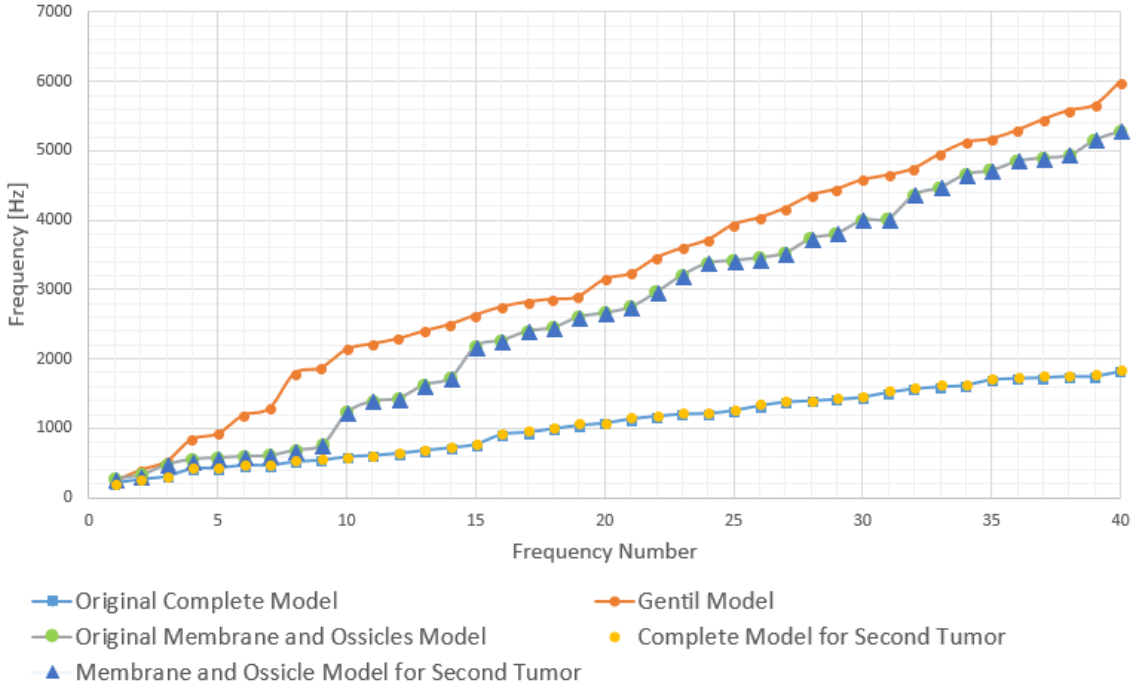

Figure 6.27 – Comparison of second tumor natural frequencies to prior literature [2], [4].

Figure 6.28 – Variations of value between natural frequencies for the original model and the second tumor model [2], [4].

It can be observed that the variations values found on this tumor are slightly smaller than the ones found on the first tumor, which is expected due to the fact that the sphere used on this example was smaller than the one used for the first example, thus rendering a minor impact on the overall model. Due to it´s minor variations from the original model, the behavior is expected to be similar, meaning that the frequencies of the complete and the simple model start to differ in more meaningful amounts starting from the ninth natural frequency.

The highest variation for this tumor complete model was found on the ninth natural frequency with a variation of 5,25%, where the tumor model had a frequency equal to 566,21 Hz and the original model had 537,96 Hz. For the simple model, the highest variation was found on the second natural frequency where the tumor model had a natural frequency of 309,57 Hz and the original model had a natural frequency of 264,66 Hz.

As mentioned, mostly due to it´s small size having only minor impacts on the model, this tumor example differed in small ways from the original model, thus being logical that, same as with the first tumor, it followed a close behavior as to Gentil´s work [2], especially on the first three natural frequencies, having a higher discrepancy around the fourth up to the fourteenth natural frequencies.

The second tumor model also always presented higher natural frequencies on the simple model than the ones found on the complete model.

Figure 6.29 brings the graph comparison of the natural frequencies for the third simulated model. The first natural frequency found for the third tumor was equivalent to 210,89 Hz, and as previously mentioned the original model first natural frequency is 212,25 Hz. On the simple model for the third tumor, the first natural frequency was 232,87 Hz, with the original being 264,66 Hz. The initial natural frequencies found for the third tumor were lower than the ones found on the original model, and from the eighteenth frequency onwards the values were higher than the original´s complete model. Figure 6.30 shows the variation of values for the natural frequencies between the third tumor model and the original model for the forty first natural frequencies, and Table 6.17 brings the value for the average variation, the highest variation and the first variation.

Table 6.17 – Variation statistics for the third tumor regarding natural frequencies.

Complete Model for the Third Tumor	
Variation in Natural Frequencies	*Value [%]*
First Natural Frequency	*0,64*
Highest Variation	*17,07*
Average Variation	*6,35*
Membrane and Ossicles Model for the Third Tumor	
Variation in Natural Frequencies	*Value [%]*
First Natural Frequency	*14,55*
Highest Variation	*50,69*
Average Variation	*18,78*

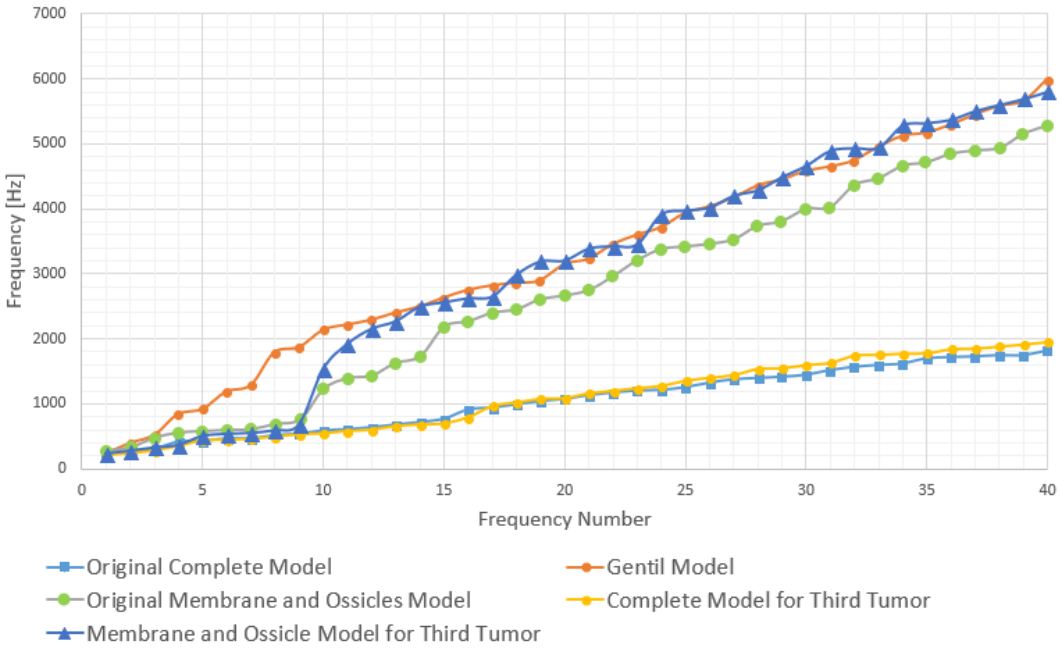

Figure 6.29 – Comparison of third tumor natural frequencies to prior literature [2], [4].

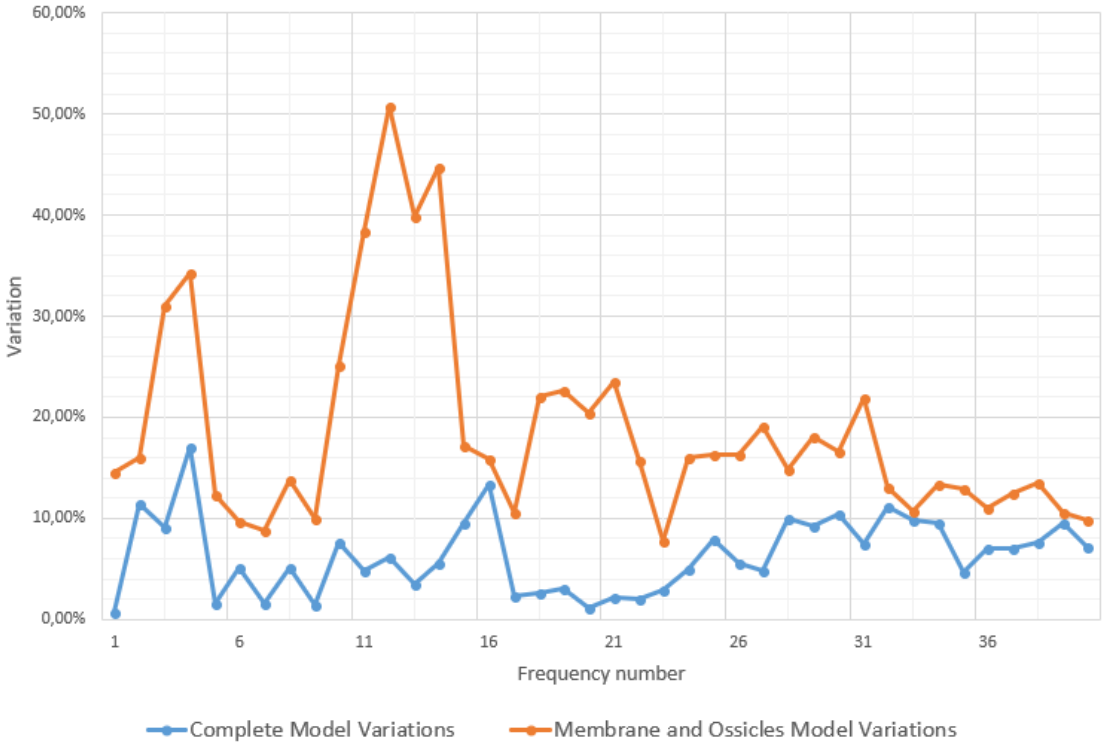

Figure 6.30– Variations of value between natural frequencies for the original model and the third tumor model [2], [4].

It is noted that the variation values for the third tumor were significantly higher than the variations found in the prior examples. That is explained due to the fact that the third tumor was the largest of all the models, thus inflicting a larger influence on the dynamic behavior of the model as a whole. It can be seen that on the complete model it still didn´t vary the values found by a large marge, possibly because even though the third tumor had a bigger size than the others, it still wasn´t significant enough for big behavioral changes for the whole model, while the simple model, which is made up of only membrane and ossicles, suffered a higher change on such behavior, and therefore had a much bigger variation than the other examples.

As previously said, the natural frequencies for the complete model of the tumor started out lower than the ones found for the original model, becoming higher after the eighteenth frequency. The simple tumor model followed a similar trend, starting out on lower values in relation to the original, and proceeding to have higher numbers from the tenth frequency onwards.

The complete model had it´s variation peak of 17,07% at the fourth natural frequency, where it´s natural frequency was equal to 345,91 Hz compared to the original model´s 417,1 Hz. The simple model had the highest variation at the twelfth frequency, with a difference of 50,69% where the tumor model had a frequency of 2152,7 Hz and the original had a frequency of 1428,57 Hz.

In comparison to Gentil´s model [2], the complete model for the tumor followed a similar behavior, having overall lower natural frequencies in comparison. The simple model, however, was the first case to reach higher values than Gentil´s model [2], which was expected, seeing as how higher the values were compared to the original model.

6.6.2 Displacement analysis

6.6.2.1 Simple model

In order to study it´s displacement behavior, the model was subjected to a range of frequencies between 100 Hz and up to 10 kHz. To better understand the results, two different nodes on the model were chosen to be observed as to how they were displaced. The first one was node number 472854, which was placed on the umbo, and the second node, of number 421800, was placed on the stirrup, and those two nodes will be the standard ones used for the remainder of this work. For the simple model of each tumor, six different sound pressure levels were used, these being 0 dB (2,0×10−5 Pa), 60 dB (2,0×10−2 Pa), 80 dB (2,0×10−1 Pa), 90 dB (6,32×10−1 Pa), 105 dB (3,56 Pa) and 130 dB (6,32×101 Pa).

Figure 6.31 brings the comparison for the umbo node displacement between all three tumor simple models and the original simple model for a sound pressure level of 0 dB (2,0×10−5 Pa), and Figure 6.32 brings the same comparison for the stirrup node displacement.

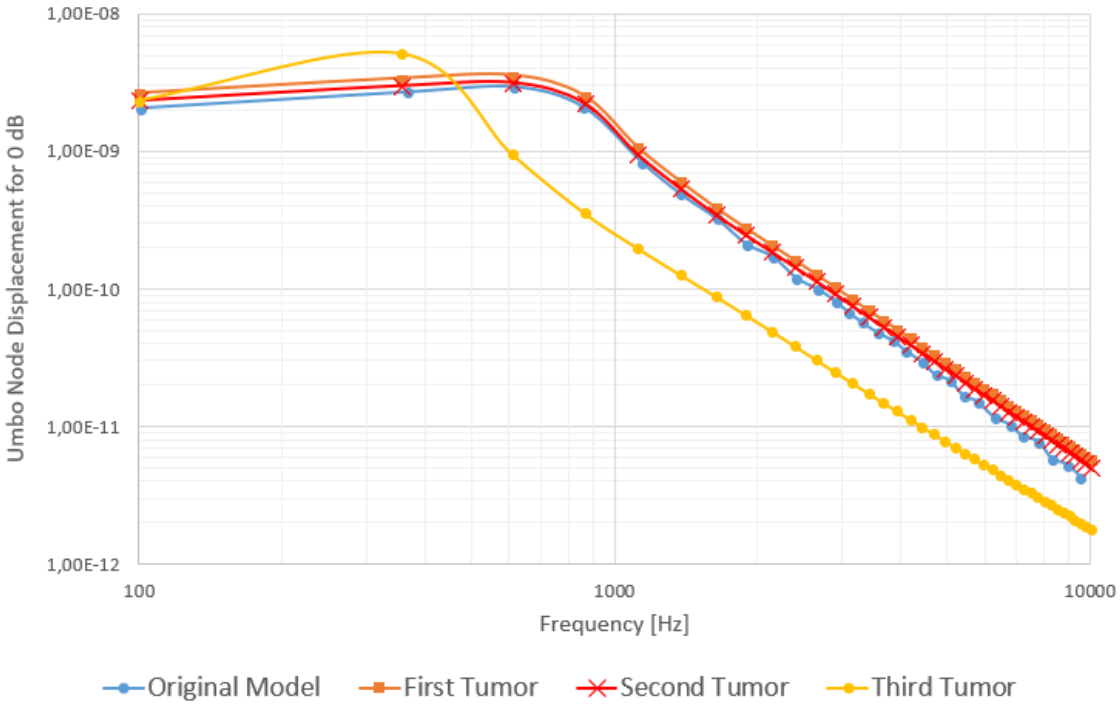

Figure 6.31 – Comparison at 0 dB sound level of umbo node displacement for the three simple tumor models and the original [4].

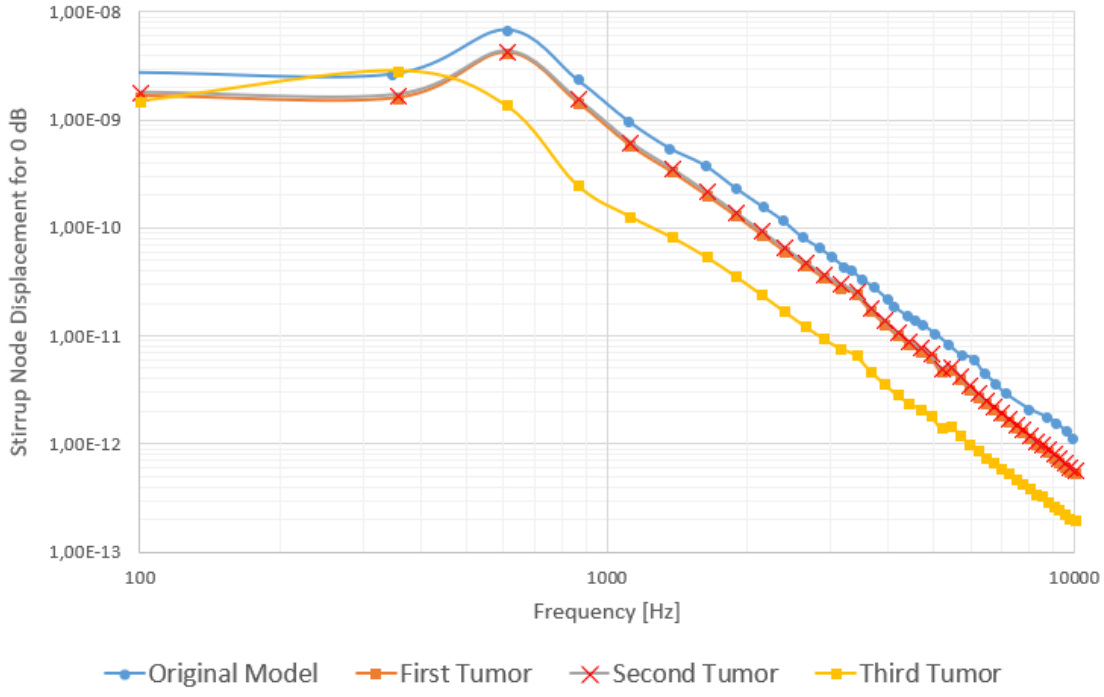

Figure 6.32 – Comparison at 0 dB sound level of stirrup node displacement for the three simple tumor models and the original [4].

Observing Figure 6.31, it is possible to observe that the three different tumor models started out on a higher displacement degree than the original model. The first and second tumor stayed on higher values of displacement, while the third tumor had an elevation peak and then proceeded to have smaller values than the others. For the stirrup node study, it can be seen that the original model had the highest starting values overall, where only the third tumor at one point had a higher value than the original, but proceeded to have the lowest values once more.

It is also notable the similar behavior for the first and second tumors. This can be explained mostly by the fact that both of them had similar sizes, and therefore affected the model in more similar ways than when compared to the third model, which was larger, and also was placed farther apart from the other two.

Figure 6.33 brings a comparison on a sound pressure level of 60 dB (2,0×10−2 Pa) for the original model and the three tumor models for the umbo node, while Figure 6.34 brings the same comparison for the stirrup node.

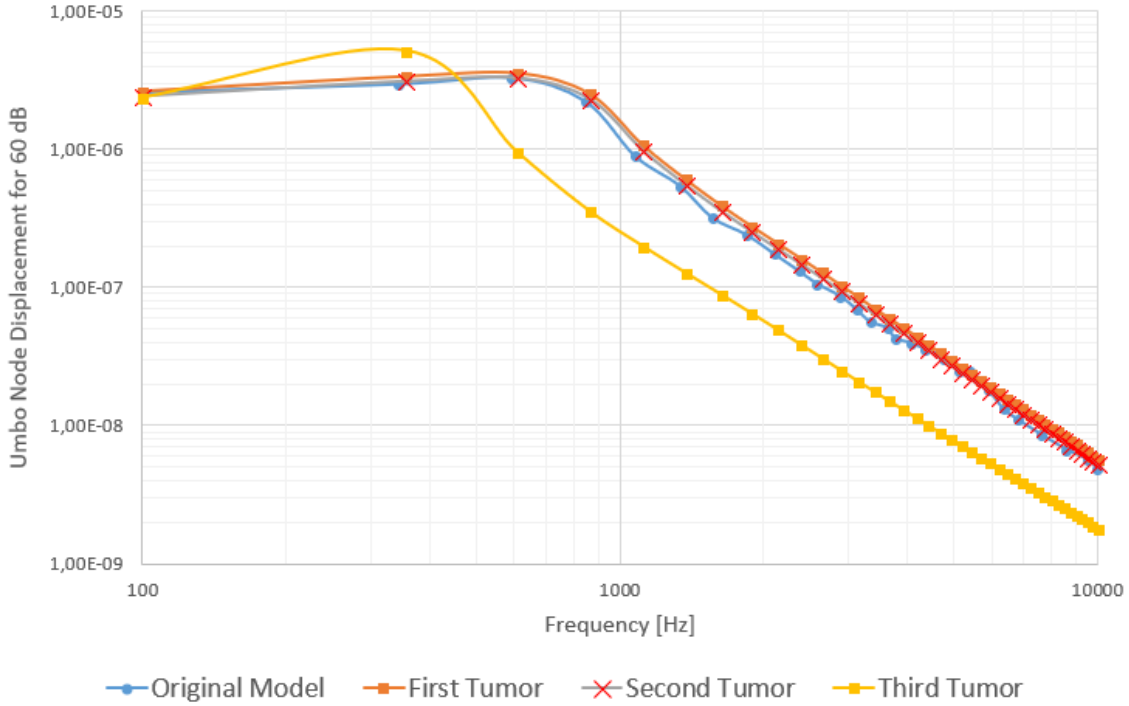

Figure 6.33 – Comparison at 60 dB sound level of umbo node displacement for the three simple tumor models and the original [4].

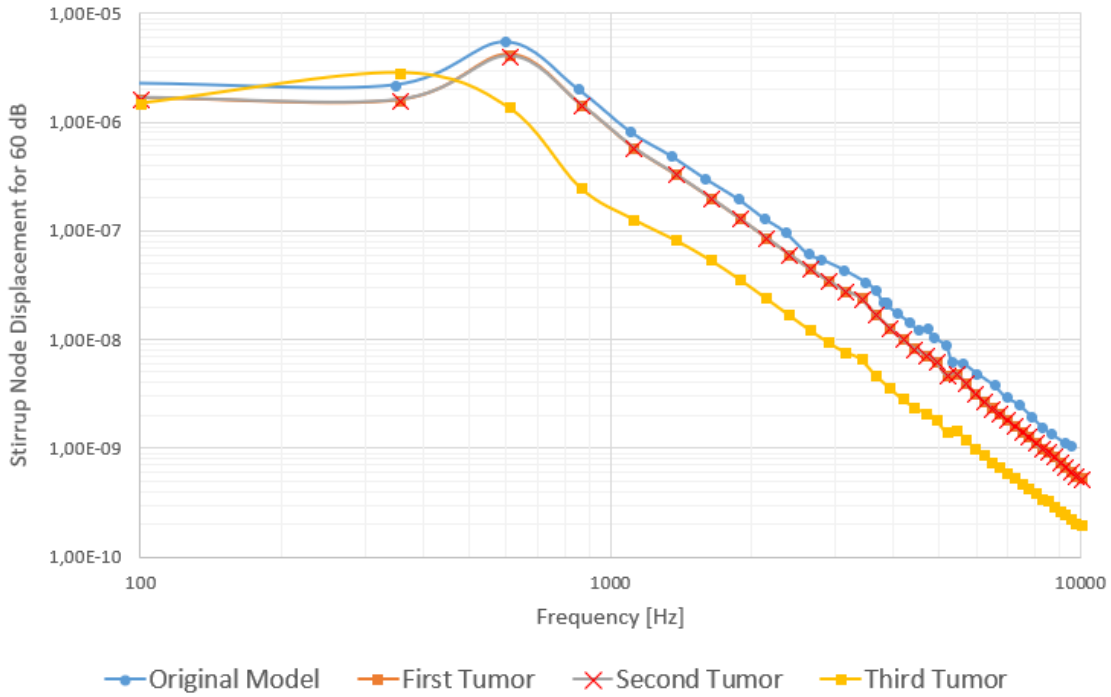

Figure 6.34 – Comparison at 60 dB sound level of stirrup node displacement for the three simple tumor models and the original [4].

It is observed in Figures 6.33 and 6.34 that the three tumor simple models followed the same kind of behavior for the sound pressure level of 0 dB, in which the two first tumors stay at slightly higher values than the original model throughout the whole study for the umbo node, while the third tumor has a peak of displacement at 354 Hz with a displacement of 5,18×10−6 mm, then proceeding to have lower displacements at higher frequencies than the other models.

On the stirrup node study, the models also followed the same pattern as the one observed for the 0 dB. The first two had slightly lower displacements than the original model through all levels of frequency, while the third tumor had the highest value observed at 354 Hz with a displacement of 2,91×10−6 mm, and then proceeded to have the lowest values of displacement for the rest of the frequency levels.

Figure 6.35 and figure 6.36 bring the comparison for a sound pressure level of 80 dB (2,0×10−1 Pa), with other literature data.

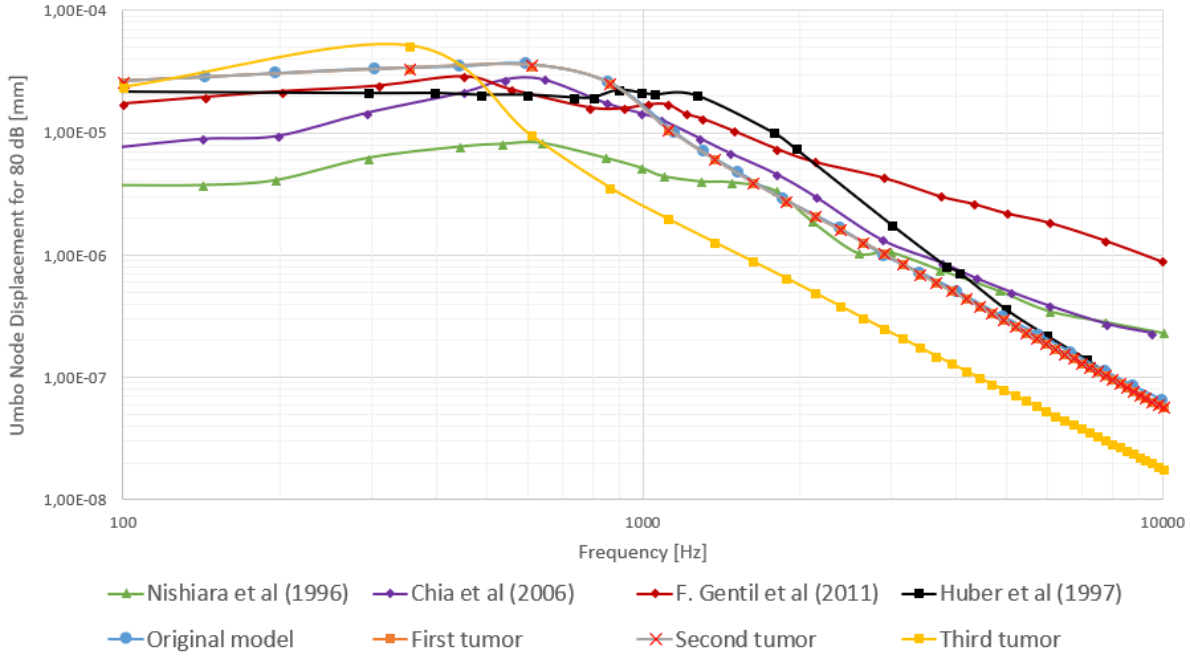

Figure 6.35 – Comparison at 80 dB sound level of umbo node displacement for the three simple tumor models [2], [4], [56]–[58].

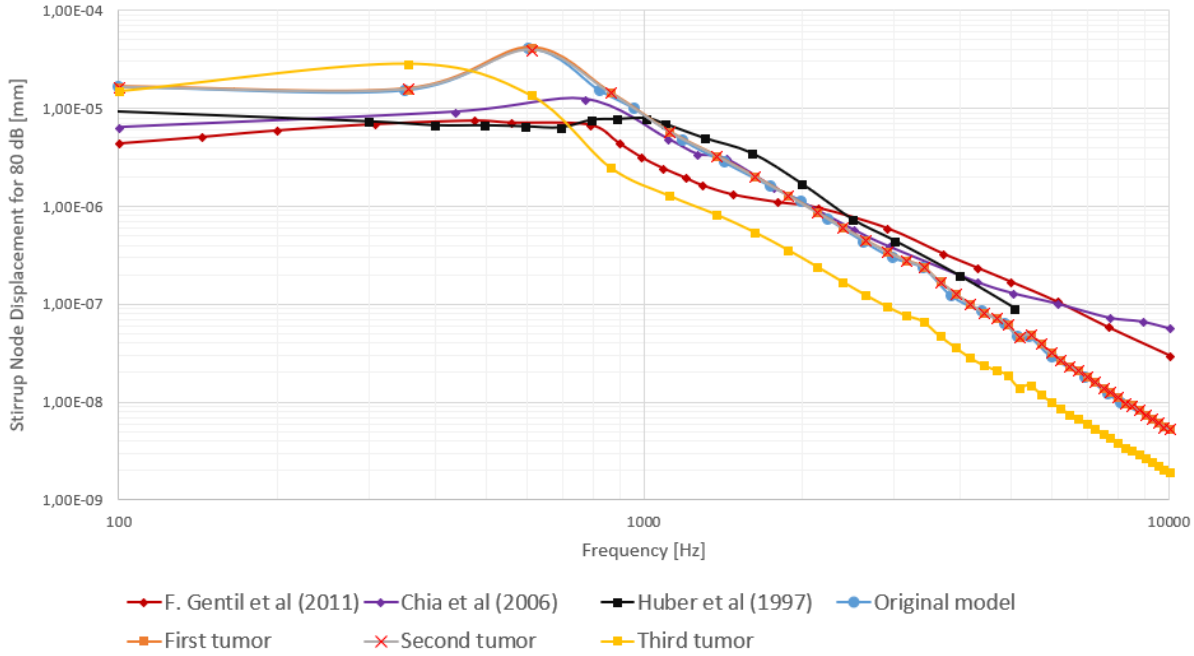

Figure 6.36 – Comparison at 80 dB sound level of stirrup node displacement for the three simple tumor models [2], [4], [56]–[58].

Regarding the literature present in the comparison, Gentil´s work was previously mentioned [47], and it determinates the displacements on the umbo and on the stirrup for a sound pressure

level of 80 dB through a model containing the membrane and the ossicles, considering the ligaments to have a hyperplastic behavior.

Chia *et al* [57] simulates through the FEM method the middle ear, built on the membrane and the ossicles, and compared it´s results to Nishihara [58]. Huber *et al* [56] published experimental data for the umbo´s displacement and the stirrup´s platinum from 10 temporal bones. Nishihara *et al* [59] also published experimental data, obtained from sixty-four people with hearing considered normal, whom were induced thirty-four different tones at 80 dB SPL on a frequency range varying between 195 Hz and 19433 Hz on the tympanic membrane, and then measured the displacement of the umbo through a laser instrument.

As observed in Figures 6.35 and 6.36, the first two tumors continued to keep similar behaviors between each other and to the original model, which are all relatively close to the results found on Gentil *et al* [47] on the lowest frequencies observed, having higher variations towards the higher frequencies. The results presented by Nishihara *et al* [59]and Chia *et al* [57] have a lower umbo displacement for lower frequencies than the other results, while getting increasingly higher values relative to the other works when on higher frequencies. The work from Huber *et al* [56] shows the most similarity to the results found for the models. The third tumor had the highest values for low frequencies in relation to prior literature, and then proceeded to have the lowest values among them all for higher frequencies.

The behaviors observed for the stirrup displacement are of equivalent patterns in regards from one study to another. While on lower frequencies the values are generally close, from the frequency of approximately 4 kHz onwards the models for all three tumors stay lower than previous literature.

Figures 6.37, 6.38 and 6.39 bring the ratio for the displacements between the umbo node and the stirrup node for 80 dB (2,0×10−1 Pa) for each of the three tumors.

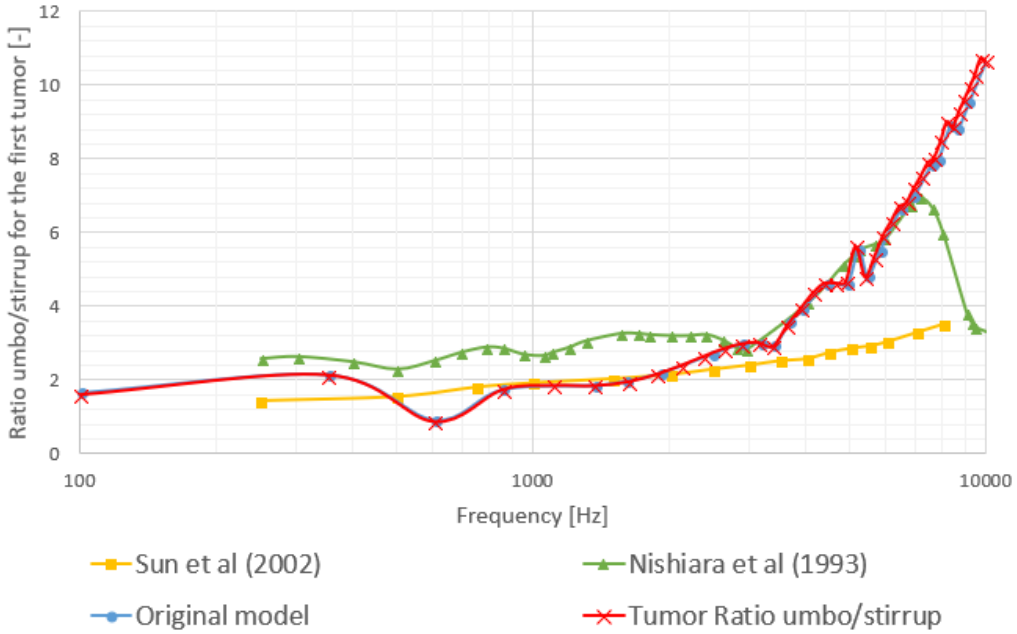

Figure 6.37 – Ratio for the umbo node displacement and the stirrup node displacement at 80 dB for the first tumor [4], [46], [59].

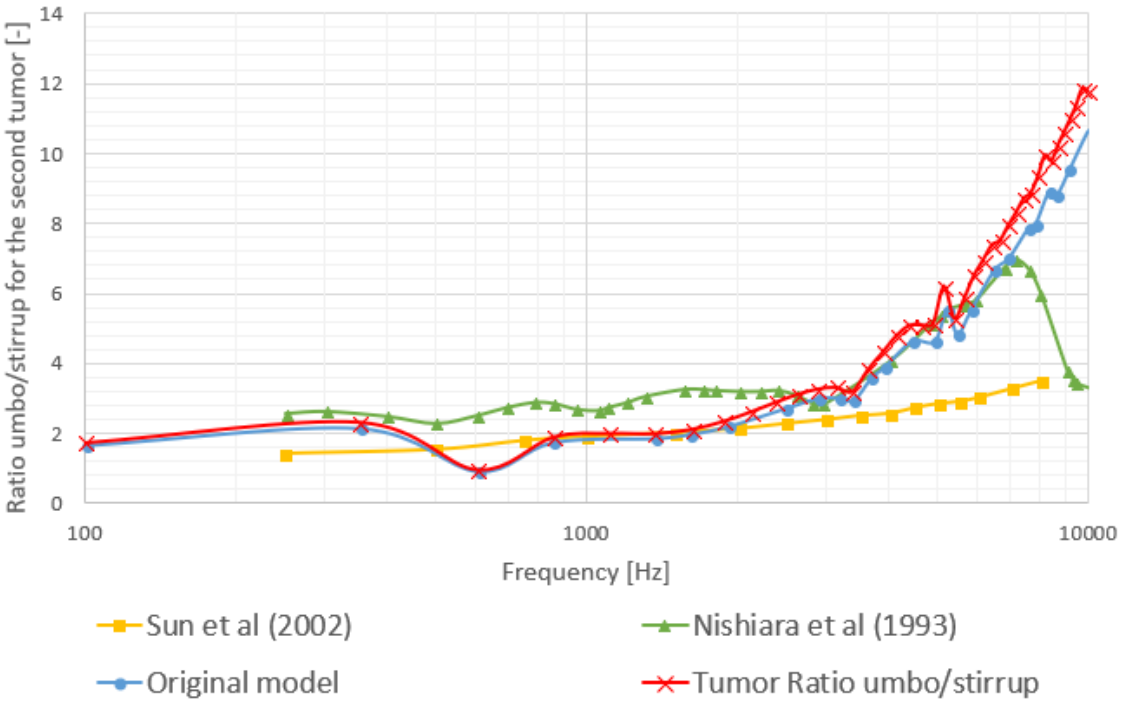

Figure 6.38 – Ratio for the umbo node displacement and the stirrup node displacement at 80 dB for the second tumor [4], [46], [59].

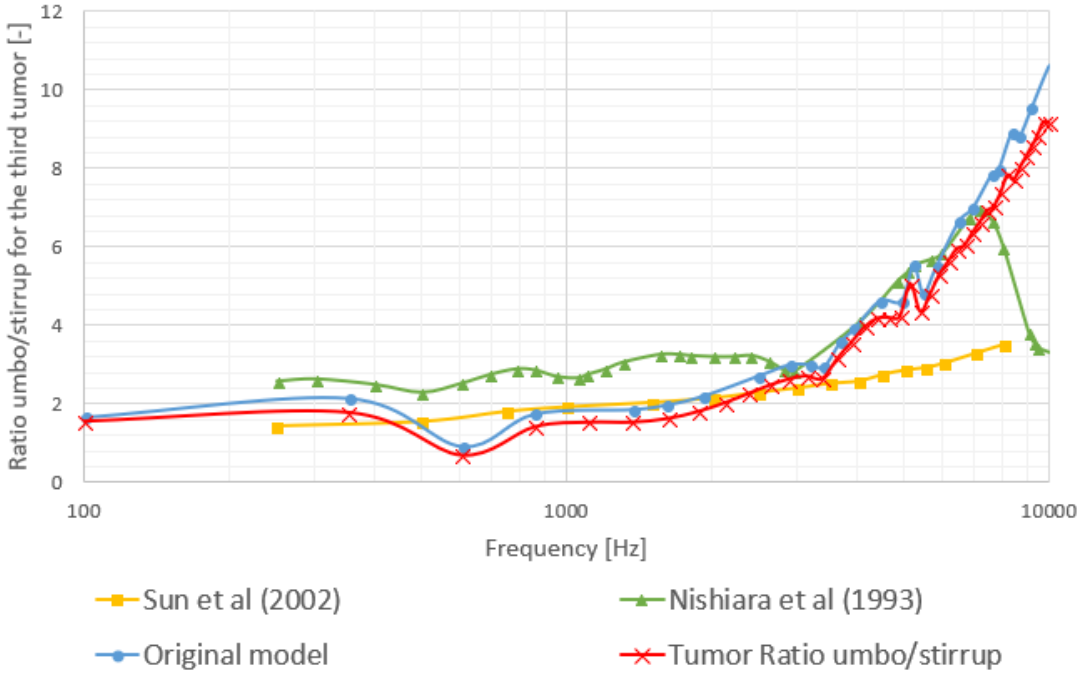

Figure 6.39 – Ratio for the umbo node displacement and the stirrup node displacement at 80 dB for the third tumor [4], [46], [59].

The first two tumors stayed on approximate ratio as the original model for lower frequencies, with the second tumor having differentiate values for higher frequencies, while the third tumor had a lower ratio throughout the whole study. In lower frequencies, between 100 Hz and approximately up to 2 kHz the ratio stays nearly constant, always around 2, showing a behavior that is practically independent from the frequency, while on higher frequencies the ratio escalates, making it so that at 10 kHz frequency the first two tumors have a ratio up to 11, and the third tumor a ratio up to 9.

The three tumors followed approximate behaviors at the lower frequencies as previous literature, but for the highest frequencies, between 7 kHz and 10 kHz, the models had a peak on the ratio number, while Nishihara *et al* [58] has a drop of value on this range of frequency, and Sun *et al* [46] presents an increasing ratio on these frequencies, but on a much smaller scale than the rise seen on the models. The variation between each tumor ratio and the original model is shown at Figure 6.40.

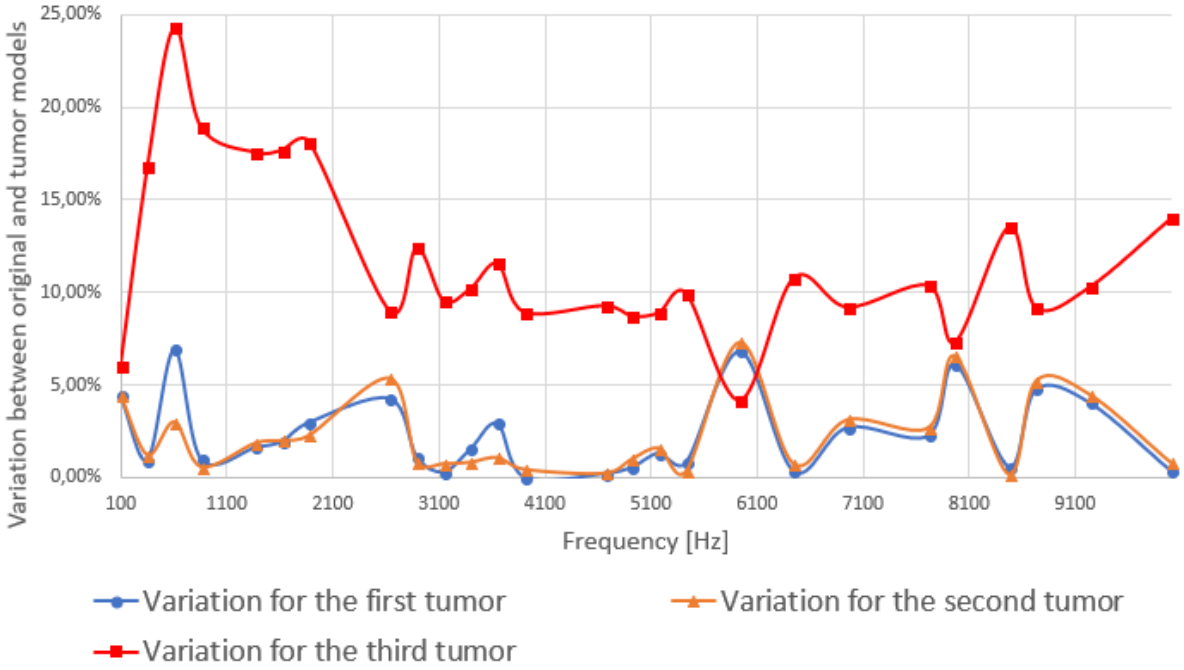

Figure 6.40 – Variation between the ratios found on the original model and the tumor models.

As expected from observing Figures 6.37, 63.8 and 6.39 the first two models, which stayed in close vicinity with the original model, had smaller variations when compared to the third tumor, which mostly had a higher discrepancy over the original model, with the exception at frequency 5,9 kHz, where it got closer results to the original than the other two. Table 6.18 brings the initial variation, highest variation and average variation for each tumor.

Table 6.18 – Variation statistics for the tumor models regarding umbo and stirrup displacements ratio.

Variation for the first tumor	
Variation	*Value [%]*
First displacement	*4,46*
Highest Variation	*6,95*
Average Variation	*2,36*
Variation for the second tumor	
Variation	*Value [%]*
First displacement	*4,47*
Highest Variation	*7,32*
Average Variation	*2,27*
Variation for the third tumor	
Variation	*Value [%]*
First displacement	*6,07*
Highest Variation	*24,3*
Average Variation	*11,8*

Figures 6.41 and 6.42 bring the comparison for the umbo and stirrup node displacement with previous literature, on a sound pressure level of 90 dB (6,32×10−1 Pa).

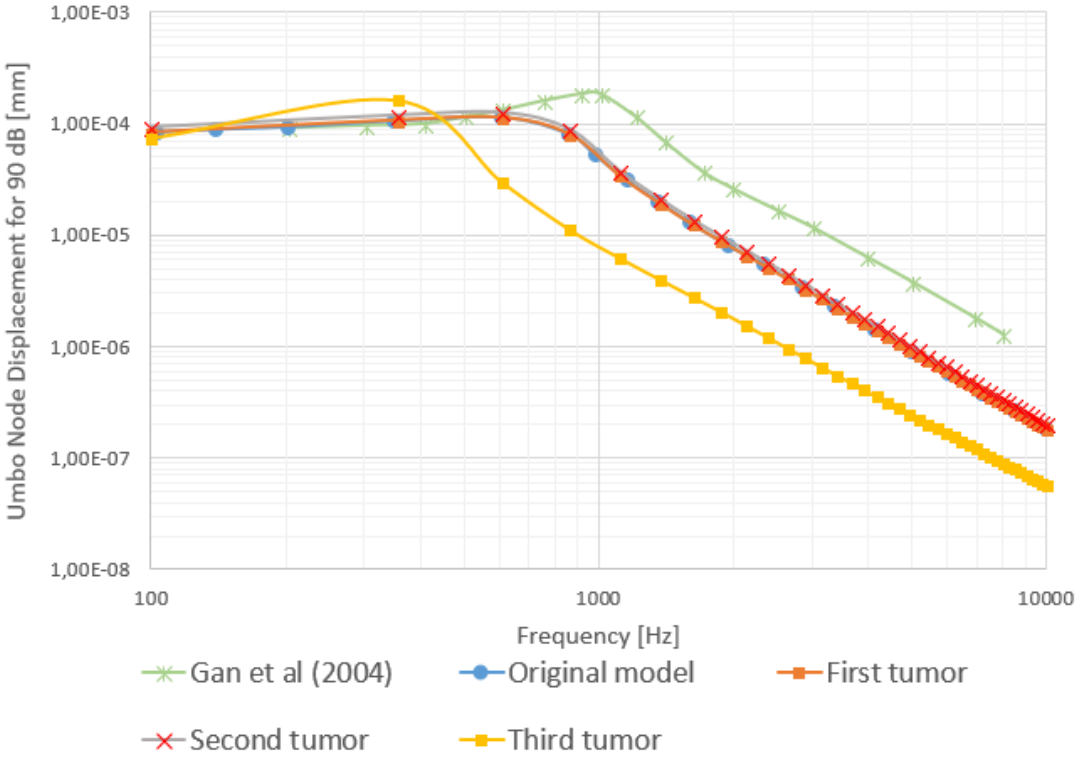

Figure 6.41 – Comparison at 90 dB sound level of umbo node displacement for the three simple tumor models [4], [45].

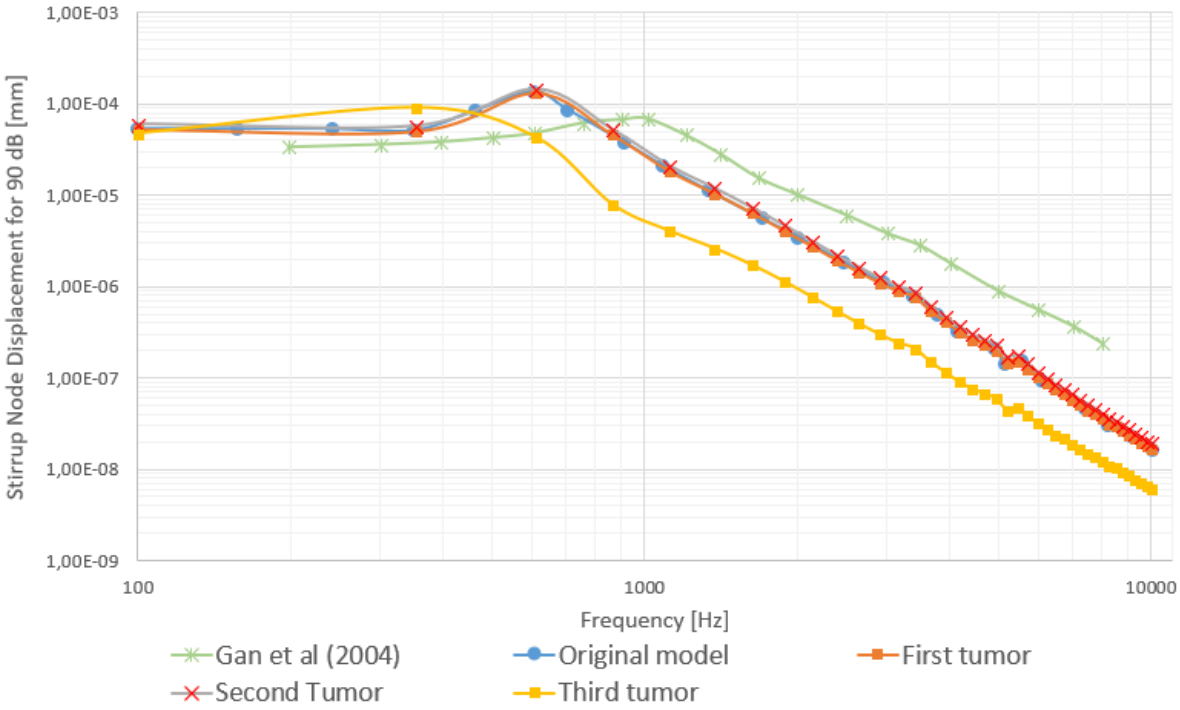

Figure 6.42 – Comparison at 90 dB sound level of stirrup node displacement for the three simple tumor models [4], [45].

The first two tumors once more stayed with a very similar behavior in regard to the original model, while the third tumor had a differential behavior having a spike of displacement at a lower frequency equivalent to 9,19×10−5 mm at 353,8 Hz frequency, then proceeding to have the lowest amounts of displacements for the highest frequencies.

It is also verified that the results from Gan *et al* [45] have good similarities. The umbo node displacement has very similar values for the first two tumors, being practically the same for the lower frequencies, and at higher frequencies the results for all the models are lower than the ones found by Gan *et al* [45]. For the stirrup node displacement, the results from the models had higher values at lower frequencies, while having lower values for higher frequencies, specially the third tumor model, which had significantly lower values at such frequencies.

Figures 6.43 and 6.44 bring the comparison for the umbo and stirrup node displacement with previous literature, on a sound power level of 105 dB.

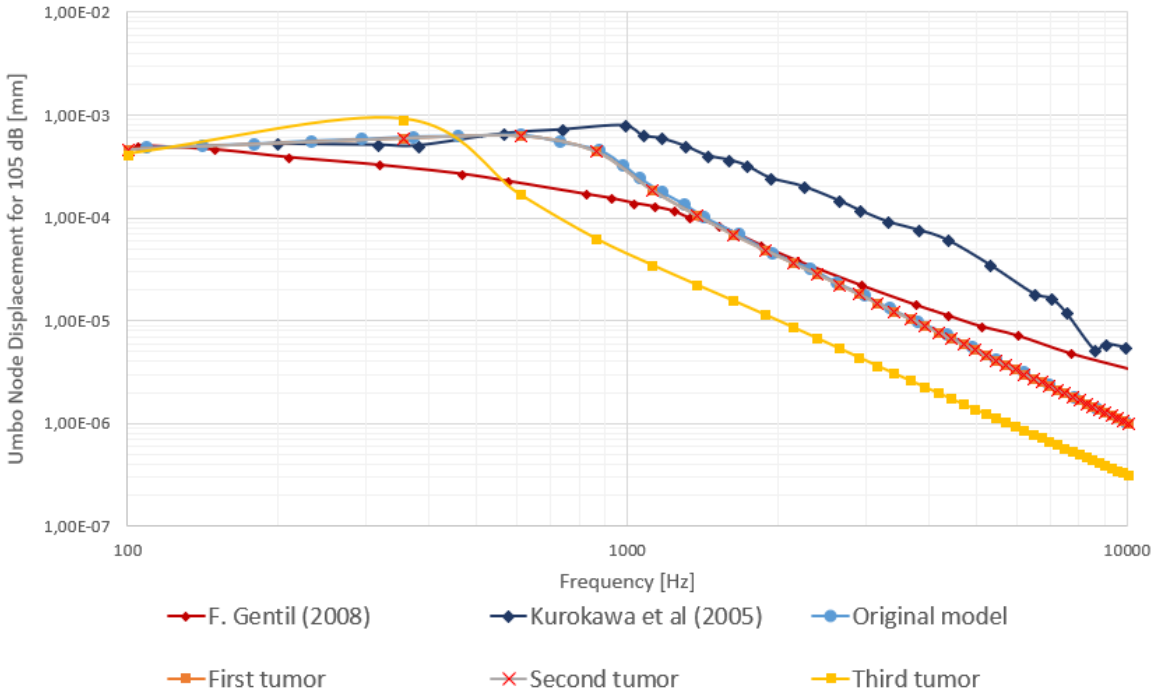

Figure 6.43 – Comparison at 105 dB sound level of umbo node displacement for the three simple tumor models [2], [4], [60].

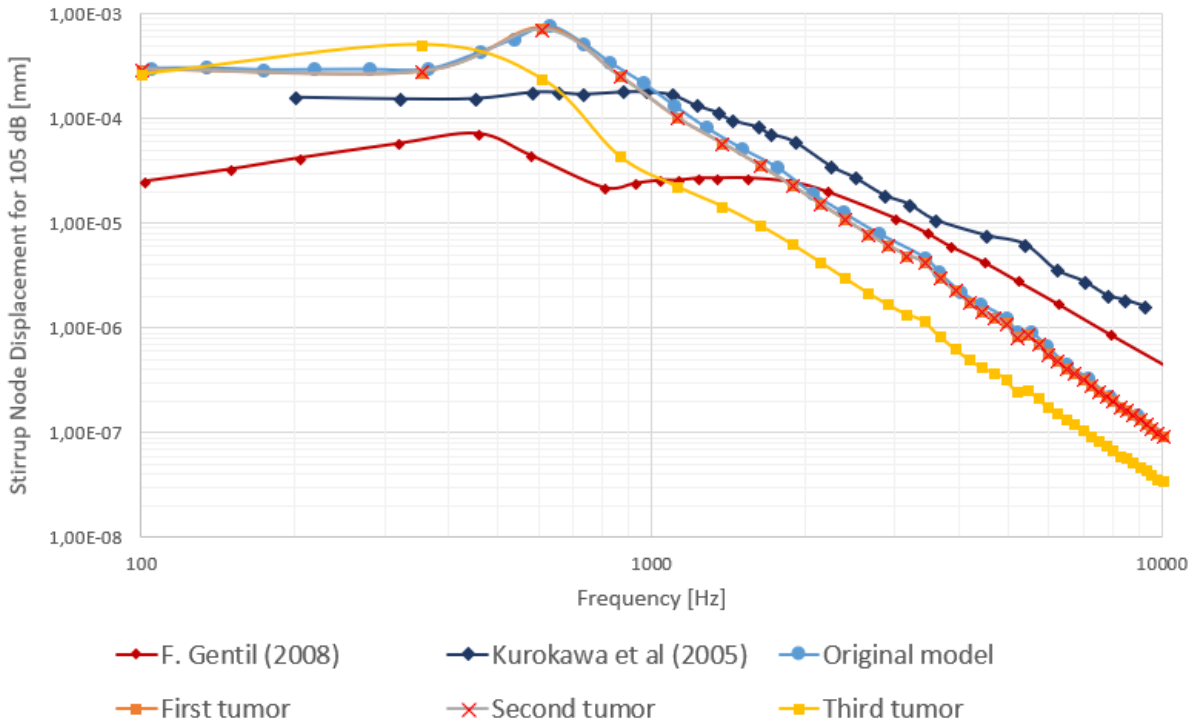

Figure 6.44 – Comparison at 105 dB sound level of stirrup node displacement for the three simple tumor models [2], [4], [60].

The data from Gentil *et al* [2] brings results from the displacement on the umbo and on the stirrup´s platinum, based on the model built on the membrane and the ossicles, while assuming hyperplastic behavior the membrane. Kurokawa *et al* [60] obtained the displacement on the umbo and on the stirrup´s platinum based on six male temporal bones, with ages ranging between 61 and 74 years, through the instrument Lase Doppler vibrometer. The results were obtained on a sound pressure level of 105 dB being applied over the tympanic membrane.

For both node displacements, at lower frequencies the models had a higher proximity to the values found by Kurokawa *et al* [60] on the range of lower frequencies, while resembling more the behavior of Gentil *et al* [2] on the higher frequencies.

The comparison between the original model and the tumor models for a sound pressure level of 130 dB can be seen on Figures 6.45 and 6.46.

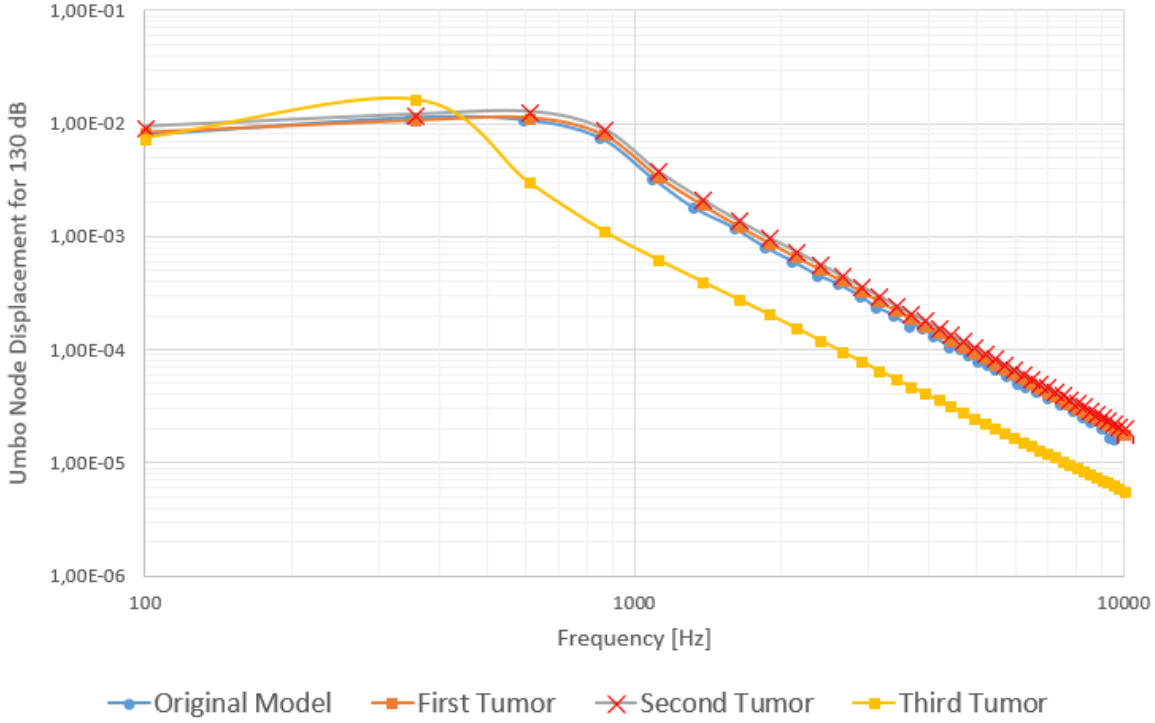

Figure 6.45 – Comparison at 130 dB sound level of umbo node displacement for the three simple tumor models [4].

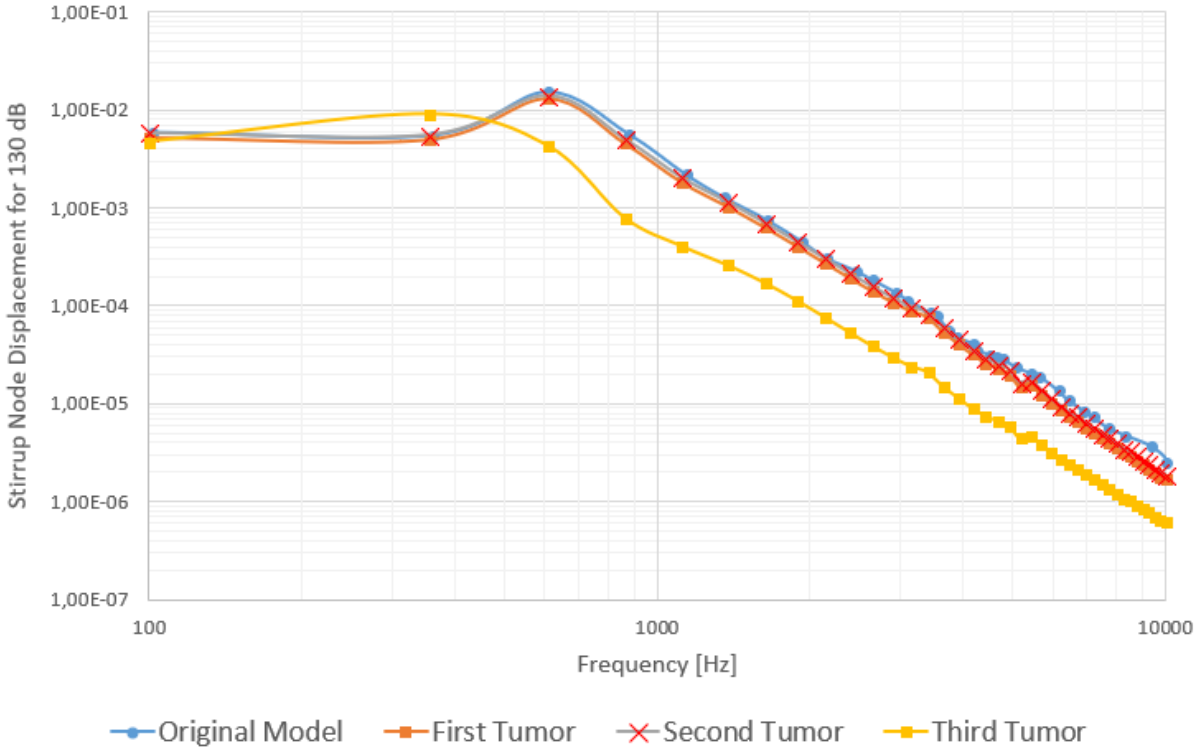

Figure 6.46 – Comparison at 130 dB sound level of stirrup node displacement for the three simple tumor models [4].

For the final sound pressure level, it is observed that the two first tumors had very high similarity to the original model throughout all the sound pressure levels. On the umbo displacement aspect, both always have had slightly higher values of displacement for the initial frequencies, while proceeding to have slightly lower values for the higher frequencies, and on the stirrup, they have had lower values overall. The third tumor throughout the entire study had a more unique behavior, having a stating value lower than the others, than at 353,8 Hz having a spike for its highest value, also higher than the values for the other models at such frequency, then proceeding to obtain the lowest displacements values overall at higher frequencies.

6.6.2.2 Complete model

The complete model was subjected to similar studies in regard to the simple model. For the complete model of each tumor, five different sound pressure levels were used, these being 0 dB (2,0×10−5 Pa), 60 dB (2,0×10−2 Pa), 80 dB (2,0×10−1 Pa), 90 dB (6,32×10−1 Pa and 130 dB (6,32×101 Pa).

Figure 6.47 brings the comparison for the umbo node displacement between all three tumor complete models and the original complete model for a sound pressure level of 0 dB (2,0×10−5 Pa), and Figure 6.48 brings the same comparison for the stirrup node displacement.

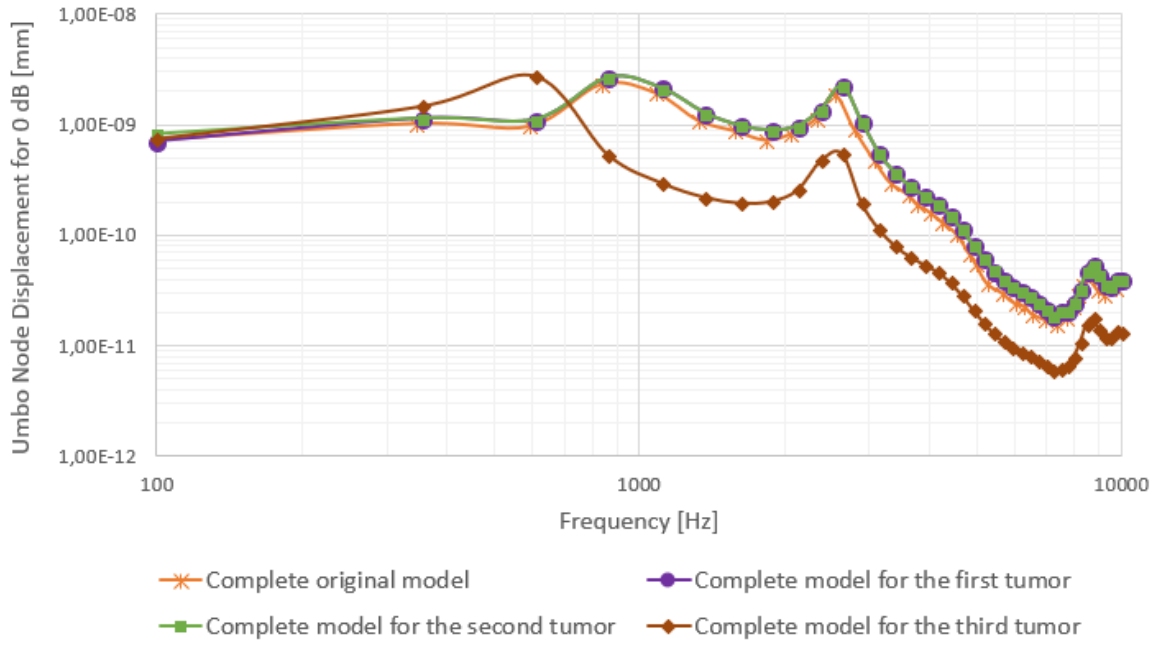

Figure 6.47 – Comparison at 0 dB sound level of umbo node displacement for the three complete tumor models [4].

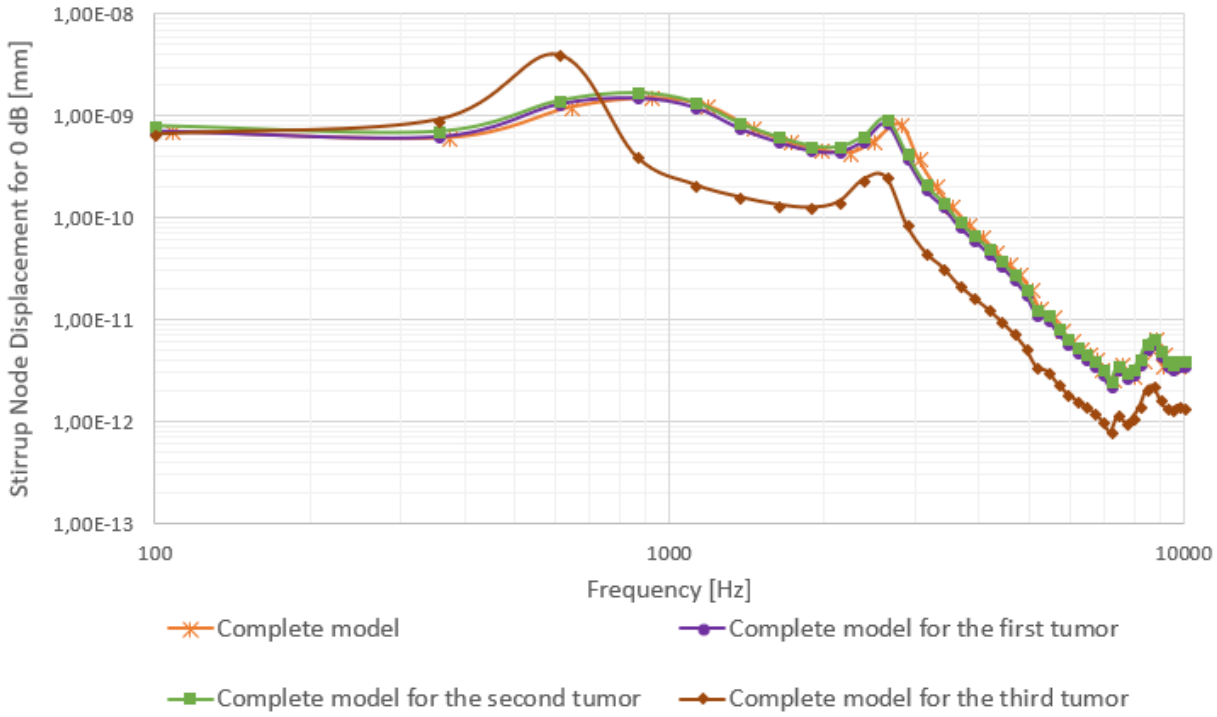

Figure 6.48 – Comparison at 0 dB sound level of stirrup node displacement for the three complete tumor models [4].

As with the studies performed on the simple models, it can be seen that also on the complete models the first two tumor models stay in close vicinity from the original model. On the umbo node displacement side, the first two tumors have slightly higher values overall when comparing to the original model, while on the stirrup node they have lower displacement values than the original on the frequency range between 2,8 kHz and 7,2 kHz, and have higher values on frequencies below and above that range.

The third tumor in both displacement cases once more show a peak of values on lower frequencies between 200 Hz and 700 Hz, then proceeding to have lower displacement values on the higher frequencies.

Figures 6.49 and 6.50 illustrate the same comparison, but for a sound pressure level of 60 dB.

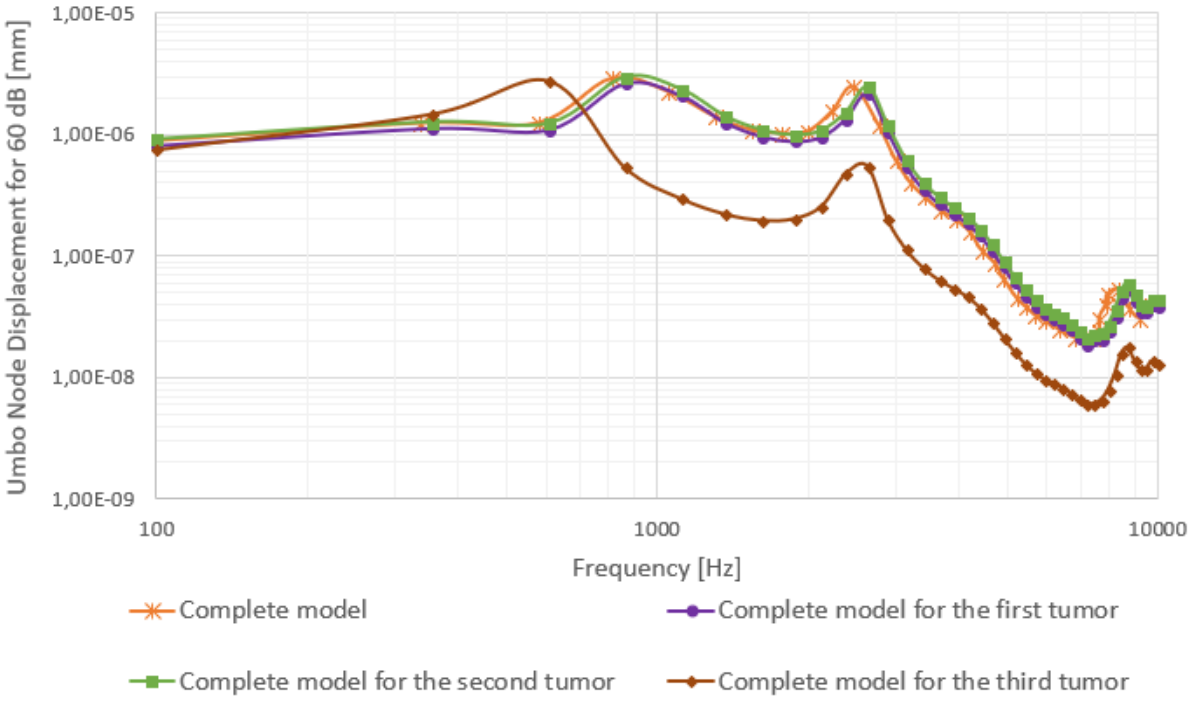

Figure 6.49 – Comparison at 60 dB sound level of umbo node displacement for the three complete tumor models [4].

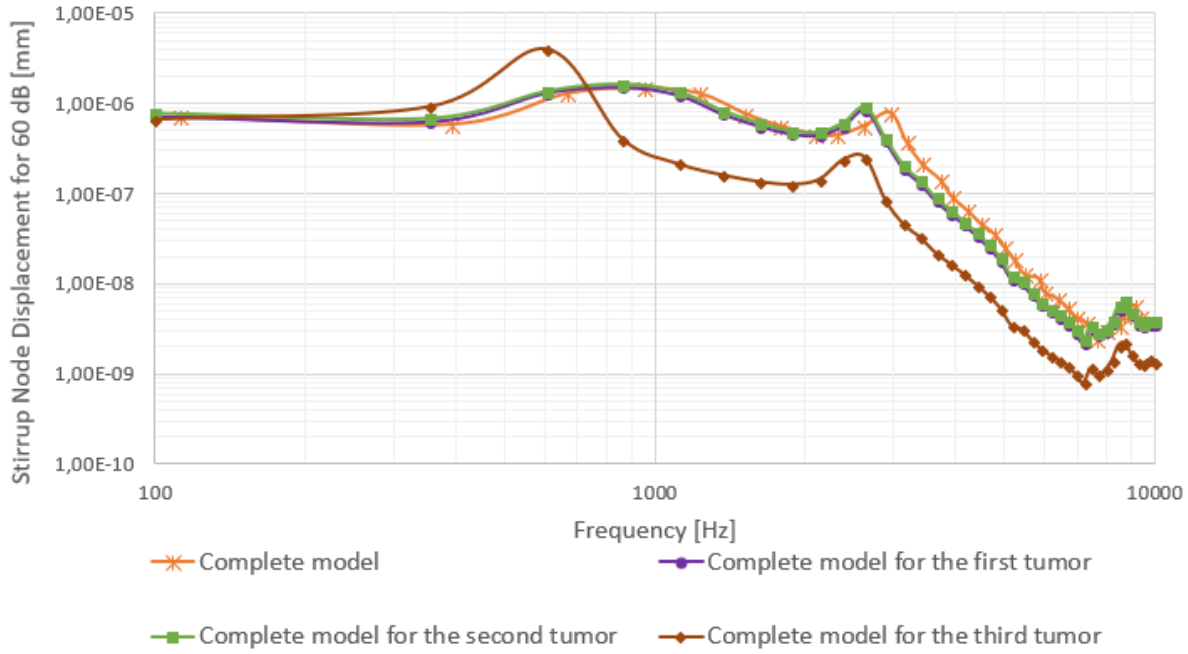

Figure 6.50 – Comparison at 60 dB sound level of stirrup node displacement for the three complete tumor models [4].

Differently from the 0 dB study, the 60 dB umbo displacement presented a situation where there were higher displacement values for the original model rather than the two first tumors, in the frequency range between 1 kHz and 2 kHz, but otherwise lower values as previously for other frequency ranges. The third tumor displayed a similar behavior to the one observed for 0 dB, having a peak displacement on lower frequencies and then proceeding to have lower values for any higher frequencies.

On the stirrup node displacement, the results obtained followed the same behavior overall as the ones found for 0 dB, with the two first tumors having a resemblance to the original model´s behavior, and the third model differentiating itself with varied numbers.

Figures 6.51 and 6.52 bring the displacement comparison for both nodes at sound pressure level 80 dB.

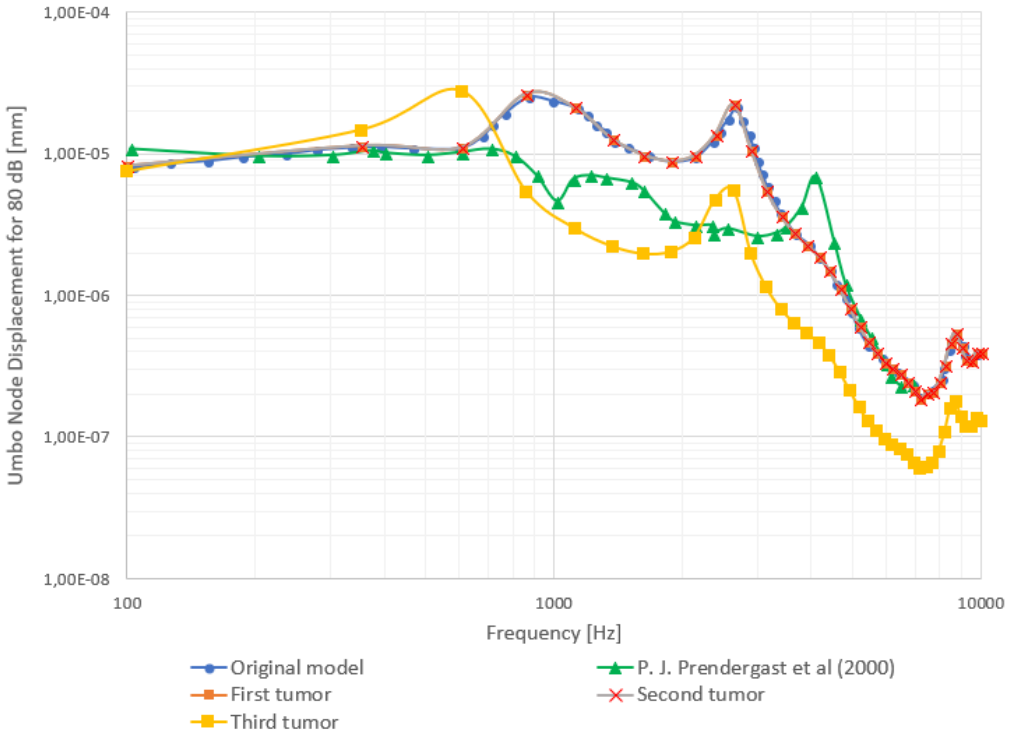

Figure 6.51 – Comparison at 80 dB sound level of umbo node displacement for the three complete tumor models [4], [61].

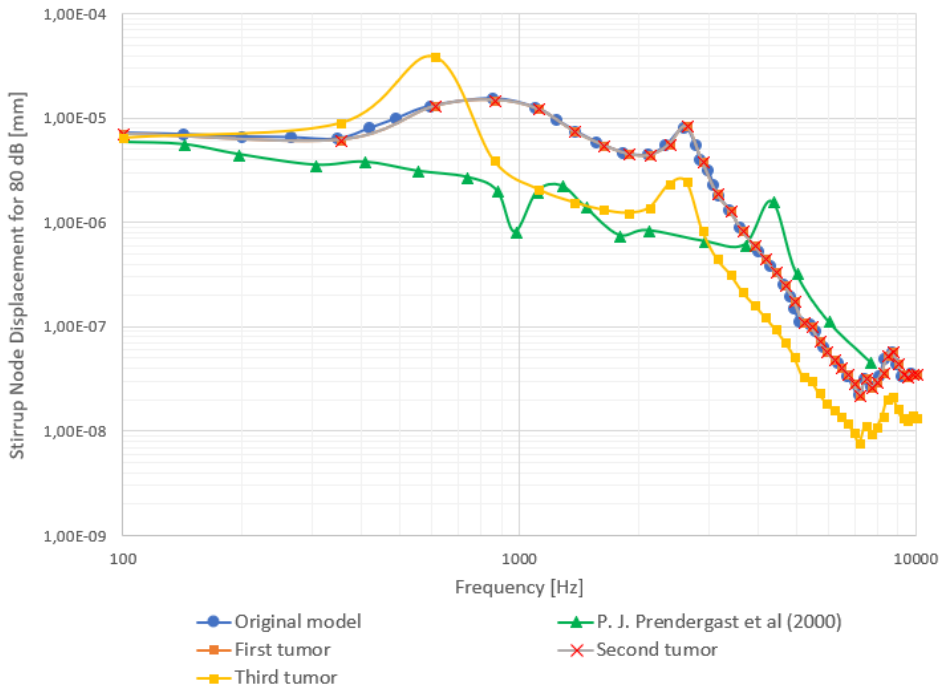

Figure 6.52 – Comparison at 80 dB sound level of stirrup node displacement for the three complete tumor models [4], [61].

The work by P.J. Prendergast *et al* [61] obtains the displacement on the umbo and on the stirrup through a tridimensional finite element model, built on the external auditive canal and the middle ear.

It is verified on the umbo displacement that the first two models, in agreement with the original mode, present a very similar displacement to the one found by P.J. Prendergast *et al* [61] for the lower frequencies, up to 800 Hz, and at the highest frequencies, starting from 5 kHz, while having different variations in between these ranges. P.J. Prendergast *et al* [61] also determines there is a resonance at frequency 4kHz, while the tumor models had it at approximately 2,6 kHz. The third tumor model also had the resonance at approximate 2,6 kHz, but apart from the resonance displacement values, it maintained lower values of displacement when compared to the literature.

The stirrup displacement has a different behavior, as it can be observed that the results from P.J. Prendergast *et al* [61] are the lowest for the lower frequencies, but after the mentioned resonance at 4 kHz it´s values are of higher displacement than the ones found for any of the models.

Figures 6.53 and 6.54 show the displacement comparison for the umbo node and the stirrup node, respectively, for a sound pressure level of 90 dB.

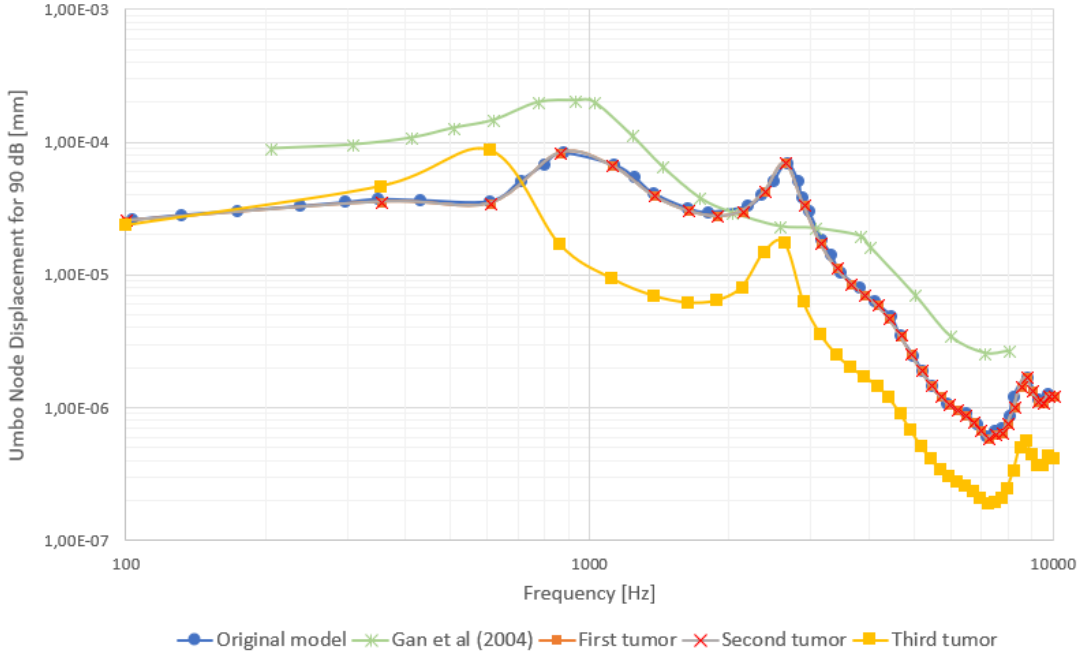

Figure 6.53 – Comparison at 90 dB sound level of umbo node displacement for the three complete tumor models [4].

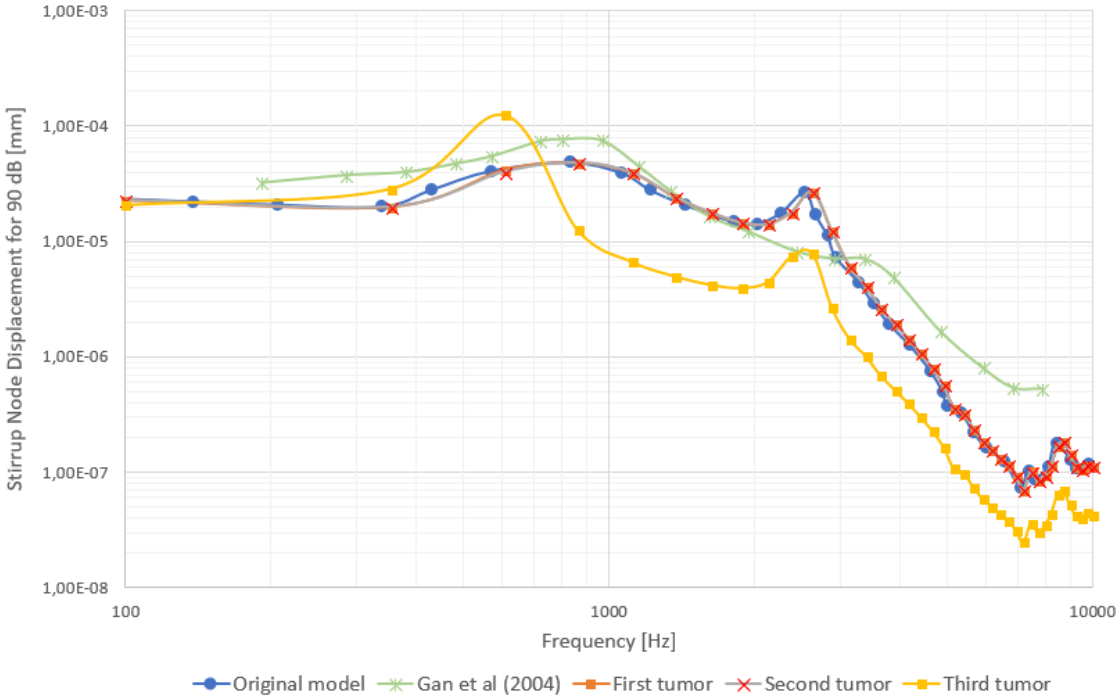

Figure 6.54 – Comparison at 90 dB sound level of stirrup node displacement for the three complete tumor models [4].

In the stirrup displacements it can be seen the first two tumors had a close behavior to the results found by Gan *et al* [45], with the results from the literature being slightly higher overall, except on the frequency range between 2 kHz and 3 kHz where the models present a peak of displacement which is not observed on the literature. The third tumor model stayed farther away from the literature values, on a lower range of displacements for both nodes.

Figures 6.55 and 6.56 bring the displacement comparison for the umbo node and the stirrup node, respectively, for the final sound pressure level of 130 dB.

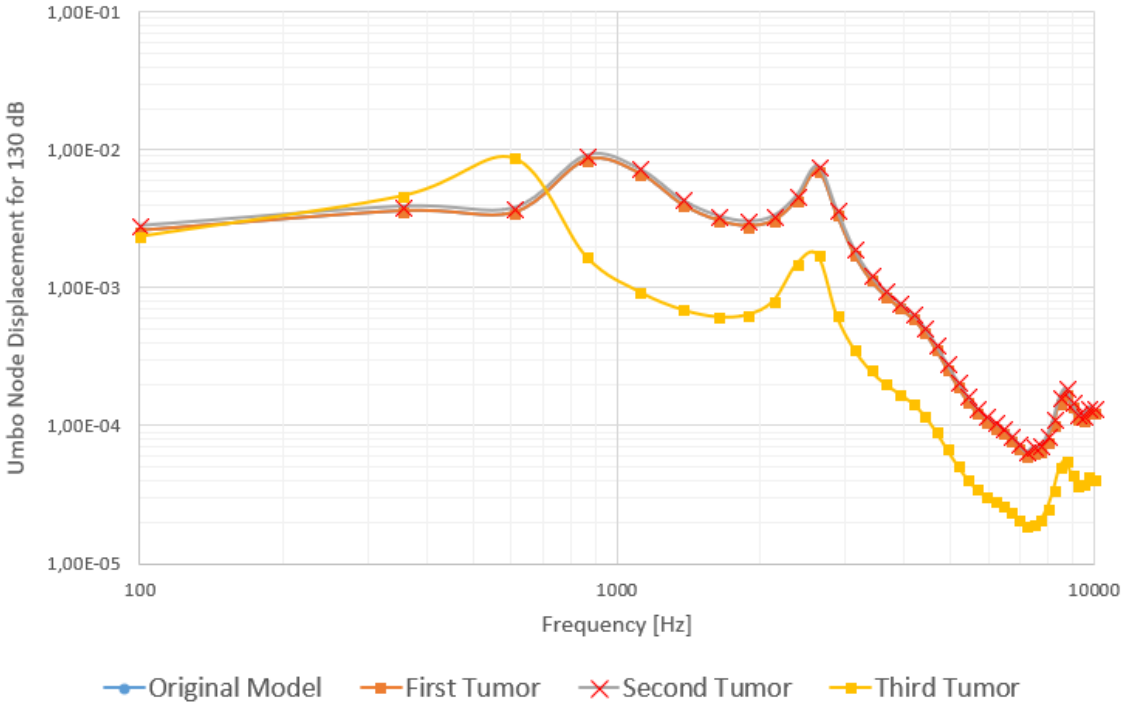

Figure 6.55 – Comparison at 130 dB sound level of umbo node displacement for the three complete tumor models [4].

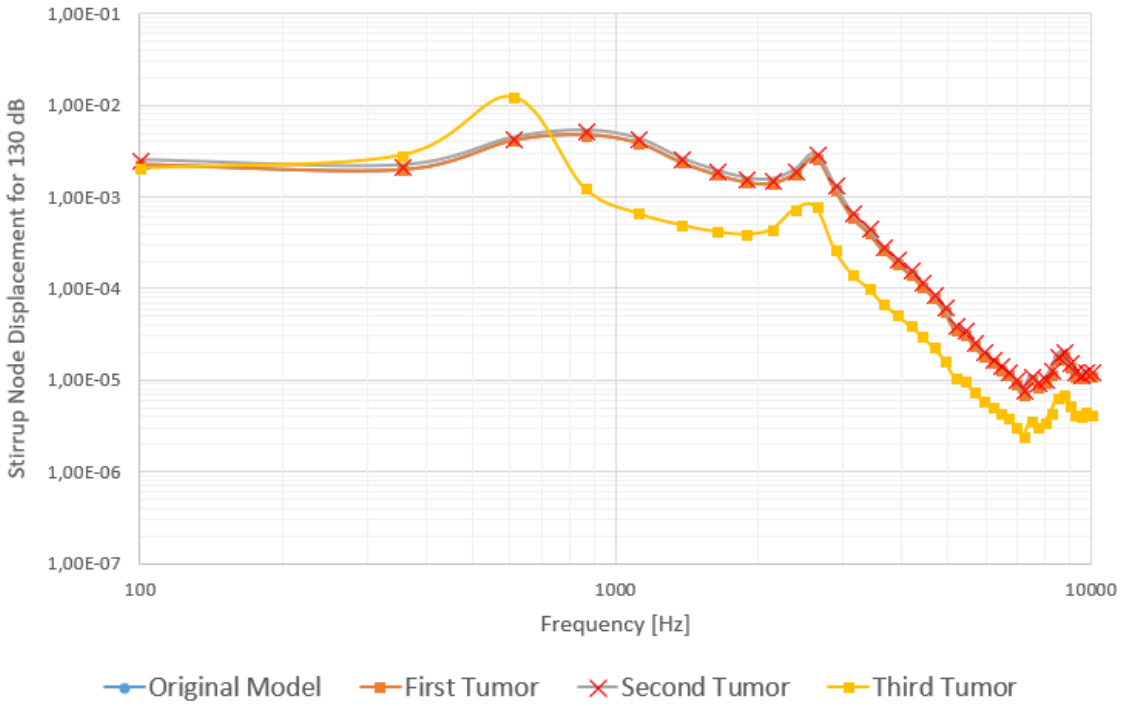

Figure 6.56 – Comparison at 130 dB sound level of stirrup node displacement for the three complete tumor models [4].

For the sound pressure level 130 dB the models continued to behave on the same way from the other levels, where the first two tumors remained very similar from each other, with the second have slightly higher values overall. The third tumor once more followed a pattern to have higher displacements for a low frequency, due to a resonance, and then proceeded to have lower displacements for all the higher frequencies.

7 CONCLUSIONS

The present work presented as objective the creation of tumor-type bodies and the further insertion of such bodies into a tridimensional model of the human ear in order to study any differences they could cause on the dynamic behavior of the model. In order to do that, two different models were applied: one model built only on the membrane, ossicles, ligaments, muscles and a fraction of the temporal bone, and a second, more complete model, which had everything from the first model plus air on the external auditory canal and on the tympanic cavity. All the mechanical properties were obtained from previous literature.

Whenever possible, data from additional previous literature was added to compare to the new behavior of the models, such situations happening when the test performed for any previous literature were similar to the simulations put to run at the time.

There were three different tumor bodies inserted to observe any behavioral changes. The first was of intermediate size, applied directly to the anvil of the middle ear, and given the same properties to the parts it was attached. The second, of small size, was inserted inside the stirrup ossicle, also given mechanical properties similar to the part it was attached. The third tumor was of a larger size, and was placed on the tympanic membrane to simulate a glomus tumor. Since the real glomus tumor is mostly built of blood, the mechanical properties used for this tumor body were similar to those of blood, also found on previous literature.

The first type of simulation the models were put to run had as objective the comparison for the natural frequencies, then comparing the results to the original model and to extra previous literature. It was possible to conclude that the small and intermediate sized tumors had very similar behaviors to the original model, thus showing they didn´t have a large impact. The third tumor model, however, posed a bigger difference on the results, showing it caused a significant change on the natural frequencies.

The second type of simulation had as objective the determination of displacements on key locations of the model, more precisely a node located on the umbo and a node located on the stirrup, on several sound pressure levels. The sound pressure levels applied varied from 0 dB up to 130 dB. On the simple model, this pressure is directly applied to the membrane, while on the complete model it is applied on the air on the entrance of the external auditory canal.

In all the pressure levels, the model was subjected to frequencies on the range between 100 Hz and 10 kHz. Similar to what could be observed on the natural frequency results, the first two tumors always kept on similar behavior as the ones found for the original model, thus not demonstrating to have a significant impact, while the third tumor continued to show a more unique set of resulting data, resulted from it´s more impactful presence.

For future works, it can be considered that this kind of study can be applied to virtually any pathology, as long as it has a physical interaction on the parts of the model. It can also be studied the ear behavior for differential air pressures, found on high peaks and mountains, or the bottom of the sea.

8 References and bibliography.

[1] G. Karki, “Human Ear: Structure and Anatomy -,” 2018. [Online]. Available: http://www.onlinebiologynotes.com/human-ear-structure-anatomy/. [Accessed: 05-Apr-2018].

[2] Gentil, F., *Estudo Biomecânico do Ouvido Médio*. 2008, Faculdade de Engenharia da Universidade do Porto.

[3] T. Belytschko, W. Liu, and B. Moran, *Nonlinear finite elements for continua and structures. 2000*, vol. 16. 2000.

[4] B. Areias, “Simulação biomecânica do ouvido humano, incluindo patologias do ouvido médio,” 2014, Faculdade de Engenharia da Universidade do Porto.

[5] Gentil, F., Jorge, R., Ferreira, A., Parente, M., Moreira, M., Almeida, A., *Estudo do efeito do atrito no contacto entre os ossículos do ouvido médio*, in *Internacional de Métodos Numéricos para Cálculo y Diseño en Ingeniería*. 2007. p. 177-187..

[6] Domingues, J., Mendonça, F., Almeida, J., Pereira, S., Sousa, M.T., rev., *Anatomia cirúrgica do osso temporal*. 2011.

[7] R. W. Baloh, “Harold Schuknecht and Pathology of the Ear,” *Otol Neurotol*, vol. 22, pp. 113–122, 2001.

[8] R. Putz, R., Pabst, *Sobotta*, vol. Tomo 1. 2000.

[9] Bento, R.F., *Tratado de Otologia*. 1998: EDUSP. 482.

[10] F. H. Netter, *Atlas of Human Anatomy 5th Edition*. 2011.

[11] L. Testut, *Traité d’Anatomie humaine – organes des sens , tome septieme.* .

[12] “Bones of the middle ear.” [Online]. Available: https://www.mayoclinic.org/diseases-conditions/hearing-loss/multimedia/ear-infections/sls-20077144?s=4.

[13] Garbe, C.A., *Estudo biomecânico para reabilitação do ouvido médio humano*, in *Engenharia Biomédica*. 2010, Faculdade de Engenharia da Universidade do Porto.

[14] Marques, M.C., *Estudo Biomecânico para a Reabilitação do Ouvido Médio Humano*, in *Bioengenharia*. 2012, Faculdade de Engenharia da Universidade do Porto.

[15] Seeley, R., Stephens, T., Tate, P., *Anatomia e Fisiologia*. 6ª ed. 2003.

[16] Standring, S., *GRAY'S Anatomia*. 40 ed. 2010.

[17] Junqueira, L.C., Carneiro, J., *Histologia Básica*. 11 ed. 2008, Rio de Janeiro.

[18] D. C. Meldau, “Aparelho Vestibular - Equilíbrio humano.” [Online]. Available: https://www.infoescola.com/anatomia-humana/aparelho-vestibular/. [Accessed: 10-Jul-2018].

[19] L. E. Kinsler, *Fundamentals of acoustic*. Wiley, 2000.

[20] Halliday, Resnick, and Walker, *Fundamentos de Física.*, 8th ed. .

[21] López, M.R., *Acústica arquitectónica aplicada*. 1999: Paraninfo.

[22] Guerra, R., *Acústica Curso de Terapêutica da Fala*. 2006, Faculdade de Ciências e Tecnologia da Universidade do Algarve, Departamento de Física.

[23] “Sound Power Level.” [Online]. Available: https://www.engineeringtoolbox.com/sound-power-level-d_58.html. [Accessed: 10-Jul-2018].

[24] Gentil, F., *Psicoacústica*. 2013/2014.

[25] “System One Audio | Fletcher Munson Correctie.” [Online]. Available: http://www.system1audio.com/fmc.html. [Accessed: 10-Jul-2018].
[26] R. Elliott, “ESP - Frequency, Amplitude and dB.” [Online]. Available: http://sound.whsites.net/articles/fadb.htm. [Accessed: 10-Jul-2018].
[27] Rodrigues, J.D., *Apontamentos de Vibraçoes de Sistemas Mecânicos*. 2013, Departamento de Engenharia Mecânica: Faculdade de Engenharia da U.PORTO..
[28] Beer, Johnston, Mazurek, and Eisenberg, *Mecânica Vetorial para Engenheiros*, 9th ed. 2011.
[29] P. R. Kurka, *Vibrações de Sistemas Dinâmicos: Análise e Síntese*. 2015.
[30] “ISO 1683:2015 - Acoustics -- Preferred reference values for acoustical and vibratory levels.” [Online]. Available: https://www.iso.org/standard/64648.html. [Accessed: 11-Jul-2018].
[31] F. T. Dias, J. P. Cruz, R. A. F. VALENTE, and R. J. A. SOUSA, *Método dos Elementos Finitos*, 1st ed. 2007.
[32] J. Carter, “Moore’s Law |.” [Online]. Available: http://pointsandfigures.com/2015/04/18/moores-law/. [Accessed: 11-Jul-2018].
[33] D. Logan, *A First Course in the Finite Element Method*, 4th ed. 2007.
[34] R. Savaris, “Método dos Elementos Finitos Aplicado à Placa Quadrada com Furo Circular Central,” 2017, Faculdade de Engenharia da Universidade do Porto.
[35] A. A. Vieira, “Teoria do circulo de mohr.” [Online]. Available: https://pt.slideshare.net/TEC_pts/teoria-do-circulo-de-mohr. [Accessed: 11-Jul-2018].
[36] M. M. Akiyoshi, A. P. da Silva, R. Pereira, and V. C. Pandolfelli, “Importância da utilização de propriedades avaliadas em função da temperatura para a simulação computacional de cerâmicas refratárias,” *Cerâmica*, vol. 48, no. 306, pp. 70–78, Jun. 2002.
[37] G. P. Nikishkov, *Introduction To The Finite Element Method*. University of Aizu, 2004.
[38] O. C. Zienkiewic and R. L. Taylor, *The Finite Element Method*, 5th ed. 2000.
[39] A. H. Nielsen, “The visible ear,” Aalborg university, 2005.
[40] *Abaqus Analysis User's Manual*. 2012.
[41] Wever, E.G. and M. Lawrence, *Physiological acoustics*. 1982: Princeton University Press.
[42] Donaldson and Miller, *Anatomy of the ear.*, 1st ed. 1973.
[43] M. E. Ravicz, W. T. Peake, H. H. Nakajima, S. N. Merchant, and J. J. Rosowski, “Modeling flexibility in the human ossicular chain: Comparison to ossicular faxation data,” 2004.
[44] Mukherjee, S., A. Chawla, and B. Karthikeyan, *A review of the mechanical properties of human body soft tissues in the head, neck and spine.* Institute of Engineers Journal. **87**.
[45] Gan, R.Z., B. Feng, and Q. Sun, *Three-dimensional finite element modeling of human ear for sound transmission.* Ann Biomed Eng, 2004. **32**(6): p. 847-59.
[46] Q. Sun, R. Z. Gan, K.-H. Chang, and K. J. Dormer, “Computer-integrated finite element modeling of human middle ear,” *Biomech. Model. Mechanobiol.*, vol. 1, no. 2, pp. 109–122, Oct. 2002.
[47] F. Gentil *et al.*, “The Influence of the Mechanical Behaviour of the Middle Ear

Ligaments: A Finite Element Analysis," *Proc. Inst. Mech. Eng. Part H J. Eng. Med.*, vol. 225, no. 1, pp. 68–76, Jan. 2011.

[48] Obrist, D., *Numerical simulation of the endolymph flow in a semicircular canal.* PAMM, 2007. **7**(1): p. 4100029-4100030..

[49] Issakainen, J., et al., *Method for calibration of step length and arrangement utilizing the method*. 2005, Google Patents

[50] Bergman, T.L. and F.P. Incropera, *Fundamentals of Heat and Mass Transfer*. 2011: Wiley.

[51] Azhari, H., *Appendix A: Typical Acoustic Properties of Tissues*, in *Basics of Biomedical Ultrasound for Engineers*. 2010, John Wiley & Sons, Inc. p. 313-314.

[52] R. Jyung, "Glomus Tumors | American Hearing Research Foundation." [Online]. Available: https://www.american-hearing.org/disorders/glomus-tumors/. [Accessed: 11-Jul-2018].

[53] M. Leverson, "Glomus Tumors (Tympanicum Jugulare) - Ear Surgery Information Center." [Online]. Available: http://www.earsurgery.org/learn/ear-tumors/tumors-of-the-middle-ear-mastoid/glomus-tumors-tympanicum-jugulare/. [Accessed: 11-Jul-2018].

[54] J. Cutnell and K. Johnson, *Physics*, 4th ed. 1998.

[55] Rescale, "Numerical Simulation of Blood Flow in Flexible Arteries Using Fluid-Structure Interaction | Rescale." [Online]. Available: https://blog.rescale.com/numerical-simulation-of-blood-flow-in-flexible-arteries-using-fluid-structure-interaction/. [Accessed: 11-Jul-2018].

[56] Huber, A., et al. *The vibration pattern of the tympanic membrane after placement of a total ossicular replacement prosthesis*. in *Proceeding of the International Workshop on middle ear mechanics in research and otosurgery. Dresden, Germany*. 1997.

[57] Liu, T.-C., et al., *Computer aided three-dimensional reconstruction and modeling of middle ear biomechanics by high-resolution computed tomography and finite element analysis.* Biomedical Engineering: Applications, Basis and Communications, 2006. **18**(05): p. 214-221.

[58] Nishihara, S. and R. Goode, *Measurement of tympanic membrane vibration in 99 human ears.* Middle ear mechanics in research and otosurgery. Dresden University of Technology, Dresden, Germany, 1996: p. 91-93.

[59] Nishihara, S., H. Aritomo, and R.L. Goode, *Effect of Changes in Mass on Middle Ear Function.* Otolaryngology -- Head and Neck Surgery, 1993. **109**(5): p. 899-910.

[60] Kurokawa, H. and R.L. Goode, *Sound pressure gain produced by the human middle ear.* Otolaryngology--Head and Neck Surgery, 1995. **113**(4): p. 349-355.

[61] Ferris, P. and P. Prendergast, *Middle-ear dynamics before and after ossicular replacement.* Journal of Biomechanics, 2000. **33**(5): p. 581-590.